Cellular and Molecular Mediators of Bronchiolitis Obliterans-like Pathological Changes in a Murine Model of Chlorine Gas Inhalation

by

Emily Grace O'Koren

Department of Immunology
Duke University

Date:_____

Approved:

_____
Michael D. Gunn, Supervisor

_____
You Wen He, Chair

_____
Garnett Kelsoe

_____
Mari Shinohara

_____
Barry Stripp

Dissertation submitted in partial fulfillment of
the requirements for the degree of Doctor
of Philosophy in the Department of
Immunology in the Graduate School
of Duke University

2013

ABSTRACT

Cellular and Molecular Mediators of Bronchiolitis Obliterans-like Pathological Changes in a Murine Model of Chlorine Gas Inhalation

by

Emily Grace O'Koren

Department of Immunology
Duke University

Date:_____
Approved:

_____
Michael D. Gunn, Supervisor

_____
You Wen He, Chair

_____
Garnett Kelsoe

_____
Mari Shinohara

_____
Barry Stripp

An abstract of a dissertation submitted in partial fulfillment of the requirements for the degree of Doctor of Philosophy in the Department of Immunology in the Graduate School of Duke University

2013

Abstract

Bronchiolitis Obliterans (BO) is a major cause of chronic airway dysfunction after toxic chemical inhalation. The pathophysiology of BO is not well understood, but epithelial cell injury has been closely associated with the development of fibrotic lesions in human studies and in animal models of both toxin- and transplant-induced BO. However, while almost all cases and models of BO include epithelial injury, not all instances of epithelial injury result in BO, suggesting that epithelial damage *per se* is not the critical event leading to the development of BO. In this dissertation, we describe a model of chlorine (Cl_2)-induced BO in which mice develop tracheal and large airway obliterative lesions within 10 days of exposure to high (350 ppm), but not low (200 ppm), concentrations of Cl_2 gas. Lesions develop in a series of well-demarcated pathological changes that include epithelial denudation, inflammatory cell infiltration by day 2 after exposure, fibroblast infiltration and collagen deposition by day 5, and in-growth of blood vessels by day 7, ultimately leading to lethal airway obstruction by days 9-12. Using this model, we were able to test our hypothesis that loss of epithelial progenitor cells is a critical factor leading to the development of obliterative airway lesions after chemical inhalation. Indeed, these lesions arise only under conditions and in areas in which basal cells, the resident progenitor cells for large airway epithelium, are eliminated by Cl_2 exposure.

The molecular pathways contributing to BO development are not well understood. Mechanisms of epithelial injury differ across BO models, but we hypothesized that after the inciting injury, BO models share common pathways. We compared microarray analysis from day 5 non-BO- and BO-inducing chemical injuries and subsequently identified biological pathways that may contribute to BO

pathogenesis. Our findings add support to pathways previously implicated in BO development and more importantly, suggest potential new pathways and molecular mediators of BO. Furthermore, we evaluated the efficacy of therapeutic inhibition of neovascularization or inflammation to prevent Cl_2-induced BO. To date, our therapeutic interventions were ineffective. Nonetheless, our findings suggest that in the context of Cl_2-induced BO, vascular endothelial growth factor receptor 2 (a mediator of neovascularization) and inducible nitric oxide synthase (a mediator of inflammation) are not critical in BO pathogenesis.

In sum, our work introduces and characterizes a novel Cl_2-induced murine model of BO. Using this model we demonstrated that in the absence of basal cells, epithelial regeneration does not occur and regions of epithelial denudation persist from which an aberrant repair process is initiated, leading to obliterative airway lesions. Our findings suggest that, irrespective of the cause, loss of epithelial progenitor cells may be a critical factor leading to the development of BO. Furthermore, our gene expression analysis implicates novel mediators and signaling pathways in the development of BO. Our analysis lays the foundation for more rigorous exploration of these targets in the pathogenesis of BO.

Dedication

To my parents, Anthony and Mari O'Koren.

Contents

List of Tables

List of Figures

Abbreviations

AHR, airway hyperreactivity

b.m., basement membrane

BALF, bronchoalveolar lavage fluid

BO, bronchiolitis obliterans

Clara cells, secretory cells

C.T., connective tissue

Cl_2, chlorine

DAVID, the Database for Annotation, Visualization and Integrated Discovery

EC, endothelial cell

FA, filtered air

FEV_1, forced expiratory volume in 1 second

G-protein, guanosine nucleotide-binding protein

H&E, hematoxylin and eosin

HIF, hypoxia inducible factor

HOCl, hypochlorous acid

IPA, Ingenuity Pathway Analysis

NO, nitric oxide

NOS2, iNOS, inducible nitric oxide synthase

OCl-, hypochlorite ion

PAMPs, pathogen-associated molecular patterns

RADS, reactive airway dysfunction syndrome

RXR, retinoid x receptors

SE, subepithelial

SO_2, sulfur dioxide

Sulfo-NHS-biotin, sulfosuccinimidobiotin

TREM-1, triggering receptor expressed on myeloid cells 1

VEGF, Vascular endothelial growth factor

VEGFR-1, vascular endothelial growth factor receptor 1

VEGFR-2, vascular endothelial growth factor receptor 2

Acknowledgements

I would like to gratefully and sincerely thank Dr. Michael Dee Gunn for his guidance, understanding, and a lot of patience during my graduate studies. Working in the Gunn lab has made me a better scientist by fostering my curiosity and creativity and, most importantly, by my learning how to translate them into meaningful science. Dee's support, especially in the face of extraordinary circumstances, was paramount in the successful completion of my degree and reflects strength of character that I greatly admire. For everything you've done for me, I thank you.

To all of the members of the Gunn lab, thank you for making lab life engaging and friendly. I'd especially like to thank Andrea Yu for her advice, encouragement, and, above all, her friendship.

I would like to express my deepest appreciation to my committee members for their expertise and support. Additionally, thanks to Brigid Hogan and her lab members for introducing me to the exciting world of airway epithelium. They were very generous with both their knowledge and skills. I also want to extend my gratitude to Michael William Foster for enriching my appreciation of pulmonary science.

I am also grateful for the camaraderie of my friends at Duke, especially Jacquie, Ian, and Ebeth, with whom I have celebrated and commiserated the experience of graduate school. Finally, I have been blessed with the overwhelming support of my entire family. My success is the direct result of the opportunities their determination and hard work has afforded me. Most especially, I want to thank my parents, to whom this dissertation is dedicated. I could not have succeeded without them. Thank you for your unwavering love and encouragement.

1. Overview

A basic understanding of airway epithelium, bronchiolitis obliterans (BO), animal models of BO, and chlorine (Cl_2) gas will be required to contextualize the research discussed herein. For this purpose, I have included an overview of each of these subjects.

1.1 Airway epithelium homeostasis and repair

Respiratory epithelium interfaces with the environment and serves as a critical physical and functional barrier to airborne particulate-matter, pollutants, and pathogens. To meet the challenges of constant environmental exposure, the epithelium has adopted a wide range of specialized effector cells, including secretory cells, ciliated cells and basal cells [1]. The diversity of the epithelium changes from proximal to distal airways, which likely reflects changing barrier and lung function requirements. Here, we will review airway anatomy and the cell types that comprise the respiratory epithelium. Additionally, the airways possess great capacity to repair after injury. We will discuss normal repair processes and the epithelial progenitors that contribute to the restitution of normal epithelium.

The overall structure of the airways is much like the roots of a tree. Air travels down successively smaller airways from conducting to respiratory airways. The major conducing airways begin with the trachea before branching into bronchi, and then proximal bronchioles. The respiratory airways include distal bronchioles and branch into alveolar ducts and sacs where the majority of oxygen exchange occurs [2]. Cellular diversity changes along the length of the airway. In mice, proximal airways, including the trachea and bronchi, are comprised of pseudostratified epithelium [1]. Ciliated and secretory (Clara) cells line the airway and are located above a layer of basal cells.

Ciliated cells are columnar-shaped with cilia protruding into the lumen. These cells are critical for debris clearance, and they function in concert as a part of the mucociliary escalator that moves mucus and particulate matter up and out of the respiratory tract [3]. Ciliated cells decrease in numbers along the bronchioles. Clara cells are also columnar-shaped and secrete small molecules into the airway, including lung surfactant and Clara cell secretory protein [1]. These products serve to inactivate harmful substances that enter the airway. Basal cells are cuboidal-shaped cells that are situated at the bottom of the epithelium with wide bases that attach to the basal lamina. Strong evidence supports that basal cells are progenitor epithelial cells during homeostatic conditions and especially after injury [4]. The epithelium of the trachea and bronchi transitions from pseudostratified to simple columnar along the bronchioles and is mainly comprised of ciliated and Clara cells. Finally, the alveolar ducts and sacs are comprised of specialized epithelial Type 1 and Type 2 cells that are uniquely adapted to assist in gas exchange [1].

Epithelium type and cell distribution vary among species. In contrast to the murine airways described above, human airways are lined by pseudostratified epithelium from the trachea down to the distal bronchioles, and these bronchioles are approximately 0.5mm in diameter when the epithelium transitions into simple cubodial epithelium that lack basal cells [5]. These disparities in anatomy are a challenge to researchers who are restricted to murine models for experimentation. In terms of size and cellular composition, the mouse trachea is representative of the first six generations of the human airways [5]. The mouse trachea, but not lower airways, contains basal cells that sit beneath the luminal epithelium and function similarly to human airway basal cells in their ability to give rise to epithelial cells during normal homeostasis and after injury [4, 6].

Under normal homeostatic conditions, epithelial cell turnover is slow with less than 5% of cells proliferating concurrently [7]. However, the airway possesses great capacity for repair after injury. The repair response greatly depends on the severity of the injury, which can be broadly divided into four different degrees [8]. The first degree consists of cellular irritation, not resulting in death, and is thought to be reversible with minimal need for proliferation as a mechanism of repair. The second degree inflicts partial necrosis or apoptosis of mature epithelial cells, and basal cells are unaffected. Repair primarily consists of a quick burst of proliferation from local mature epithelial cells or proliferation and differentiation of local progenitor cells. The third degree of injury involves the majority of mature epithelial cells undergoing necrosis or apoptosis and shedding from the airway wall; the majority of basal cells survive. This type of injury is evident after toxic gas inhalation, such as sulfur dioxide (SO_2) and lower concentrations of Cl_2 [9, 10]. The fourth degree of injury is similar to the third, except that the majority of basal cells do not survive. This type of injury is most often seen in large areas of mechanical injury or even after inhalational exposure to high concentrations of chemicals [10, 11]. It is important to note that the injury inflicted by inhalational irritants is often dependent on toxicant dose and duration of exposure.

In response to injuries involving desquamation, normal epithelial repair is thought to occur in three stages [12-14]. First, basal cells spread and migrate to cover denuded epithelium. Second, these cells proliferate, with self-renewing basal cells remaining near the basal lamina and daughter cells forming upper layers of transitory squamous metaplasia. Lastly, the upper layers remodel to form a pseudostratified layer of mature, differentiated mucociliary epithelium. It is important to note that the exact epithelial progenitor cells responsible for repair vary along the airway and into the lung; identification of these progenitors is an active area of research [14, 15]. However,

extensive epithelial lineage tracing implicates basal cells as the primary progenitor in the pseudostratified epithelium of mice after desquamation of the airways [4, 5].

1.2 Bronchiolitis obliterans

BO is a form of chronic obstructive airway disease in which small airways are compressed and narrowed by fibrosis and inflammation. The resulting fixed airway obstruction leads to dyspnea, typically on exertion, which is often progressive [16-18]. Currently, BO is the most prominent feature of chronic rejection after lung transplantation and is the leading cause of death beyond the first year post transplant [18, 19]. Lung transplantation is the most recognized cause of BO, but less recognized causes include collagen vascular disease, gastroseophageal reflux, inhalation of toxic chemicals, viral infections, and hematopoetic stem cell transplantation [16, 20]. In the case of toxin inhalation, BO has been documented following exposures to a wide variety of chemicals, including Cl_2, ammonia, methyl isocyanate, mustard gas, and diacetyl, the cause of "popcorn worker's lung" [21, 22].

Diagnosis of BO is often difficult, relying on a combination of clinical and physiological parameters. The hallmark clinical finding is reduced forced expiratory volume in 1 second (FEV_1) in the absence of other identifiable causes [20]. It is common for BO to develop in patches, making it possible to go undiagnosed in transbronchial biopsies. Additionally, no diagnostic guidelines exist for BO identification via radiographic findings, although expiratory CT scans may aid in identifying air-trapping that can occur from small airway narrowing [20]. Because diagnosing BO is often difficult, its true incidence may be underestimated. In one recent study, 78% of U.S. Iraq and Afghanistan veterans who presented with unexplained dyspnea and underwent lung biopsy had pathologic evidence of BO, despite, in most cases, having normal chest x-rays and pulmonary function tests [23].

Pathologically, BO can be divided into two forms: proliferative and constrictive. In proliferative BO, connective tissue breeches the airway lining and then proliferates within the lumen to form tissue masses, akin to granulation tissue [24]. This is often seen as an acute inflammation-mediated process and, in some cases, responds to corticosteroid treatment [16]. In contrast, constrictive BO is an irreversible fibrotic thickening of the submucosa that concentrically constricts the small airways from beneath the airway epithelial lining [16]. It is not clear whether constrictive BO is the final outcome of persistent and severe proliferative BO, or if these represent distinct responses to differing types of airway injury [25]. To date, therapeutics for constrictive BO have met with limited success and serve mostly to slow the progression of the disease, not cure it. The majority of therapeutics are immunosuppressants, including cyclosporine, azithromycin (an antibiotic that also suppresses activation of myeloid cells), statins, and aggressive prevention of known risk factors such as gastroesophageal reflux and infections [20, 26, 27]. Even so, constrictive BO is associated with high mortality [17, 18].

BO is a complex disease that can arise from multiple factors, including ischemia, inflammation, immune-mediated rejection and epithelial injury. The interplay between these factors in the pathogenesis of BO remains unclear. Tissue ischemia can be induced by transplantation and anti-endothelial immune responses. Recent studies demonstrated that reducing lung transplant ischemia by revascularizing bronchial arteries, in addition to the pulmonary artery, resulted in fewer incidents of acute rejection and infection, and delayed the onset of BO[28, 29]. This study directly implicates transplant ischemia as an inciting factor of BO. It is proposed that ischemia-induced hypoxia leads to inflammation, another BO-associated factor. Immune cells are capable of oxygen sensing through intracellular accumulation of hypoxia inducible factors (HIFs); HIFs enhance

cell activation and inflammatory functions [30]. It has been proposed that hypoxia perpetuates a pro-inflammatory environment that is permissive to innate immune cell-mediated tissue damage and/or the development of alloimmune rejection of donor tissue. In the case of immune-mediated rejection, acute rejection is a well-documented risk factor for BO after lung transplant. A recent study demonstrated that as few as one incidence of minimal acute rejection significantly increased the risk of BO complications[31]. Rejections can initiate compliment cascades and inflammation that lead to tissue damage [32-34]. Additionally, pulmonary infection is a significant risk factor for BO after transplant [20, 35]. It is thought that the immune response to the pathogen induces pro-inflammatory cytokines and increases antigen presentation at the site of infection, creating an environment conducive to alloreactive T cell priming and, ultimately, graft rejection [35].

The common theme to all these inciting factors is tissue damage, from which aberrant fibrotic responses progress into BO. More specifically, several lines of evidence suggest that epithelial cell injury is the most critical pathogenic factor. In a mouse model of allogeneic mismatched orthotopic lung transplantation characterized by severe vascular rejection but no epithelial injury, obliterative airway disease did not occur [36]. However, in a mouse tracheal transplant model, an alloresponse to epithelium was sufficient to induce obliterative airway disease [37]. In non-transplant murine studies, chronic depletion of mature epithelial cells, either Clara cells or Type II alveolar cells, results in abnormal re-epithelialization and a fibrotic response [38, 39]. In the case of chemical-associated BO, epithelial injury is also a common feature of almost all human instances and animal models, further supporting the view that epithelial damage is a critical factor in the pathogenesis of BO. The research herein investigates mechanisms through which chemical-induced epithelium injury initiates BO.

1.3 Animal models of bronchiolitis obliterans

Several animal models of BO have emerged over the past two decades, each with their own advantages and limitations. It is generally agreed that large animal models such as pigs are apt to be the most clinically relevant due to their anatomic similarity to humans, but such models are labor intensive, low throughput and extremely costly. To overcome those challenges, small rodent models were created; however, the size discrepancy between human and rodents has been a persistent criticism. Here, we will briefly discuss the various small animal models of transplant and non-transplant BO.

Transplant animal models of BO include both heterotopic and orthotopic transplantation of tracheas, lungs, and bone marrow [40]. The most common model is heterotopic transplantation, which involves excising the trachea and implanting it intraperitoneally or subcutaneously in an allogenic or syngenic recipient mouse. The development of BO is alloimmune-dependent as syngenic transplants are protected [19, 41]. Approximately 10 days post transplant, the allograft exhibits epithelial damage and immune cell infiltration. At 21 days, tissue remodeling is evident with granulation-like tissue obstructing the lumen. The major advantages of the model are its reproducibility, technical simplicity, and gross similarity to the human disease pathology. However, there are major disadvantages. Unlike in humans, the allograft is subjected to immediate tissue ischemia (depending on diffusion from the surrounding extrapulmonary environment), is no longer a functioning conduit for ambient air, and is removed from the influence of the pulmonary-specific milieu.

Orthotopic tracheal transplantation overcame the disadvantages of heterotopic transplantation in that a section of a donor trachea surgically replaces the trachea of an allogenic recipient. This allows the allograft to remain an integral part of the airway. Disadvantages of this model are that it is technically very difficult, and BO development

is less reproducible [19]. In contrast to the heterotopic model, the majority of othotopic transplants does not develop BO, or develops a less severe BO [36]. Further investigation revealed that the allografts were reepithelialized with recipient-derived epithelium, preventing immune-mediated epithelial cell death. Restoration of the epithelial barrier was enough to prevent BO. This model demonstrates the critical importance of epithelial integrity in the pathogenesis of BO.

BO lesions have also been reported in an orthotopic bone marrow transplantation model. This model involves lethally irradiating mice, then transferring back bone marrow cells back with or without spleenic T cells. Two months post transplant, 15-50% of mice showed evidence of BO. This model is also dependent on alloimmune mechanisms. However, such low frequencies of BO development would require large cohorts of mice to ensure statistical significance of findings, decreasing its feasibility for testing therapeutics.

Non-transplant models of BO include the administration of toxins, many of which arose from clinical findings in humans who were accidently exposed to various irritants that resulted in BO. For instance, the chemical papaverine was implicated in the development of BO in a cohort of humans after they consumed raw plants that contained high levels of the compound [42]. Intratracheal installation of papaverine in rats led to BO development by 4 weeks post exposure [43]. Human clinical observations have led to similar BO models using chronic aspiration of gastric fluid in rats, oral administration of oleic acid in dogs, intratracheal installation of diacetyl in rats, and toxic gas inhalation in mice [10, 22, 44, 45]. Commonly reported events preceding BO development include epithelial damage, sometimes to the extent of denudation, and increased inflammatory cell infiltration into the airways. The major advantages of non-transplant models of BO are their technical simplicity, the airways remain functional and

exposed to the pulmonary milieu, and BO pathogenesis, especially fibrotic responses, can be studied in the absence of robust alloimmune responses. However, most of the studies characterizing these models were highly descriptive, with a major focus on late-stage BO identification. The studies lacked comprehensive analysis of early events that contribute to BO pathogenesis.

1.4 Chlorine: an industrial commodity and a pulmonary toxicant

Inhalation of toxic chemicals, such as Cl_2, can result in mild to severe lung dysfunction or even death[46]. Cl_2 is one of the top manufactured toxic gases in the world and is primarily used in the production of industrial products. The U.S. produces around 15 million tons of Cl_2 each year [47]. Typically, Cl_2 is transported and stored in large quantities, making spills and ruptures of Cl_2 containers a potential risk to nearby residential areas[47]. In one instance, a train derailed in Graniteville South Carolina, releasing 42-60 tons of Cl_2 gas. Nine exposure victims died, and 71 victims were hospitalized[48]. The most common exposures occur as occupational hazards or when mixing common household cleaners[49, 50]. Besides accidental exposures, Cl_2 gas was and is currently utilized in warfare and terrorism[47, 51]. As a result of its easy accessibility and toxicity, the U.S. government listed Cl_2 gas as a likely chemical agent for use in chemical attacks, making development of therapeutics for Cl_2 gas inhalation of great importance[52].

Direct mechanisms by which Cl_2 causes lung injury are better understood than indirect mechanisms. Cl_2 is a water-soluble greenish-yellow gas that preferentially dissolves into the upper airways where it depletes anti-oxidants then generates reactive intermediates (HOCl and OCl-) and chloromines. These toxic agents damage and disable proteins, inhibit Na^+-dependent fluid clearance, and increase epithelium permeability and death[53, 54]. Anti-oxidant treatments were shown to successfully curtail the

chlorination of biological molecules by inhibiting the generation of Cl_2 intermediates and thus mitigating direct mechanisms of Cl_2 injury[55]. Indirect mechanisms are not clearly understood, but studies have highlighted the importance of inducible nitric oxide synthase (NOS2, an enzyme known to catalyze copious amounts of nitric oxide). The role of NOS2 in Cl_2 injury will be discussed in greater detail in Chapter 4.

In humans, predominant physiological responses to Cl_2 gas inhalation are wheezing, dyspnea, increased airway hyperreactivity (AHR) and hypoxia that, short-term, are consistent with acute lung injury and, long-term, can develop into reactive airways dysfunction syndrome (RADS) [47, 48]. Immediate medical treatment for Cl_2 exposure focuses on decontamination and alleviating symptoms instead of directly combating pathologic causes. Supportive care includes oxygen support and bronchodilators to control airway constriction[56]. The majority of exposure victims have transient lung abnormalities that return to normal within a few days or weeks after exposure,[50, 56] but there are studies that report persistent declines in lung function in a portion of exposure victims. A study by Schwartz et al. followed 13 construction workers who were accidentally exposed to Cl_2 gas. Twelve years after exposure, 5 of the 13 workers exhibited persistent elevated AHR[57]. Another study by Bherer et al. evaluated 71 workers who had been repeatedly exposed to Cl_2 over the span of several months. Eighteen to 24 months post exposure, 41% of the workers exhibited elevated AHR[58].

In sum, as a leading industrial commodity, Cl_2 contributes greatly to the health and convenience of modern society. It is used in the production of plastics, paper, and other goods, and its strong disinfecting properties are employed as a major method of water purification. Such ubiquitous handling of Cl_2 mutually increases the potential of

occupational and domestic exposures. Further research is required to identify and develop therapeutics that target specific mechanisms of Cl_2-induced airway injury.

2. Loss of basal cells precedes bronchiolitis obliterans-like pathological changes in a murine model of chlorine gas inhalation

2.1 Introduction

The exact pathogenesis of BO remains unclear. As mentioned above, potential contributing factors include innate and adaptive immune responses, tissue ischemia, and chronic epithelial cell injury [37, 59-61]. Specifically, epithelial injury is a common feature of almost all human instances and animal models of toxic chemical inhalation associated with the development of BO, supporting the view that epithelial damage is a critical factor in the pathogenesis of BO. However, evidence suggests that epithelial injury *per se* is not sufficient for the development of BO. Some animal models demonstrate widespread death of epithelial cells, but repair normally with no evidence of fibrotic lesion development. In animal models that display obliterative airway lesions, both the frequency and the anatomic distribution of these lesions is much less than the extent of epithelial damage. These findings suggest that some factor beyond acute epithelial cell injury is required for the development of BO. We previously mentioned 4 degrees of epithelial injury, the last of which kills epithelial progenitor cells called basal cells. We hypothesized that basal cell death is the critical factor that initiates BO pathogenesis.

Here, we describe a novel murine model in which obliterative airway lesions with the pathologic appearance of proliferative BO rapidly develop in the tracheas and primary bronchi of mice exposed to high doses of Cl_2 gas. The sequence of cellular events that occurs during the development of these obliterative airway lesions includes epithelial cell death, failure of re-epithelialization, inflammatory cell infiltration, fibroblast infiltration, collagen deposition, and angiogenesis, ultimately leading to lethal

airway obstruction within 10 days. Moreover, in a comparison of different doses of Cl_2 exposure, we determined that the BO lesions only develop under conditions and in areas in which basal cells are eliminated by toxic gas exposure. In the absence of basal cells, epithelial regeneration does not occur and regions of epithelial denudation persist, from which an aberrant repair process is initiated that leads to obliterative airway lesions. Our findings suggest that, irrespective of the cause, loss of epithelial progenitor cells may be a critical factor leading to the development of BO. Results in this chapter have been reprinted with permission of the American Thoracic Society[10].

2.2 Materials and methods

Mice and survival studies. Mice were 8-9 week-old C57Bl/6 females, purchased from Charles River Laboratories (Wilmington, MA). CX3CR1$^{GFP/GFP}$ mice were provided by D. Littman (New York University, New York, NY) and crossed with C57Bl/6 mice to produce CX3CR1$^{+/GFP}$ mice. All animal experiments were conducted in accordance with National Institutes of Health guidelines and protocols approved by the Animal Care and Use Committee at Duke University.

Chlorine exposure. 1% percent Cl_2 in nitrogen was purchased from Airgas National Welders (Research Triangle Park, NC). Mice were placed within individual holders and exposed for a 30 minute duration to Cl_2 (Airgas National Welders, 1% Cl_2 in nitrogen) or filtered air (FA) via a nose-only inhalation chamber (Figure 1). Cl_2 concentrations within the chamber were regulated upstream by mixing 1% Cl_2 gas into filtered air and were calibrated to deliver Cl_2 concentrations specifically between 175 to 350 ppm. Control mice were exposed to FA under the same experimental conditions of temperature and relative humidity. After exposure, mice were returned to vivarium housing and monitored during recovery periods ranging between 1-14 days.

Histology and immunofluorescence. For trachea dissection, the airways were exposed via a midline incision through the skin and peritoneum extending through the rib cage and up to the epiglottis. The trachea was exposed, and the rib cage was opened along the midline of the sternum. The heart was removed; then the airway-esophagus combination was removed and cut free below the epiglottis. The tissue was washed briefly in PBS to remove blood. The esophagus and lung tissue were separated from the trachea. To remove air bubbles, PBS was gently pushed though the remaining airway with a 23 gauge needle and 3 ml syringe. Tracheas were fixed in 4% paraformaldyhde for 3 hours at 4 degrees C. For paraffin sections, tissues underwent PBS washing, alcohol dehydration, xylene clearing and paraffin embedding. Sections were cut 8μm thick and then stained with hematoxylin and eosin (H&E). For frozen sections, tissues were washed with PBS several times then washed in 15% and 30% sucrose, respectively, for 1 hour. Tissues were left overnight in half 30% sucrose, half OCT at 4 degrees C then embedded into OCT. Tracheas were serially cut into 12μm thick cross sections, proximally to distally. Frozen tissues were stained with H&E or the primary anti-bodies: rabbit anti-cytokeratin 5 (Covance, Emeryville, CA), rat anti-e-cadherin (Zymed/Invitrogen, Grand Island, NY), rat anti-CD31 (BD Pharmingen, San Jose, CA), rat biotinylated anti-CD11b (Biolegend, San Diego, CA), rabbit biotinylated anti-collagen I (Rockland, Gilbertsville, PA). Fluorescence-conjugated secondary antibodies were all from Molecular Probe/Invitrogen (Grand Island, NY). Images were taken with an inverted confocal laser scanning microscope (Zeiss LSM 510; Carl Zeiss, Jena, Germany). To maintain high resolution of complete tracheal rings, multiple images of tracheal sections were taken at low magnification and then layered to create a composite image. In some composites, peritracheal tissues were omitted.

Quantification of epithelium. The length and thickness of tracheal epithelium was measured in photomicrographs of distal tracheal sections using the ruler function on the Zeiss LSM image browser. All analyzed tracheal sections were cut from the distal trachea. For the quantification of % epithelialized circumference on day 5 post Cl_2, the total distance of tracheal circumference that stained positive for e-cadherin or cytokeratin 5 was divided by the total tracheal circumference as measured along the basal lamina. Epithelial thickness was measured at 200μm intervals around the total length of e-cadherin$^+$ or cytokeratin 5$^+$ epithelium in each transverse tracheal section. Areas of denuded epithelium were not included in thickness quantification.

Sulfosuccinimidobiotin tracheal labeling. Mice were restrained and nose-only exposed to either 200 or 350 ppm Cl_2 for 30 minutes. On day 4 after exposure, mice were anesthetized by ketamine (100 mg/kg)/xylazine (10 mg/kg) i.p. and then given 0.25mg of EZ-Link Sulfo-NHS-Biotin, No-Weigh Format (Sulfo-NHS-Biotin) (Pierce Biotechnology, Rockford, IL, USA) intranasally in a total of 30ul. Immediately before administration, Sulfo-NHS-Biotin was reconstituted with molecular grade water. Tracheas were harvested either 4 hours or 3 days after Sulfo-NHS-Biotin administration (corresponding to day 4 or day 7 post Cl_2 exposure, respectively). Tracheas were processed as frozen sections then stained, and imaged as described above.

For quantification of subepithelial Sulfo-NHS-Biotin staining, one cross section per trachea (from the distal region) was analyzed using the Zeiss LSM image browser. The length of biotin staining was defined as the length of the basal lamina under which consecutive biotin staining was present. Non-consecutive biotin stains in the same tracheal cross section were counted as independent stains. The length of lesions was defined as the length of the basal lamina along which intraluminal lesion was present.

Tracheal cell isolation and flow cytometric analysis. Tracheas were dissected (same as stated above), cleaned of surrounding connective tissue, cut into several smaller pieces and then digested for 40 minutes in media containing: 1.5 mg/ml collagenase, .4 mg/ml DNase I, 5% FBS and 10mM HEPES in HBSS. Tissues were gently vortexed every 10 minutes during incubation. The disassociated tissue was strained through a 70μm cell strainer. Cells were washed with PBS then counted, 1.0-5.0 x 10^6 cells were stained in PBS with Live/Dead Aqua (Molecular Probes). Cells were washed then blocked for 10 minutes at 4 degrees C in a blocking buffer: 10 mM EDTA, 1% BSA, 5% normal mouse serum, 5% normal rat serum, and 1% Fc block (eBioscience, San Diego, CA) in PBS. Cells were stained with antibodies for 30 minutes, total volume 100ul, then washed three times and analyzed using a BD LSRII flow cytometer (BD Pharmingen, San Jose, CA). Antibodies used included: CD45-Qdot605, CD31-eflour450, and Ly6G-AF700 from eBioscience and CD11b-PE-Cy7, Ly6C-V450 from BD Pharmingen (BD Pharmingen, San Jose, CA)). Although cells were stained with CD31 and Ly6C, neither of these markers were used for specific gating. Neutrophils were gated on singlets, $CD11b^+$, $Ly6G^+$ cells. Non-neutrophil myeloid cells were gated on singlets, $CD11b^+$, $Ly6G^-$ cells.

Statistics. Numerical data are presented as mean, mean ± SD, or mean ± SEM, as indicated in the figure legends. The comparison between survival curves was performed with the log-rank test using GraphPad Prism software (GraphPad, San Diego, CA). All data are analyzed by Student's *t* tests using Prism software, as indicated in the figure legends. Pearson correlation coefficients were generated using Prism software.

2.3 Results

2.3.1 Obliterative airway lesions develop in mice exposed to high dose Cl_2

We developed a model of Cl_2-induced lung injury in which up to six mice can be simultaneously exposed to a given concentration of Cl_2 gas by nose-only inhalation (Figure 1). In preliminary dose-ranging studies, we determined that exposure to 175-250 ppm Cl_2 for 30 minutes results in minimal acute mortality. However, during our studies, we observed that a small number of mice exposed to Cl_2 appeared to symptomatically recover from the acute effects of Cl_2, but then developed severe respiratory distress requiring euthanasia on days 6-12. A similar unexplained late mortality in Cl_2-exposed mice has been described previously [62]. To further explore this phenomenon, mice were exposed to a higher dose of Cl_2 (350ppm for 30 min). Rather than recover, 75% of mice exposed to 350ppm Cl_2 develop a distinct pattern of labored breathing between days 6-12 which progresses to severe respiratory distress requiring euthanasia within 24 hours (Figure 2A). In comparison, only 16% of mice exposed to 200ppm Cl_2 require euthanasia (Figure 2A). On pathological examination, all of the mice that develop labored breathing display grossly visible obliterative airway lesions. These lesions occur most commonly in the lower third of the trachea and in the main stem bronchi and have the appearance of granulation tissue. In transverse histological sections of the tracheas, obliterative airway lesions occlude greater than 80% of the airway lumen (Figure 2B). These obliterative lesions contain both connective tissue and inflammatory cells and display incomplete epithelial coverage at the lesion/airway interface (Figure 2C). Overall, the cellular composition and appearance of these lesions closely resemble the histopathology of human proliferative BO lesions [63].

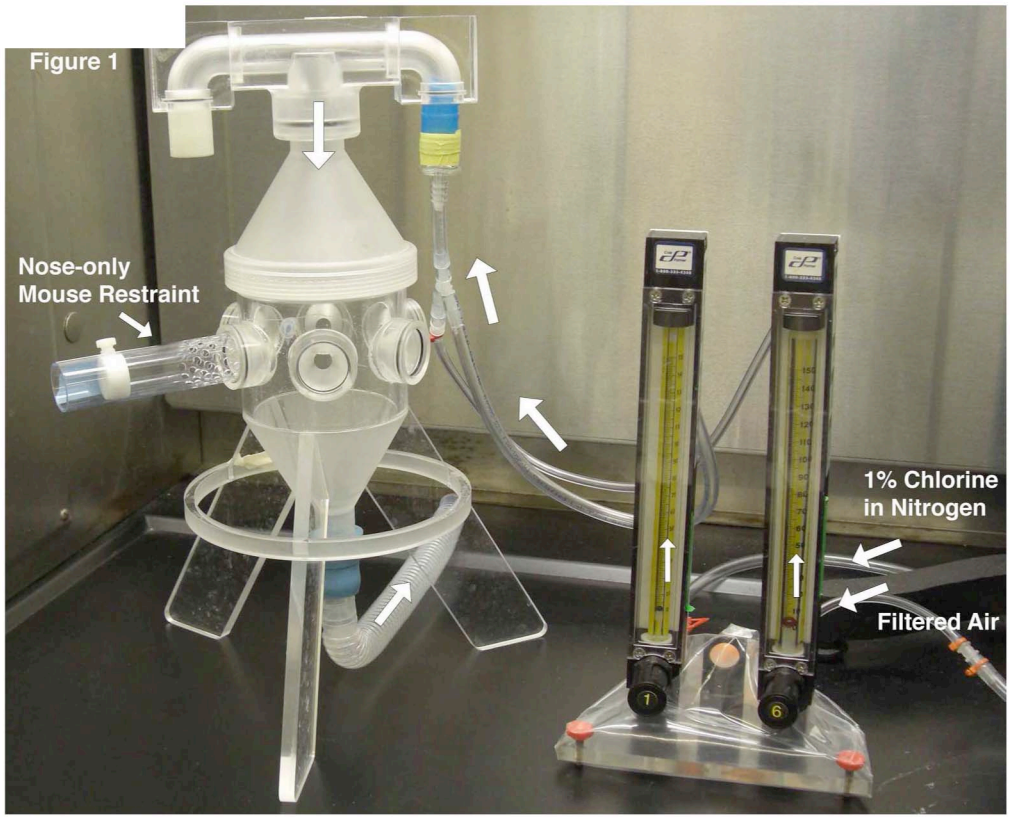

Figure 1: Nose-only restraints and exposure apparatus.

Mice were individually restrained in tubes that were specially designed such that the nose of the mouse protrudes from the tube. The nose-only mouse restraints fit securely into one of six available holders that access the interior of the exposure chamber. When properly loaded, only the mouse's nose protrudes into the exposure chamber. Gas flow into the chamber is regulated by Cole Palmer flow meters. Filtered air runs through the first flow meter at 4 L/min. 1% Cl_2 balanced in nitrogen runs through the second flow meter at varied rates. The output from the regulators are mixed just prior to entering the top of the exposure chamber. The bottom of the exposure chamber is vented into the fume hood exhaust.

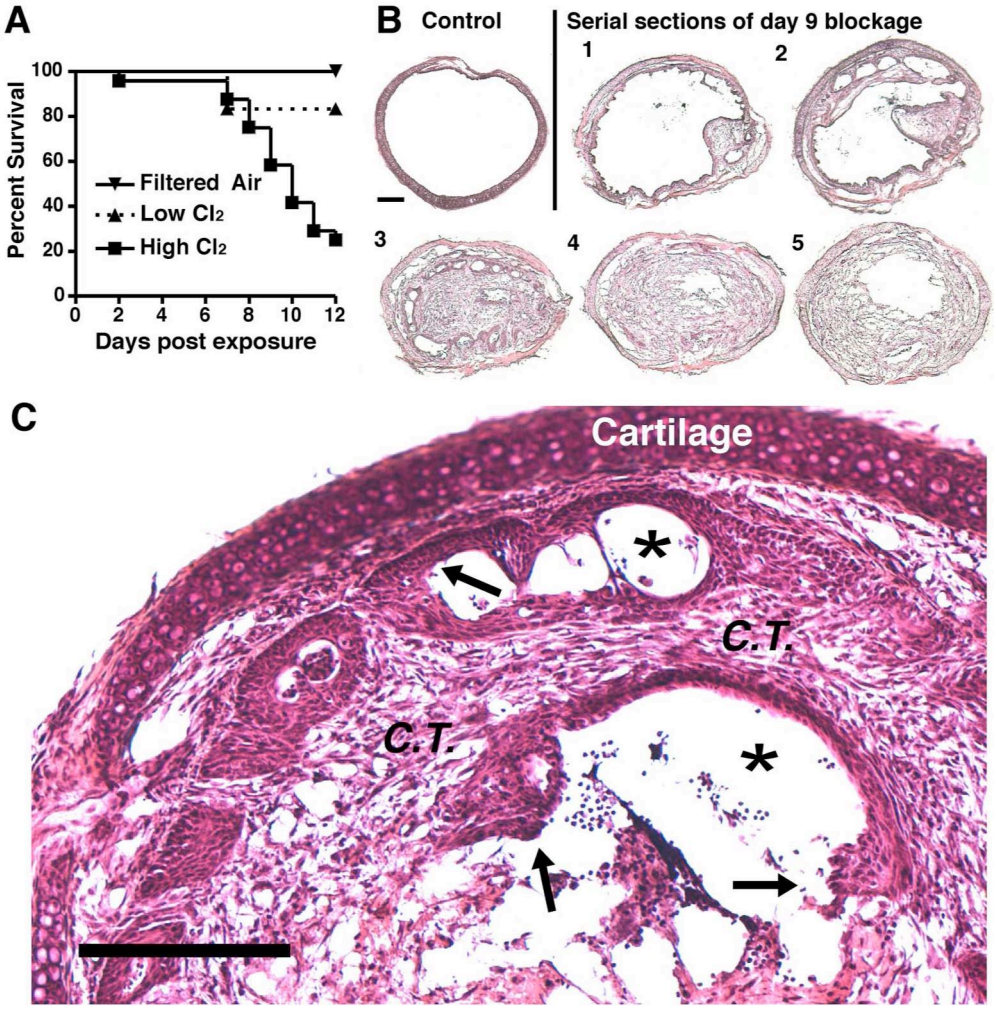

Figure 2: High concentrations of Cl_2 induce lethal obliterative airway lesions.

A) Survival after exposure to filtered air (n=3 mice), low dose Cl_2 (200ppm, n=6), or high dose Cl_2 (350ppm, n=24). p=.0337 between high and low dose survival curves by log-rank test. B) Transverse sections from an unexposed trachea and a mouse euthanized 9 days after high dose Cl_2. Sections 1-5 indicate order of sections, anterior to posterior. Sections are representative of 16 tracheas similarly examined. Scale bar is 200μm. C) Day 9 blockage exhibiting abnormal re-epithelialization (arrows), connective tissue (*C.T.*) invasion and nearly complete occlusion of the lumen (asterisk). Scale bar is 200μm.

2.3.2 Lesion formation coincides with basal cell but not luminal epithelial cell death

To determine if the increased frequency of obliterative airway lesions in mice exposed to 350ppm Cl_2 is due to more severe epithelial injury in these animals, we compared the fate of airway epithelium in mice exposed to low (200 ppm) and high (350 ppm) Cl_2. Three hours after low dose Cl_2 exposure, tracheas display large regions in which luminal epithelial cells (ciliated and Clara cells) are necrotic and are beginning to slough off (Figure 3B,H). By 24 hours, the necrotic epithelium sloughs off, revealing a thin layer of simple squamous cells (Figure 3C,I). In contrast, 3 hours post high dose Cl_2 exposure, many regions contain luminal epithelial cells that are swollen and lack cilia but remain attached to the tracheal wall (Figure 3H,K). By 24 hours, the epithelium is still attached but is clearly necrotic; it displays widespread cellular swelling and loss of nuclei (Figure 3E,L). Over the next 10 days, the great majority of mice exposed to low dose Cl_2 display complete epithelial repair with no evidence of fibrotic lesions (data not shown), while mice exposed to high dose Cl_2 develop obliterative airway lesions.

These findings suggest that acute epithelial damage alone is not sufficient to induce obliterative airway lesions. This view is consistent with our findings in a different model of toxic chemical exposure, SO_2 inhalation, which we have previously described in detail [1, 4]. As with 200 ppm Cl_2, mice exposed to SO_2 display widespread luminal epithelial necrosis, sloughing of epithelium revealing a layer of simple squamous cells, and complete epithelial repair after 14 days, with no evidence of obliterative lesion formation [4]. In this model, we observed that tracheal basal cells survive SO_2 exposure, proliferate, and give rise to relatively large patches of descendants that include both Clara and ciliated cells, thus acting as the progenitor cells for tracheal

epithelium after chemical injury. Recent evidence suggests that basal cells also act as the progenitor cells for epithelial repair after Cl_2 inhalation [64].

To determine if the differences in epithelial repair we observe in mice exposed to low versus high doses of Cl_2 are due to differences in basal cell survival, we examined tracheas for the presence of basal cells after low and high dose Cl_2 exposure. Immunohistochemical staining with anti-e-cadherin marks both luminal epithelial and basal cells. To specifically identify basal cells we co-stained with anti-cytokeratin 5, a basal cell-specific marker. Our analysis demonstrates that basal cells remain viable and present in normal numbers, relative to unexposed mice, after low dose Cl_2 exposure (Figure 3G,J). In these sections, most of the mature columnar, luminal epithelium (e-cadherin$^+$ cytokeratin 5$^-$) is absent and the epithelium replacing it consists primarily of basal cells (e-cadherin$^+$, cytokeratin 5$^+$). In contrast, mice exposed to high dose Cl_2 display numerous large areas of trachea that are completely devoid of cytokeratin 5$^+$ basal cells (Figure 3M). The epithelial cells in these regions remain attached, are swollen, and display faint e-cadherin$^+$ staining, but no longer have nuclei at 24 hours post injury (Figure 3L). These findings strongly suggest that the chemical-induced loss of basal cells is a critical event in the course of toxin exposure. It is known that if basal cells remain viable, they can serve as a source of progenitor cells for rapid epithelial repair. Here, we propose that in the absence of basal cells, re-epithelialization does not occur and a fibrotic response is initiated.

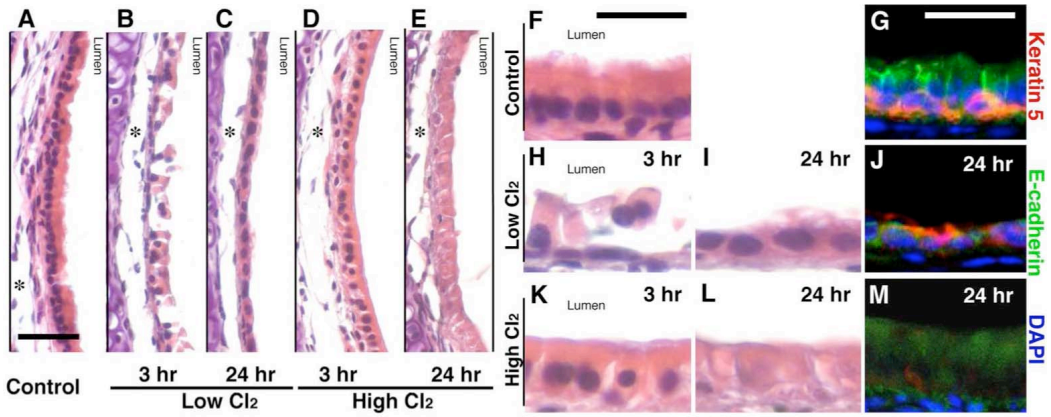

Figure 3: Exposure to high Cl_2 results in basal cell death.

Photomicrographs of H&E-stained tracheas from unexposed mouse (A,F); after low dose Cl_2; 3 hrs (B,H), 24 hrs (C,I); or after high dose Cl_2; 3 hrs (D,K), 24 hrs (E,L). Immunofluorescent staining of: uninjured trachea (G), 24 hrs after low (J) and high (M) dose Cl_2. E-cadherin (green), cytokeratin 5 (red), DAPI (blue). Panels are representative of 5-6 tracheas at each time. Scale bar is 20μm for A-E and 25μm for F-M. Asterisks denote a fixation artifact.

2.3.3 Basal cell loss correlates with reduced tracheal re-epithelialization

To determine the consequences of basal cell loss on epithelial repair, inflammation, and fibrosis, we examined the time course of these events in mice exposed to low and high dose Cl_2. In general, normal epithelial repair is thought to occur in three stages [12, 13, 65]. First, basal cells spread and migrate to cover denuded epithelium. Second, these cells proliferate, with self-renewing basal cells remaining near the basal lamina and daughter cells forming upper layers of transitory squamous metaplasia. Lastly, the upper layers remodel to form a pseudostratified layer of mature, differentiated mucociliary epithelium.

By day 5 after Cl_2 exposure, it is clear that low and high dose Cl_2-exposed tracheas undergo markedly different rates of epithelial repair. After low dose Cl_2 exposure, the entire trachea is reepithelialized; the thickened e-cadherin$^+$ luminal epithelium with basal cells (e-cadherin$^+$ cytokeratin 5$^+$) residing near the basal lamina is characteristic of the second phase of epithelial repair (Figure 4A). There is no evidence of cellular migration into the lumen. In contrast, by day 5 after high dose Cl_2 exposure, necrotic epithelium is no longer attached to the airway wall, but, on average, 49% of the tracheal circumference lacks both mature epithelium and basal cells, as indicated by the absence of e-cadherin and cytokeratin 5 staining (Figure 4B, insets 4 and 6, 4F). In those areas that do contain epithelium, this consists of a single layer of cells, some of which are cytokeratin 5$^+$, indicating the presence of basal cells (Figure 4B, insets 3 and 5). On average, the epithelium is 50% less thick than after low dose Cl_2 exposure (Figure 4E). These observations suggest that even in areas where basal cells survive, their decreased numbers significantly retard epithelial repair. In large areas of epithelial necrosis caused

by high dose Cl_2, the basal lamina is exposed to the lumen, whereas after low dose Cl_2 exposure, it is covered by regenerating epithelium (Figure 4C,D). In addition, by day 3 after high dose Cl_2 exposure, the necrotic epithelium that initially remained adherent to the tracheal wall becomes displaced into the lumen where it is retained as a mass of necrotic cells (Figure 4D).

By day 7 after low Cl_2 exposure, the trachea remains fully epithelialized. Most of the transitory squamous metaplasia has remodeled into normal pseudostratified epithelium (Figure 4G,I). In contrast, after high Cl_2, the epithelium forms disorganized patches, varying in stages of repair (Figure 4H,J). In some areas, connective tissue has fused with the trachea wall, preventing re-epithelialization of the original basal lamina. Additionally, the epithelium has begun surrounding the invading connective tissue in places, but there are still denuded areas where obliterative lesions interface directly with airspace.

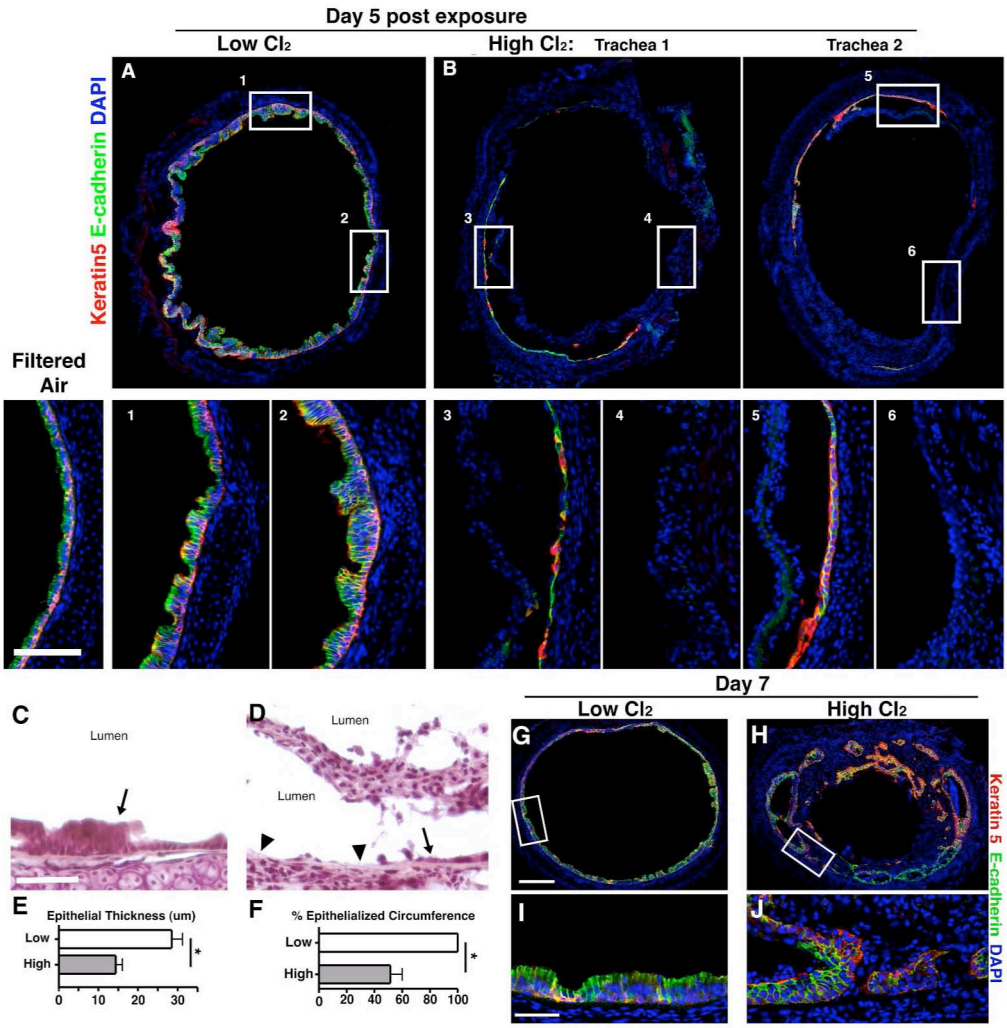

Figure 4: Basal cell loss results in aberrant re-epithelialization.

Immunofluorescent staining of epithelium 5 days after low (A) or high (B) dose Cl_2. Two individual tracheas are shown in B. Boxed areas in top row are magnified in the bottom row and correspond by number. E-cadherin (green), cytokeratin 5 (red), DAPI (blue). Scale bar is 200μm. H&E staining of epithelium 5 days after low (C) or high (D) dose Cl_2. Epithelium is denoted by black arrows and denuded epithelium by arrowheads. Scale bar is 50μm. Quantification of % epithelialized tracheal circumference (E) and epithelial thickness (F) 5 days after exposure to low or high dose Cl_2 (n=3; *, $p<0.05$ by student's t test, data are presented as mean ± SEM). Immunofluorescent staining of epithelium 7 days after low (G,I) or high (H,J) dose Cl_2. Scale bar is 200μm for G and H. Scale bar is 25μm for I and J. All panels are representative of 5-6 tracheas at each time.

2.3.4 Obliterative lesions originate from areas of denuded epithelium

While the above findings demonstrate an overall association between the occurrence of epithelial denudation and the formation of obliterative airway lesions, they do not directly demonstrate that obliterative lesions arise from areas of epithelial denudation. To address this issue, we developed a technique that would allow us to track the fate of individual lesions in individual animals. To label areas of epithelial denudation, we administered sulfosuccinimidobiotin (Sulfo-NHS-biotin) to mice intranasally 4 days after low or high dose Cl_2 exposure. Sulfo-NHS-biotin is comprised of esters of biotin that are highly reactive, cell impermeable, and form stable amide bonds with primary amines found on the surfaces of living and non-living organic material [66]. To confirm that this technique specifically labels areas of epithelial denudation, tracheas were harvested 4 hours after Sulfo-NHS-biotin administration (on post exposure day 4) and stained with anti-e-cadherin and streptavidin to localize intact epithelium and covalent biotin attachment, respectively.

All tracheas harvested 4 hours after Sulfo-NHS-biotin administration demonstrate uniform staining for biotin on epithelial surfaces. In addition, there is biotin staining of exposed basement membrane areas and/or subepithelial connective tissue that is highly dependent on the presence and extent of epithelial denudation. Tracheas with no visible epithelial denudation typically display one or more small areas of subepithelial biotin staining (Figure 5A) whose total length averages 390 ± 281μm (Figure 5E). In contrast, tracheas with visible regions of epithelial denudation typically display one large area of subepithelial biotin staining (Figure 5B) whose total length averages 2411 ± 1070 μm (Figure 5E). The length of subepithelial staining in individual mice closely correlates with the length of associated epithelial denudation (Figure 5F, r =

0.920, $p < 0.0001$). Moreover, the length of this subepithelial staining, when measured from the center of epithelial denudation, either equals or slightly exceeds the length of epithelial denudation (Figure 5G). These results demonstrate that Sulfo-NHS-biotin staining accurately labels the extent and position of epithelial denudation.

To determine if obliterative airway lesions arise from areas of epithelial denudation in individual mice, a separate study was performed in which mice were exposed as before to low or high dose Cl_2, and then administered Sulfo-NHS-Biotin after 4 days. In these studies, however, the tracheas were harvested 3 days later rather than at 4 hours to allow time for repair or lesion formation. In these samples, surface staining of airway epithelial cells was not detected, probably due to membrane turnover of labeled live cells, but areas of subepithelial staining remained visible. No intraluminal lesions were found in sections that contained less than 300μm of subepithelial staining, suggesting that the development of such lesions requires a certain amount of epithelial denudation (Figure 5H). In contrast, all sections with >300μm of subepithelial staining contained intraluminal lesions. In individual mice, the length of tracheal wall covered by intraluminal lesions closely correlates with the length of subepithelial staining (Figure 5 I, $r = 0.995$, $p<0.0001$). Lesions, when measured from the center of biotin staining, typically equal or slightly exceed the length of the associated biotin stain (Figure 5 J). These findings demonstrate that intraluminal lesions arise from areas of epithelial denudation and suggest that the size of intraluminal lesions is determined by the extent of epithelial denudation.

We also graphed the data points in Figures 5E and H in a manner that reflects the exposure group from which each data point was generated (Figure 6). Data points representing short lengths of biotin staining and associated with no visible denudation or lesions were primarily generated after exposure to low Cl_2. In contrast, data points

representing long lengths of biotin staining and associated with visible denudation or lesions were primarily generated after exposure to high Cl_2.

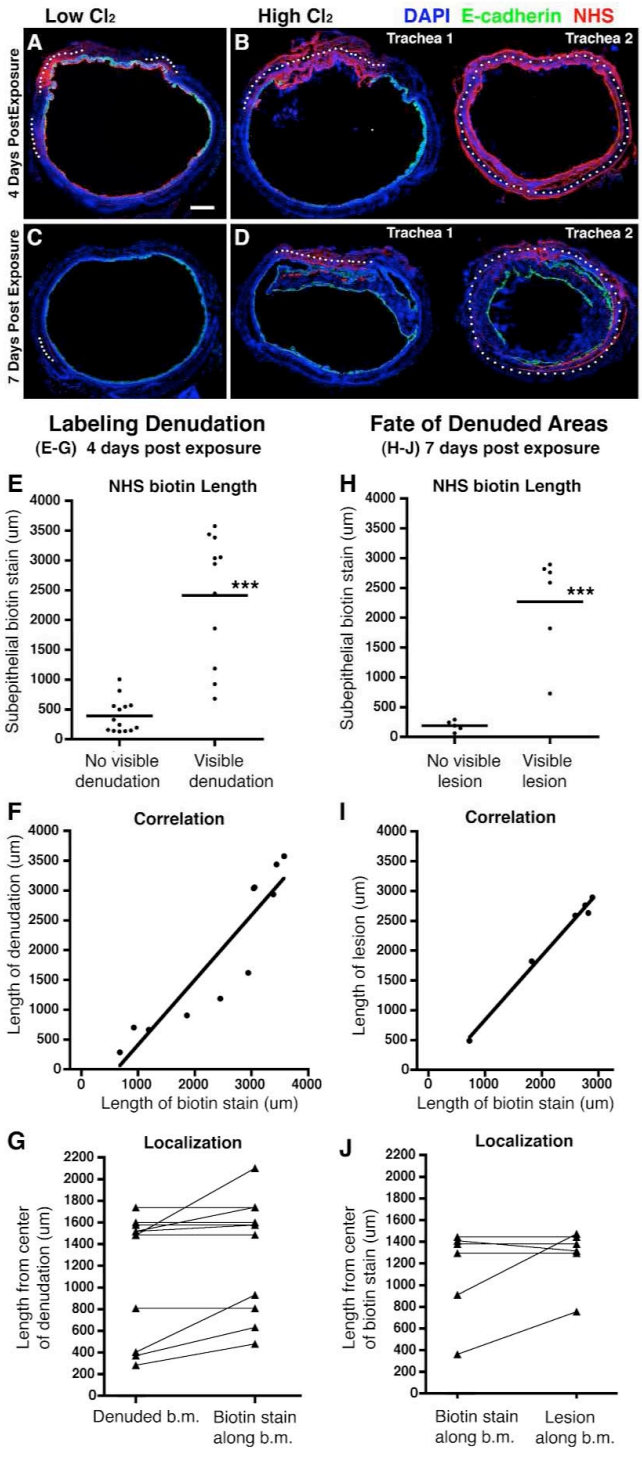

Figure 5: Tracheal blockages originate from areas of denuded epithelium.

Mice were exposed to low or high dose Cl_2 then intranasally given the labeling agent Sulfo-NHS-biotin 4 days post exposure. (A and B) Immunofluorescent staining of e-cadherin and biotin 4 hours after administration of NHS-biotin in mice that were exposed to low or high dose Cl_2. Images are representative of multiple tracheas; low Cl_2 n=5 and high Cl_2 n=10 (2 examples are shown in B). (C and D) Immunofluorescent staining of e-cadherin and biotin 3 days after biotin labeling (7 days post exposure to low or high dose Cl_2). Images are representative of multiple tracheas; low Cl_2 n=3 and high Cl_2 n=7 (2 examples are shown in D). Scale bar is 200μm. White dots mark regions of subepithelial biotin staining. The lengths of these regions was measured along the basement membrane (b.m.) for quantitation. (E) The length of subepithelial biotin staining in areas with or without visible denudation. n=15 tracheas ; ***p<.0001 by student t test. (F) Correlation between length of biotin staining and the length of epithelial denudation; r=.920, p<.0001. n=10 tracheas. (G) The length of biotin staining in areas of denuded epithelium was measured from the center of the denuded area outward in each direction. For each data point, the length is an average of the left and right extensions. n=10 tracheas. (H) The length of subepithelial biotin staining in areas with or without visible lesions. n=10 tracheas; ***p<.0001 by student t test. (I) Correlation between length of biotin staining and the length of luminal lesions; r=.995, p<.0001. n=6 tracheas. (J) The length of lesions measured from the center of the associated biotin staining outward in each direction. For each data point, the length is an average of the left and right extensions. n=6 tracheas.

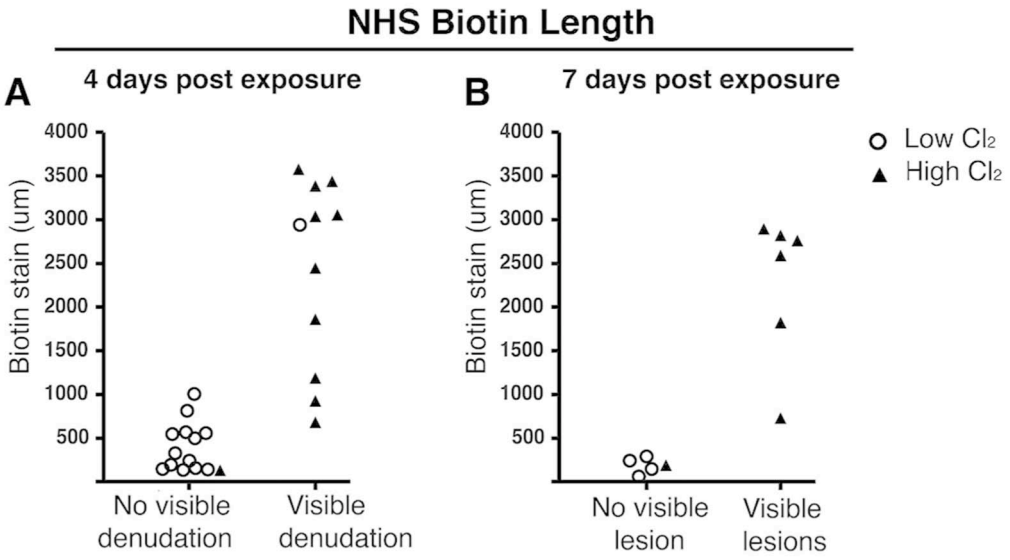

Figure 6: Length of NHS biotin staining by Cl_2 exposure group.

The length of subepithelial biotin staining in areas with or without visible denudation; low Cl_2 n=5 and high Cl_2 n=10. (B) The length of subepithelial biotin staining in areas with or without visible lesion; low Cl_2 n=3 and high Cl_2 n=7.

2.3.5 Inflammatory cell infiltration precedes airway intraluminal fibrosis

To better define the specific cellular events that are associated with the development of intraluminal lesions, we examined the time course of inflammation, collagen production, and vascularization in mice exposed to 350ppm Cl_2. By day 2 after exposure, $CD11b^+$ cells, consisting of both neutrophils and macrophages, begin to infiltrate the dead epithelium (Figure 7A, B). By day 5, infiltration by $CD11b^+$ cells is substantial (Figure 7G), with macrophages (arrowheads) and neutrophils (small arrows) being the predominant cell types (Figure 7E, F). By day 7, myeloid cell infiltrates decrease (Figure 7 I-K) but in many cases reappear when mice develop terminal respiratory distress on or around day 9 (Figure 7 M-O). Higher magnification images of CD11b and collagen I staining are provided in Figure 8.

To quantify these inflammatory cell infiltrates, whole tracheas from mice exposed to low or high dose Cl_2 were digested into single cell suspensions, then subjected to flow cytometric analysis. In mice exposed to low dose Cl_2, numbers of total tracheal cells and monocytes/macrophages ($CD11b^+Ly6G^-$) are significantly increased at day 5 only, with no increase in neutrophils (Figure 7 Q-S). In mice exposed to high dose Cl_2, numbers of total tracheal cells and monocytes/macrophages are significantly increased at all time points and the number of neutrophils significantly increased on days 3 and 7 (Figure 7 Q-S). These findings demonstrate that inflammatory cell infiltration, especially of monocytes/macrophages precedes the development of intraluminal lesions, which are typically observed on day 7 after Cl_2 exposure.

At the time when infiltration of monocytes/macrophages is peaking, around day 5 post-exposure, collagen-producing cells begin to infiltrate the cellular mass (Figure 7 H, white arrows). Once this begins, the deposition of collagen producing fibroblasts and

connective tissue within the airway lesion increases rapidly (Figure 7 F,J,N and H,L,P). Consequently, tracheas can progress from being totally patent to near totally occluded over a period of 4 days (Figure 7 E,I,M).

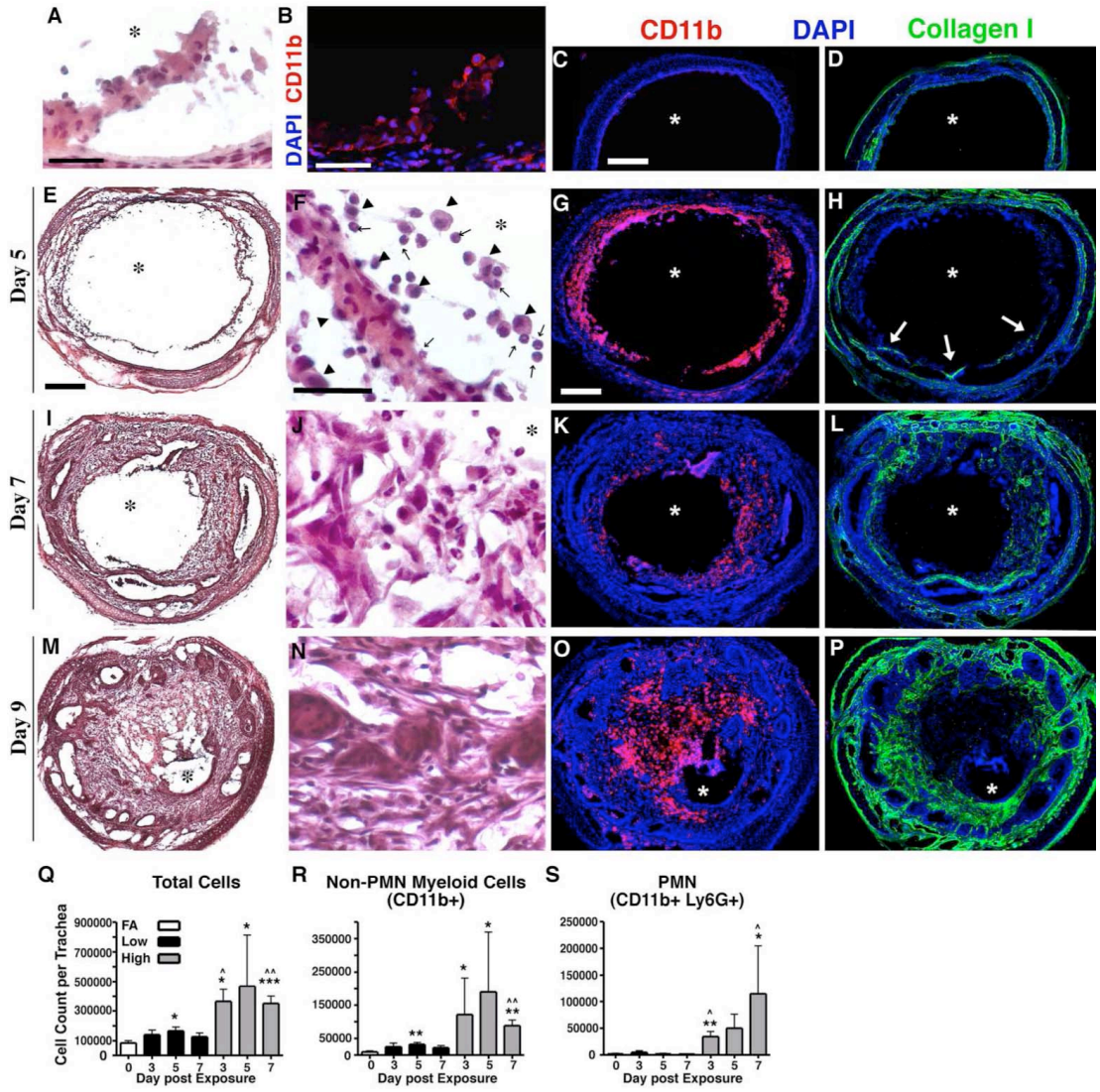

Figure 7: Loss of epithelial integrity results in inflammatory cell infiltration, mesenchyme infiltration, and collagen deposition.

H&E staining of tracheal epithelium 2 days after exposure to high dose Cl_2 (A). Immunofluorescent staining for CD11b (red) in a similar day 2 tissue section (B). In A and B, scale bar is 25μm. Immunofluorescent staining of either CD11b (red) or collagen I (green) in a control tracheal section and sections harvested on day 5, 7 and 9 after high dose Cl_2; CD11b (C,G,K,O respectively); collagen I (D,H,L,P respectively); scale bar is 200μm. In H, white arrows denote collagen 1^+ cells infiltrating the lumen. H&E staining of tracheal sections harvested on days 5, 7 and 9 after high dose Cl_2 (E,I,M respectively; scale bar is 200μm), (magnified images F,J,N respectively; scale bar is 25μm) In F, arrowheads denote macrophages while small arrows denote neutrophils. All tissue sections are representative of 5-6 tracheas at each time. Asterisks denote the lumen. Using flow cytometry, total cells (Q), non-neutrophil CD11b+ cells (R), and neutrophils (S) were quantified from tracheal digests from mice exposed to FA, low, or high dose

Cl_2. Bars represent mean ± SD for 5-8 mice per group. *p<0.05; ** p<0.005;***p<.0001 in comparison to FA by student t test. ^p<0.05; ^^ p<0.005 in comparison to day-matched low dose Cl_2 by student's t test.

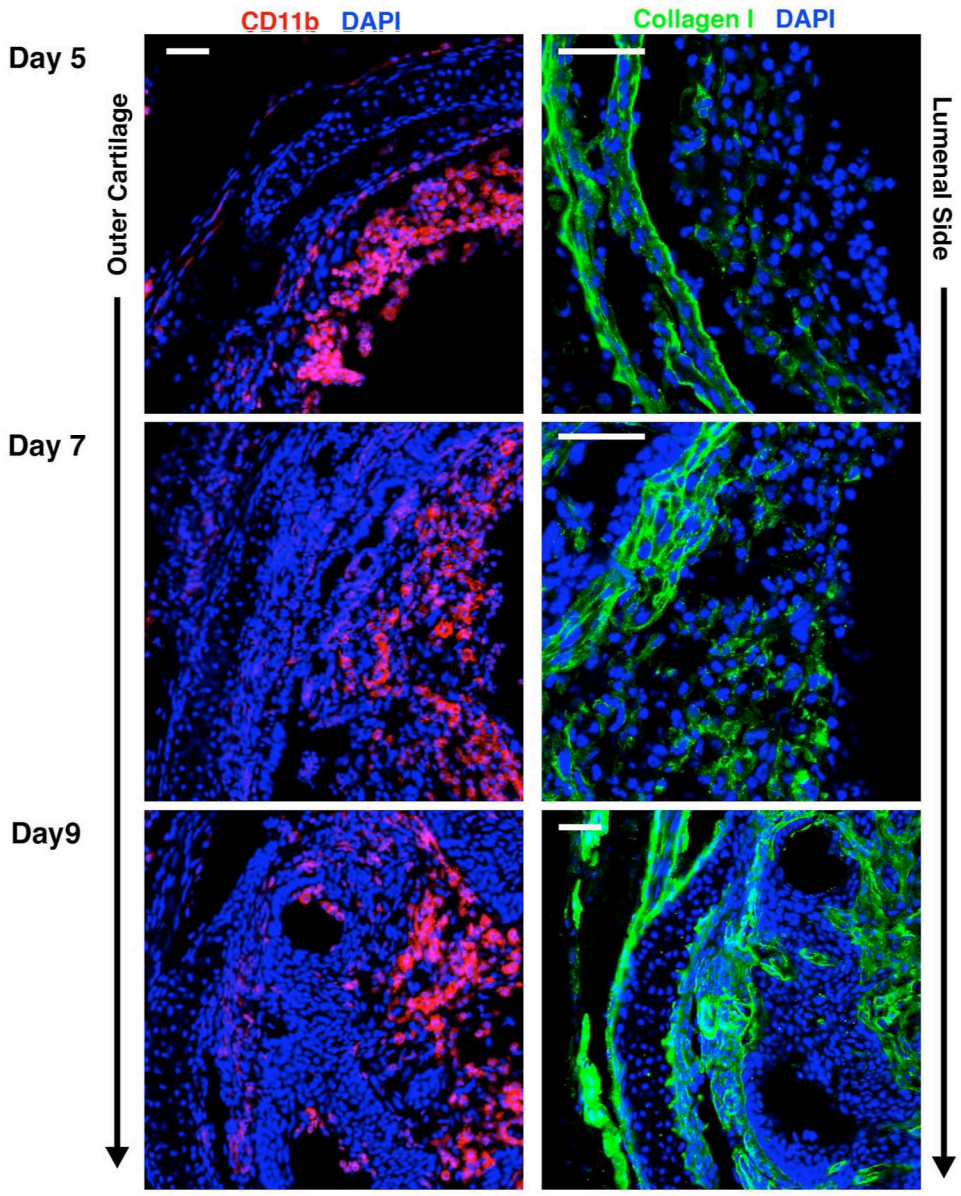

Figure 8: CD11b$^+$ inflammatory infiltrates and collagen I$^+$ infiltrates.

Magnified images of immunofluorescent staining for either CD11b (red) or collagen I (green) in sections harvested on day 5, 7 and 9 after high dose Cl_2; scale bars are 50μm.

2.3.6 Vascularization of obliterative airway lesions is a late event

To determine if vascularization plays a significant role in the development of obliterative airway lesions, we performed immunohistochemistry for the endothelial cell (EC) marker PECAM-1 on tissue sections over the course of lesion development. Prior to exposure, tracheal blood vessels lie just below the basal lamina (Figure 9A). EC remain in this position though day 5 post Cl_2 exposure (Figure 9 B,C). By day 7, EC begin to penetrate the basal lamina into the developing obliterative lesions (Figure 9 D,E arrows). This corresponds to the time of rapidly increasing cellularity within obliterative lesions. By day 9, obliterative airway lesions are highly vascularized (Figure 9F). These findings suggest that vascularization does not play a role in the initiation of obliterative airway lesions.

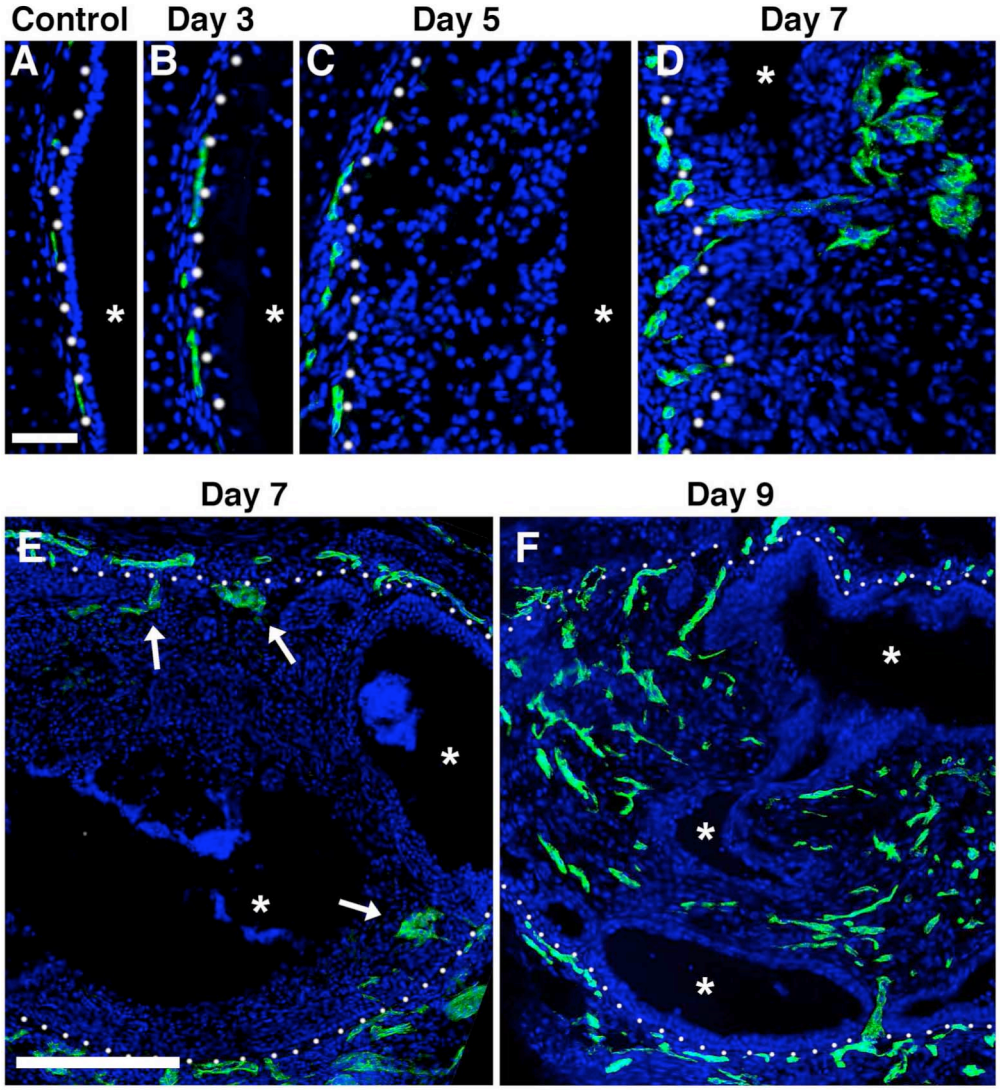

Figure 9: Vascularization of tracheal blockages.

Immunofluorescent staining of endothelial cells (PECAM-1, green) in an uninjured trachea and tracheas harvested 3 (B), 5 (C), 7 (D,E), and 9 (F) days after exposure to high dose Cl_2. Whites dots denote the basal lamina. White arrows denote endothelial sprouts into the lumen. Asterisks denote the lumen. Tissue sections are representative of 5-6 tracheas at each time. Top panel, scale bar is 50μm. Bottom panel, scale bar is 200μm.

2.4 Discussion

BO is a debilitating and potentially lethal disease resulting from the narrowing of the airways by fibrosis and inflammation. The pathogenesis of BO is not clearly understood but may involve immune components, tissue ischemia, and epithelial damage [38, 63]. The majority of BO cases, animal and human, include epithelial damage, but not all cases of epithelial damage result in BO. Here, we find that loss of basal cells is closely associated with the development of obliterative airway lesions in a model of acute toxin-induced airway injury. This conclusion is based on several findings. First, we demonstrate that the extent of acute injury to luminal epithelial cells does not correlate with the development of obliterative airway lesions. Second, we find that development of such lesions occurs only under conditions and in areas in which basal cells are eliminated. Third, we find that loss of basal cells is closely associated with a failure to re-epithelialize regions of epithelial denudation. Fourth, we find that obliterative airway lesions arise only at sites of epithelial denudation and that the size of such developing lesions closely correlates with the extent of epithelial denudation. To our knowledge, this is the first demonstration that intraluminal fibrotic lesions arise specifically at sites of epithelial denudation. Taken together, our findings suggest a clear mechanism by which loss of basal cells leads to airway intraluminal fibrosis. This mechanism is consistent with human pathological studies in which obliterative airway lesions appear to arise from areas of epithelial denudation[63].

Although our findings demonstrate strong correlations among basal cell loss, persistent regions of epithelial denudation, and the development of airway intraluminal fibrosis, they do not directly prove that basal cell loss is the cause of airway intraluminal fibrosis. Such proof will likely require the targeted preservation or elimination of basal

cells in an animal model. However, several other associative studies have been performed that support our overall conclusion. It is known that only some toxic chemical exposures lead to the development of BO. Our findings would suggest that the ability of individual chemicals to cause BO is directly related to their effects on basal cells. Although data on the toxicity of specific chemicals toward basal cells is limited, the studies that are available support this conclusion. In animal models, chemicals such as naphthalene, nolidocanol, and SO_2 do not cause basal cell loss and do not cause airway intraluminal fibrosis [67]. In contrast, exposures to diacetyl and sulphur mustard, which are known to cause BO, have been shown to cause basal cell depletion [68, 69]. For any given chemical, there will also be a dosage effect, as demonstrated by our comparison of Cl_2 dosages. In addition, a recent study comparing Cl_2-induced lung injury in FVB/NJ and A/J mice found that reduced epithelial repair and increased airway fibrosis were associated with a reduced number of resident basal cells at baseline[64, 70]. Taken together, our findings and previous reports demonstrate a clear association between basal cell loss and the development of obliterative airway lesions.

According to our model, loss of basal cells does not directly stimulate obliterative airway lesion formation. Rather, it is the failure of re-epithelialization and the consequent prolonged presence of regions of complete epithelial denudation that stimulates an intraluminal fibrotic response. This view is consistent with previous studies in which epithelial denudation induced by chronic depletion of mature epithelial cells results in the development of BO-like fibrotic lesions [38, 39]. After chronic Clara cell depletion, intrabronchiolar fibrotic lesions only arise in areas of complete epithelial denudation, whereas peribronchiolar fibrosis arises in areas that maintain epithelial intergrity despite persistent epithelial injury. Pathologically, the intra- and peri-bronchiolar fibrosis are similar to human proliferative and constrictive BO, respectively.

These observations suggest that the development of proliferative versus constrictive BO may depend on the extent and timing of epithelial injury. It is also possible that proliferative BO can advance to constrictive BO. In a nitric acid-induced rat model of BO, proliferative lesions were observed after the first week of injury, followed later by the occurrence of constrictive BO [71]. We were unable to address the possibility of a transition from one pathology to another in our model, as all mice that survived high dose Cl_2 exposure displayed fully re-epithelialzed tracheas 2-3 weeks post injury with no evidence of fibrosis (data not shown). We assume these mice retained enough surviving basal cells to repair normally and avoid proliferative BO initiation.

Although our findings apply directly only to proximal airway regions that contain basal cells, it is likely that depletion of other types of epithelial progenitor cells in distal airways also leads to intraluminal fibrotic lesions. Human pathological studies demonstrate that such lesions arise by connective tissue penetrating areas of epithelial denudation [63]. Several types of distal airway and alveolar epithelial progenitor cells have been described that are distinct from basal cells [72]. It would be of interest to determine if such cells are depleted by stimuli that lead to distal airway or alveolar intraluminal fibrosis. This would include exposure to chemicals such as phosgene and chloropicrin that preferentially target the distal lung. It would also include non-toxin-related causes of BO. For example, in lung transplantation-induced BO, it is possible that immune-mediated epithelial progenitor cell death contributes to aberrant repair processes and fibrosis. Similarly, the tissue ischemia that is associated with lung transplantation may be extensive enough to eliminate epithelial progenitor cells.

The model of Cl_2-induced airway injury we describe causes the reproducible ablation of basal cells followed by the rapid development of obliterative airway lesions. Relative to other models of BO, this model offers several advantages. It is relatively

simple, requires no surgery, is highly reproducible, and results in the near total occlusion of airways within 10-12 days. Exposure of mice to high dose Cl_2 induces a well-demarcated series of pathological changes that will allow a more detailed analysis of the individual cellular and molecular events that lead from basal cell loss to airway occlusion. Because this model uses C57BL/6 mice, it is readily amenable to analysis using the large number of genetically altered mouse strains available on this background. We anticipate that this model will prove useful in elucidating the pathophysiology of proliferative BO and in the identification of potential therapeutics for this disease.

3. *In vivo* evaluation of anti-angiogenic therapeutics in Cl_2-induced bronchiolitis obliterans

3.1 Introduction

Currently, there are no therapeutics for the treatment of constrictive BO and steroid-resistant proliferative BO. A major goal of our research is to identify and evaluate therapeutics using our previously characterized Cl_2-induced BO model. We identified a well-demarcated series of pathological changes in the airways (e.g. epithelial denudation, inflammatory cell infiltration, fibroblast infiltration and collagen deposition, and in-growth of blood vessels). The necessity of each pathological change in the progression of BO is not understood. In this chapter, we present our preliminary data on the efficacy of anti-angiogenic therapeutics in the prevention of Cl_2-induced blockage formation.

Neovascularization is a common finding in human instances and animal models of BO. In a heterotrophic trachea transplantation model of BO, a 3-fold increase in vessel counts were observed in allografts compared to syngenic grafts 21 days post transplantation [73]. Additionally, lung biopsies of oleic acid-induced BO in dogs showed polys of variable size and shape in the bronchioles, most of which were neovascularized [45]. In humans, BO-affected lung tissue showed evidence of fibrovascular tissue in the airway [73].

Vascular endothelial growth factors (VEGFs) and their receptors, VEGFR-1 and VEGFR-2, are major regulators of angiogenesis [74-76]. VEGF-A is a shared ligand for VEGFR-1 and VEGFR-2, but the receptors have opposing effects. VEGFR-2 is considered the major regulator of the cellular effects of VEGF-A, including angiogenesis, and can additionally bind VEGF-E, -C, and –D. Conversely, VEGFR-1 is thought to act as a

negative regulator of VEGFR-2 through its ability to binds VEGF-A with much higher affinity, effectively sequestering the ligand away from VEGFR-2. VEGFR-1 also binds VEGF-B, PLGF-1 and -2. The VEGF receptors are primarily expressed on endothelial cells but are also expressed on many other cells types including, but not limited to, macrophages, monocytes and platelets[77, 78].

Therapeutically targeting the VEGF pathway has resulted in successful inhibition of neovascularization [79]. In particular, cancer research has taken advantage of inhibiting this pathway, since neovascularization is a major mechanism supporting tumor growth. One therapeutic strategy uses adenoviral production of soluble VEGFR-1 to increase receptor levels in the blood. Due to its high affinity, VEGFR-1 sequesters the natural ligands away from the pro-angiogenic VEGFR-2. This therapy resulted in 80% inhibition of tumor growth in a murine cancer model [80]. A different anti-angiogenic therapeutic strategy used the anti-murine VEGFR-2 antibody, DC101, to prevent the receptor's ability to bind ligand, subsequently blocking VEGFR-2 signaling. Use of DC101 in a murine tumor model also resulted in significantly decreased tumor growth and metastasis [81].

We hypothesized that blockage growth in our Cl_2-induced BO model may require neovascularization to supply nutrients to the granulation tissue and that cutting off that supply via anti-angiogenic therapies could mitigate blockage growth and protect mice from lethal airway obstruction. Here we tested the two anti-angiogenic therapies discussed above in our BO model.

3.2 Materials and methods

Chlorine exposures. Exposures were conducted as described in chapter 2 methods.

VEGFR-1 adenovirus. Adenoviral vectors were kindly provided by Dr. Christopher Kontos (Department of Medicine/Cardiology, Duke University). The vectors were first-generation E1-deleted replication-defective vectors made by Ad-Easy system (Agilent Technologies, Santa Clara, CO). Gene expression of the protein/peptide of interest was driven by human cytomegalovirus immediate/early promoter. Empty adenoviral vector was used as control (Ad-control). Approximately 2.5 to 7.5 x 10^9 pfu of adneo-VEGFR-1 or empty virus was injected into mice via tail vein.

DC101. DC101 was kindly provided by Dr. Andrew Nixon (Department of Medicine/Medical Oncology, Duke University). DC101 was produced from hybridoma cells and concentrated in media as previously described [82]. Starting 24 hours post Cl_2 exposure, mice received an i.p. injection of 800ug DC101 then subsequent i.p. injections of 400ug DC101 on days 4, 6, 7, and 8.

Soluble VEGFR-1 detection. We determined plasma soluble VEGFR-1 (R&D Systems, Minneapolis, MN) using commercial ELISA kits and according to the manufacturer's specifications.

3.3 Results

3.3.1 A VEGFR-1 ligand trap does not prevent BO blockage formation

To test if inhibition of the VEGF signaling pathway prevents blockage formation we used adenovirus overexpression of soluble VEGFR-1 to sequester natural ligands from VEGFR-2. Three days prior to chemical injury, we i.t. administered an adenovirus expressing an empty vector (ad-control) or soluble VEGFR-1 (ad-VEGFR-1). Others have demonstrated that this adenovirus preferentially infects liver hepatocytes and produces circulating levels of VEGFR-1 that are elevated for up to 2 weeks after treatment [80, 83]. Mice were then nose-only exposed to high Cl_2 for 30 minutes. Seven days post exposure, mice were sacrificed for blood and trachea harvest. Figure 10A diagrams the

experimental timeline. Serum levels of soluble VEGFR-1 were quantified, allowing us to identify positive expressers (Figure 10B). Mice with expression < 3.0 ng/ml were not included in our analysis since their expression most likely does not reach therapeutic levels. The harvested tracheas were scored by gross observation for the presence or absence of blockage (Figure 10C). There is no significant difference between the ad-control group (75% blockage positive) and the ad-VEGFR-1 group (80% blockage positive). Vessel density was not counted. Anecdotally, blood vessels were grossly visible in blockages of both groups, and blockage sizes did not differ among groups. Despite high levels of circulating soluble VEGFR-1, blockage formation was not prevented after high dose Cl_2-induced injury.

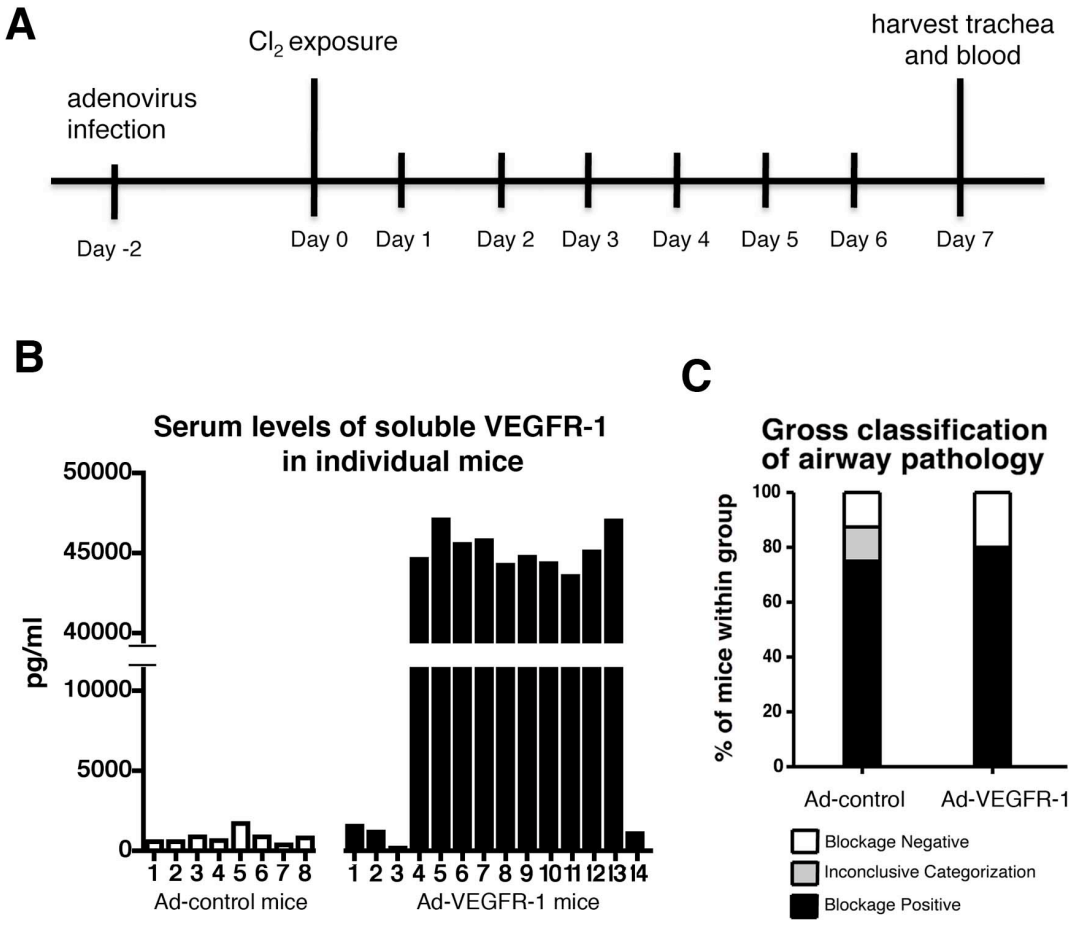

Figure 10: Overexpression of soluble VEGFR-1 by adenovirus does not prevent BO lesions

A) Experimental timeline of adenovirus administration, Cl_2 exposures and tissue harvest. B) Serum levels of soluble VEGFR-1 in individual mice 7 days post Cl_2 exposure (350ppm) and 9 days post intravenous injection with an adenovirus encoding VEGFR-1 (Ad-VEGFR-1, n=14) or control (Ad-control, n=8). C) Tracheas were harvested on day 7 post Cl_2 exposure then grossly examined and categorized based on the presence or absence of blockage formation in the airways. The categorization of one trachea was inconclusive. For, the control group n=8. For the Ad-VEGFR-1, n=10; the Ad-VEGFR-1 mice #1, 2, 3, and 14 in panel B were removed from blockage analysis due to their low levels of circulatory soluble VEGFR-1.

3.3.2 An anti-VEGFR-2 blockade does not prevent lethal BO airway obstruction

We used an alternative therapeutic strategy to inhibit VEGFR-2 signaling. The anti-murine VEGFR-2 antibody, DC101, interrupts the receptor's ability to bind ligand and prevents VEGFR-2 signaling. Mice were exposed to 30 minutes of high Cl_2. Then mice were either given PBS or 800ug of DC101 i.p. starting 24 hours post injury, then given 400ug of DC101 on days 4, 6, 7, and 8. This dose was comparable to a previous therapeutic regimen reported to significantly inhibit tumor growth in a murine cancer model [81]. Mice were monitored for two weeks, during which they were euthanized upon development of excessive labored breathing. The tracheas of euthanized mice were examined and scored by gross observation for the presence or absence of blockage. All tracheas of mice requiring euthanasia had obstructive BO blockages (data not shown). There was no statistical difference in survival between PBS and DC101-treated groups (Figure 11).

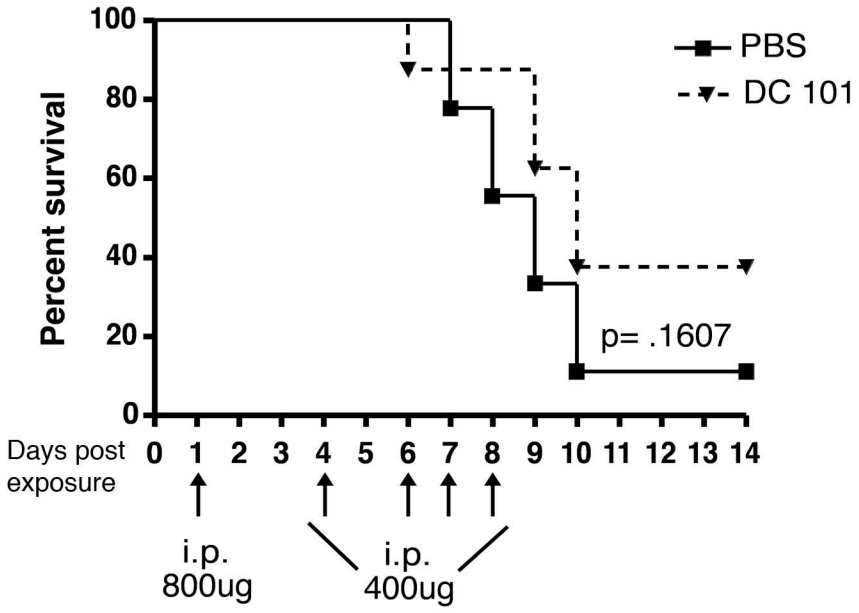

Figure 11: DC101 A VEGFR-2 specific monoclonal antibody, DC 101, does not prevent the development of lethal BO

Mice were exposed to Cl_2 (350ppm). Mice were given i.p. administrations of DC 101; 800ug on day 1, then 400ug on days 4, 6, 7, and 8. The control group was given PBS. DC 101 group, n=8; control group, n=9. The difference in survival curves was not significant; p=.1607 by log-rank test.

3.4 Discussion

Our findings suggest that inhibition of the VEGFR pathway, primarily mediated by VEGFR-2, does not protect mice from chemical-induced BO. The data obtained here were preliminary; therefore, we cannot make this claim with certainty. There are two major limitations in our study. 1) We did not validate the activation of the VEGFR-2 pathway in our injured tissue. Based on histological evidence of neovascularization, we assumed that VEGFR-2 was active. 2) We did not validate that soluble VEGFR-1 or DC101 was present at levels sufficient to inhibit VEGFR-2 activation. However, we believe that the inability of two separate VEGFR-2 inhibiting techniques to protect or alter the course of BO development strongly indicates the dispensable nature of the VEGFR-2 pathway in the development of BO.

Several studies corroborate our findings that VEGFR is dispensable for neovascularization. A study of human bronchoalveolar lavage fluid (BALF) from lung transplant patients showed no correlation between VEGF concentrations and incidents of BO [84]. Additionally, a separate study of human BALF from BO positive transplant patients demonstrated that neutralization of VEGF in the BALF did not reduce angiogenic responses measured in an *ex vivo* BALF-stimulated angiogenesis assay [73]. However, neutralization of CXCR2 ligands using an anti-CXCR2 antibody antagonist inhibited the antigenic response by more that 60% of the non-neutralized BALF controls. These findings urged us to consider alternative pathways of neovascularization.

Growing evidence implicates CXCR2 and its ligands as a biological axis of vascular remodeling in several diseases including, cancer, pulmonary fibrosis and BO. [85-89]. More importantly, Belperio et al. demonstrated greatly increased immunohistological staining for CXCR2 in human BO biopsies that colocalized to

remodeled vasculature. Subsequently, they demonstrated that a therapeutic-regimen of anti-CXCR2 antibody significantly reduced the severity of disease in a murine heterotrophic transplant model of BO. Specifically, they observed decreases in early neutrophil recruitment, reduced angiogenic activity in an *ex vivo* corneal micropocket assay of angiogenesis, and overall attenuation of BO severity (scored as an average of airway lining epithelial loss, leukocyte infiltration, extracellular matrix deposition, and luminal obliteration)[73].

The same mechanism of neovascularizton may occur in our chemical-induced BO model. It would be interesting to evaluate the effect of CXCR2 neutralization in our BO model since there are several major differences between our model and the herterophic BO model (e.g. allorejection independent vs. dependent, location: functioning airway vs. subcutaneous implantation, non-surgical vs. surgical technique). In chapter 5, we will continue our discussion on the potential involvement of the CXCR2 biological axis in our BO model with additional insight gleaned from microarray analysis of BO lesions.

4. *In vivo* evaluation of anti-inflammatory therapies in Cl_2-induced bronchiolitis obliterans

4.1 Introduction

As previously mentioned, a major goal of our research is to identify and evaluate therapeutics using our Cl_2-induced model of BO. In chapter 3, we targeted neovascularization, one of several pathological changes in the airways (e.g. epithelial denudation, inflammatory cell infiltration, fibroblast infiltration and collagen deposition, and in-growth of blood vessels). In the present chapter, we will target inflammation; specifically, we will prevent inducible nitric oxide synthase (NOS2)-mediated inflammation and determine the therapeutic efficacy of NOS2 inhibition in our model.

An indirect mechanism implicated in Cl_2-induced respiratory injury is the excessive production of nitric oxide (NO), leading to increased and persistent oxidative burden. Three nitric oxide synthases catalyze the release of nitric oxide from L-arginine. These include neuronal NOS, epithelial NOS, and inducible NOS (NOS2). Expression of *NOS2* is initiated by inflammation [90]. NOS2 is highly expressed in pulmonary macrophages, cells that respond to inflammation by generating effector molecules such as tumor necrosis factor alpha (TNF-α) and NO [91, 92]. Excessive levels of NO can be tissue-damaging. Studies suggest that, after chemical inhalation, NO produced by NOS2 interacts with superoxide to form peroxynitrite, which can cause tissue damage directly or lead to DNA strand breakage [93]. DNA damage triggers the activation of poly-ADP ribose polymerase, a DNA repair enzyme, which depletes cellular ATP, leading to necrotic cell death [94-97]. Excessive NO may also contribute to lung injury by abolishing the pulmonary vasoconstriction reflex to hypoxia [98]. A previous study showed that pharmacological inhibition of NOS2 prior to Cl_2 exposure reduces subsequent Cl_2-induced increases in AHR, however fibrotic airway changes were not

assessed [99]. It is unknown whether NOS2-produced NO contributes to fibrotic pathological changes resulting from Cl_2-exposure. In bleomycin-induced pulmonary fibrosis, airway NOS2 expression levels increase and pharmacological inhibition of NOS2 reduces disease severity and improves survival of bleomycin-challenged mice [100, 101]. This implicates NOS2 as a mediator of fibrosis. In this chapter, we sought to determine whether Cl_2-induced BO is mediated by NOS2 and to determine if NOS2 inhibitors, when used therapeutically, can prevent or delay lethal airway obstruction.

Additionally, we sought to test the efficacy of steroid therapy in our model. Not only are steroids potent suppressors of inflammation, clinical findings demonstrate that most cases of proliferative BO respond favorably to steroid treatment [24]. Histopathologically our model of Cl_2-incuded BO is more similar to proliferative than constrictive BO, so we hypothesized that use of steroids would be protective in our model. However, aggressive forms of proliferative BO exist that are not responsive to steroids. Additionally, constrictive BO responds poorly to steroid treatment and is considered irreversible. We evaluated the effect of steroid therapy in our model.

4.2 Materials and methods

Mice. C57BL/6 were purchased from Charles River Laboratories (Wilmington, MA) and Nos2 null mice (stock # 002596) were purchased from Jackson Laboratory (Bar Harbor, ME). The majority of our experiments used 10-12 week-old male mice. All animal experiments were conducted in accordance with National Institutes of Health guidelines and protocols approved by the Animal Care and Use Committee at Duke University.

Chlorine Exposures. Exposures were conducted as described in chapter 2 methods.

1400W administration. The NOS2 inhibitor 1400W (N- [[3-(aminomethyl)phenyl]methyl]- ethanimidamide, dihydrochloride ([2-[(1-iminoethyl) amino]ethyl]-l-homocysteine)) was purchased from Cayman Chemical Company (Ann Arbor, Michigan, USA). Prior to use, the compound was dissolved in PBS at 0.5 mg/ml (2.0 mM concentration). Starting 3 hours post chemical exposure and then daily for 7 days, mice received aerosolized drug or placebo treatments using the nose-only inhalation chamber. The duration of daily aerosol treatment was 30 minutes.

Statistics. The comparison between survival curves was performed with the log-rank test using GraphPad Prism software.

Solu-medrol. Starting 24 hours post Cl_2 exposure, mice received daily i.p. injections of .1mg solu-medrol, also known as methylprednisolone sodium succinate, (Pfizer, New York City, NY) for 6 days.

4.3 Results

4.3.1 Therapeutic administration of NOS2 inhibitors does not prevent lethal BO airway obstruction

To determine if pharmacologic inhibition of NOS2 can provide a benefit when administered therapeutically, we examined the survival of Cl_2-exposed mice treated with the small molecule NOS2 inhibitor 1400W. Three hours post Cl_2 exposure mice were treated with an aerosol of 1.0 mM 1400W for 30 minutes; this therapy was repeated daily for 9 days. Anecdotally, both groups of mice demonstrated similar behavior patterns. There was no difference in survival between treated and untreated groups; both groups had 50% survival at day 14 (Figure 12A).

4.3.2 *Nos2*-deficient mice are not resistant to lethal BO airway obstruction

In the above experiment, we did not validate the efficiency of aerosol delivery of NOS2 inhibitors to inhibit NOS2 activity in the lung. It is possible that the concentration of the inhibitor delivered into the airway was not sufficient for NOS2 inhibition. To overcome this challenge, we repeated the survival experiment using *Nos2*-deficient mice. There was no difference in survival between wild-type (WT) and *Nos2*-deficient mice (Figure 12B). These findings suggested that NOS2 does not play a role in the pathogenesis of BO in our model.

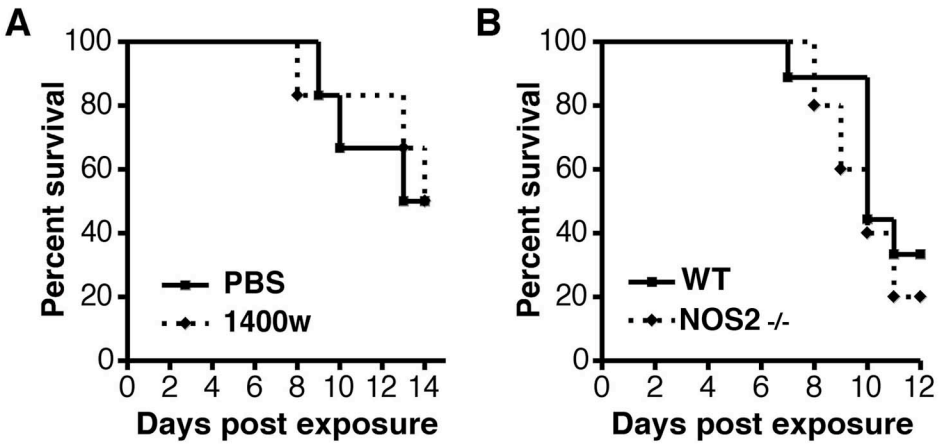

Figure 12: Pharmacological inhibition of NOS2 with 1400W does not prevent the development of lethal BO

A) Mice were exposed to Cl_2 (350ppm) then given aerosolized PBS or 1400W (.5mg/ml) starting 4 hrs post exposure and then once daily for 9 days; n=6 for each group. The difference in survival curves was not significant; p=.9086 by log-rank test. B) WT and *Nos2*-deficient mice were exposed to Cl_2 (350ppm); WT group, n=9; *Nos2*-deficient group, n=5. The difference in survival curves was not significant; p=.4847 by log-rank test.

4.3.3 Steroid Treatment does not prevent BO blockage formation

Since a large proportion of human proliferative BO can be resolved with steroid treatment, we determined if steroid treatment could resolve blockage formation in our model. Mice were exposed to 30 minutes of high Cl_2. Subsequently mice were either given PBS or 0.1mg of solu-medrol i.p. starting 24 hours post injury and then once daily. Seven days post exposure, tracheas were harvested then scored by gross observation for the presence or absence of blockage (Figure 13). There is no statistical difference between the control PBS group (60% blockage positive) and the solu-medrol group (100% blockage positive). The deviation of both groups from our historical average mortality, ~80%, is most likely due to normal variations that were exaggerated by the small number of mice in each group, n=5.

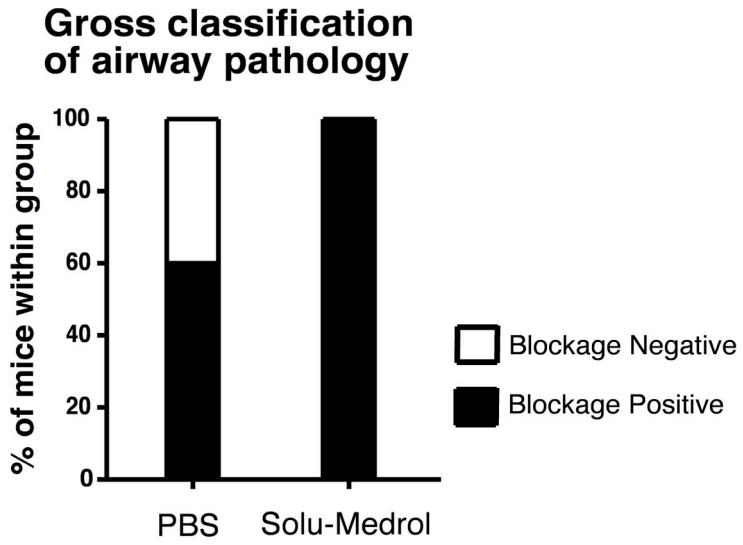

Figure 13: Steroid treatment does not prevent BO lesions

Mice were exposed to Cl_2 (350ppm) then given i.p. administrations of solu-medrol (.1mg per mouse) or PBS everyday starting 24 hours post exposure; n=5 for each group. Tracheas were harvested on day seven post exposure then grossly examined and categorized based on the presence or absence of blockage formation in the airways.

4.4 Discussion

In this chapter, we demonstrated that NOS2 is dispensable for the development of lethal airway obstruction seen after Cl_2 inhalation. Our findings were unexpected considering there is evidence that NOS2 inhibition is effective at reducing lung injury after exposure to other toxins and in other types of lung injury. For example, sheep treated with a NOS2 inhibitor after smoke inhalation demonstrate significantly decreased respiratory dysfunction and inflammation relative to vehicle-treated controls [102]. Bleomycin-induced lung injury and mortality are reduced in *Nos2*–deficient mice or mice treated with an NOS2 inhibitor [101]. Additionally, NOS2 inhibition preserves airway and pulmonary epithelial barrier function in endotoxemic mice [103]. Clearly, NOS2 contributes differentially to the multiple pathologies that can arise after Cl_2 injury (e.g. acute lung injury, reactive airway dysfunction syndrome, and fibrosis) and other pulmonary diseases. One possible explanation for our observations is that NOS2-driven pathology may depend on the enzyme's ability to generate biologically significant increases in oxidative burden. The same mechanism may not be applicable in our model since the direct mechanism of Cl_2 injury is excessive oxidization. NOS2-generated oxidative injury may not increase the oxidative burden already inflicted by Cl_2 and, therefore, is not biologically significant. However, this is a very simplistic explanation for the effects of a complex molecule, NO, that induces a wide range of physiologic effects depending on concentration and effected cell types [104]. From our data, we conclude that NOS2-generated NO is not a critical regulator of intraluminal fibrosis after Cl_2 injury.

Steroid-treatment was ineffective at preventing BO in our model. Histologically, the fibrotic blockages that developed after Cl_2 injury resembled proliferative BO,

however, they did not respond to steroid treatment in a similar manner. 65-80% of human proliferative BO resolves after corticosteroid treatment [24]. Our findings may indicate that our model represents the 20-35% of proliferative BO that does not respond to treatment. Currently, the mechanism of action for corticosteroid protection is unknown. One possible mechanism is that steroid treatment prevents additional epithelium injury by suppressing epithelial- and leukocyte-induced inflammation. The same mechanism may not be applicable in our model since the majority of epithelial cell damage occurs during and immediately after chemical exposure. Our findings suggest that steroids are not effective in treating the fibrotic processes that contribute to BO. However, a major limitation of our experiment was that we did not confirm that steroid-treatment actually reduced inflammation in our model. There is the possibility that the time between injury and airway obstruction may be too short for steroid-treatment to be effective. In our future research we intend to continue *in vivo* evaluation of inflammation-targeted therapeutics for the prevention of BO.

5. Identification of potential molecular mediators of bronchiolitis obliterans using bioinformatics

5.1 Introduction

Our selection of therapeutic targets above was solely based on histopathologic findings in the development of bronchiolitis obliterans. *In vivo* modulation of those targets with previously described therapeutic regimens did not grossly alter the progression of fibrosis. Therefore, we used microarray expression profiling of injured tracheal tissue to identify potential molecules and signaling pathways that regulate BO progression. Comparison of gene expression profiles after exposure to non-BO- and BO-inducing toxic gas inhalation allowed us to differentiate up-regulation of genes associated with normal epithelial injury/repair versus upregulation of genes specific to BO. Using cutting-edge pathway analysis software, we identified enriched biological pathways specific to BO-development and even predict upstream regulators of the disease process. Our intentions are that this rigorous analysis will result in the identification of BO-specific therapeutic targets with the potential to resolve or mitigate airway injury after Cl_2 gas inhalation injury. We will discuss the merits of the potential therapeutic targets that were identified based on current literature.

5.2 Materials and methods

Chemical exposures. Cl_2 exposures were conducted as described in chapter 2 methods. For SO_2 exposures, 8 week old female mice were placed in individual compartments of a chamber and whole body exposed to 500 ppm SO_2 in air for 3 hours, as previously described (Rawlins, 2006).

Gene expression profiling by microarray. Tracheas were dissected and cleaned of surrounding connective tissue. Each trachea was then cut into one small cylindrical segment by trimming away the bronchioles just above the bronchiole bifurcation and trimming away the proximal airways at the third or fourth tracheal ring. The tissue segment was immediately frozen in RLT buffer (RNeasy Mini Kit; Qiagen, Valencia, CA) and later bead homogenized. RNA was immediately extracted using the RNeasy Mini Kit. RNA was submitted to the Duke University microarray core facility for microarray analysis. RNA quality was checked with a 2100 Bioanalyzer (Agilent Technologies). cDNA was amplified, then Cy3-labelled cDNA was hybridized to a Whole Mouse Genome 4×44K v2 array (Agilent Technologies). Microarray cDNA was amplified from 20 ng total RNA using Ovation Pico WTA system V2 (NuGEN Technologies, San Carlos, CA, USA). Cy3-labelled cDNA was hybridized to a Whole Mouse Genome 4×44K v2 array (Agilent Technologies).

Microarray analysis. Data analysis was performed using the Partek Genomics Suite (Saint Louis, MO). First, the raw data were imported and normalized. Subsequently ANOVA statistical analysis was performed on the entire dataset searching for significant differences between exposure groups (filtered air, SO_2, low Cl_2, high Cl_2). Subsequently, significantly upregulated or downregulated genes were identified based on fold changes <-3 or >3 and a p-value of <0.01 . Hierarchical clustering analysis and

principal components analysis were performed within the software suite. To investigate functional characteristics as well as upstream regulators of specific gene lists, we used Ingenuity Pathway Analysis (IPA) (Ingenuity Systems, Redwood City, CA). IPA mapped genes and calculated P values (Fisher's exact test) in canonical pathway analysis and calculated z-scores and P values in upstream regulator analysis. The activation z-score predicts the activation state of the upstream regulator, using the gene expression patterns of the genes downstream of that regulator. An upstream regulator is considered activated if the z-score is ≥ 2 and inhibited if the z-score ≤ -2 with a P value <0.01 considered significant. The Database for Annotation, Visualization and Integrated Discovery (DAVID) v6.7 was used for molecule classification within gene lists. Specifically, we identified secreted proteins and subsequently queried for G-protein binding or growth factor activity annotations.

5.3 Results

5.3.1 Microarray analysis reveals exposure-specific gene profiles and injury severity gene profiles

To identify differentially expressed genes in non-BO- and BO-inducing inhalation injury, mice were exposed to FA (filtered air), SO_2 (500 ppm), low Cl_2 (200 ppm) or high Cl_2 (350 ppm). Tracheas were harvested for RNA extraction 5 days post exposure; this timepoint was chosen to reveal biological processes influencing the early stages of mesenchymal invasion into the airspace. Agilent whole mouse genome 4×44K v2 arrays were used to analyze the expression profiles. Table 1 summarizes the number of gene targets found to be differentially expressed by ANOVA when compared across groups. The greatest number of gene targets resulted from comparisons of high Cl_2 to either FA or low Cl_2. To ascertain the global similarities among individual samples, we performed a principal component analysis (PCA) on unfiltered gene profiles (Figure 14). Within low Cl_2 (yellow), high Cl_2 (red), and FA (green) exposure groups, individual samples clearly cluster together, suggesting that they share similar expression profiles within groups. Additionally, the three exposure groups clearly separate from each other, suggesting there exists exposure-specific expression profiles.

However, individual samples from the SO_2 (purple) exposure group did not cluster together. Instead, two of the samples were similar to the FA group, while the other two samples were similar to low Cl_2. The same trend is observed when we applied genome wide hierarchical clustering to the individual samples; FA, low Cl_2 and high Cl_2 clustered separately but $S0_2$ was divided between FA and low Cl_2 (Figure 15). We speculate that the division among the SO_2 individuals was a result of inconsistent airway injury after exposure, in which two animals were injured and two were not injured.

According to previous studies, SO_2 exposure results in airway epithelial injury similar to that of low Cl_2 [105]. In our data, two of the SO_2 exposed individuals clustered with the low Cl_2. This suggested that gene expression profiles were indicative of gross airway injury.

Table 1: Total number of genes differentially expressed between groups.

Using Partek analysis software, ANOVAs were preformed between all exposure groups. Analysis was restricted to genes with >3 or <-3 fold expression changes and a $p<0.01$.

	# of probes:	
	Up-regulated	**Down-regulated**
S02 vs FA	46	25
Low vs FA	210	55
High vs FA	1066	742
High vs S02	779	506
High vs Low	1082	1240

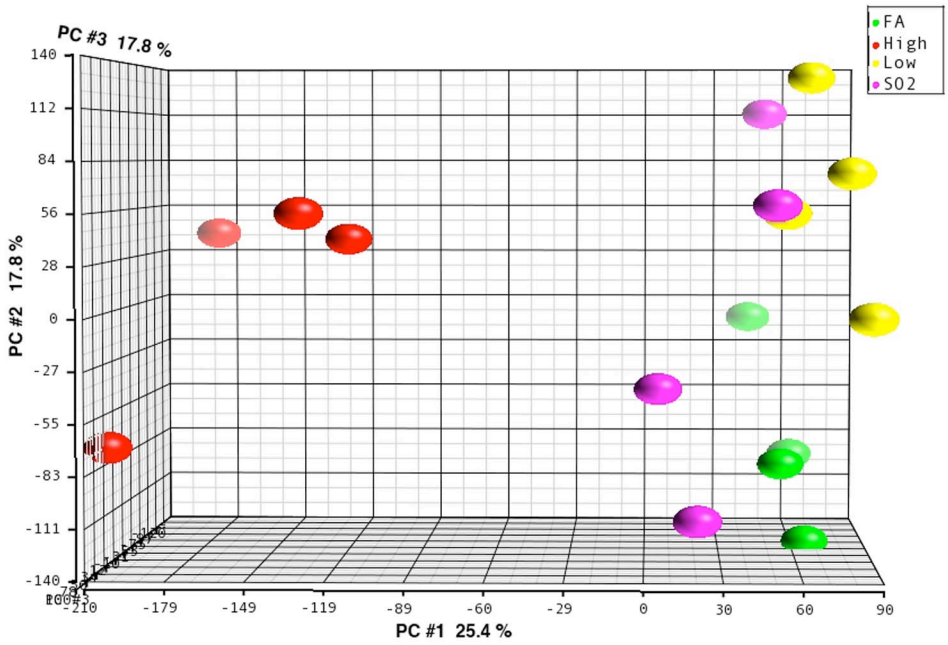

Figure 14: Principle component analysis of global gene expression.

In this analysis, the high-density gene expression data can be transformed into linearly uncorrelated variables called principle components. The samples are then graphed in three dimensions according to the 3 components with the greatest variance. The distance between individual samples correlates to expression profile similarity. PC #1 (x axis) accounted for 25.4%, PC #2 (y axis) 17.8%, and PC #3 (z axis) 11.1% of the observed variation for this data. Each point on the graph represents the expression profile of one sample. The colors for the exposure groups are as follows: low Cl2 (yellow), high Cl2 (red), and FA (green).

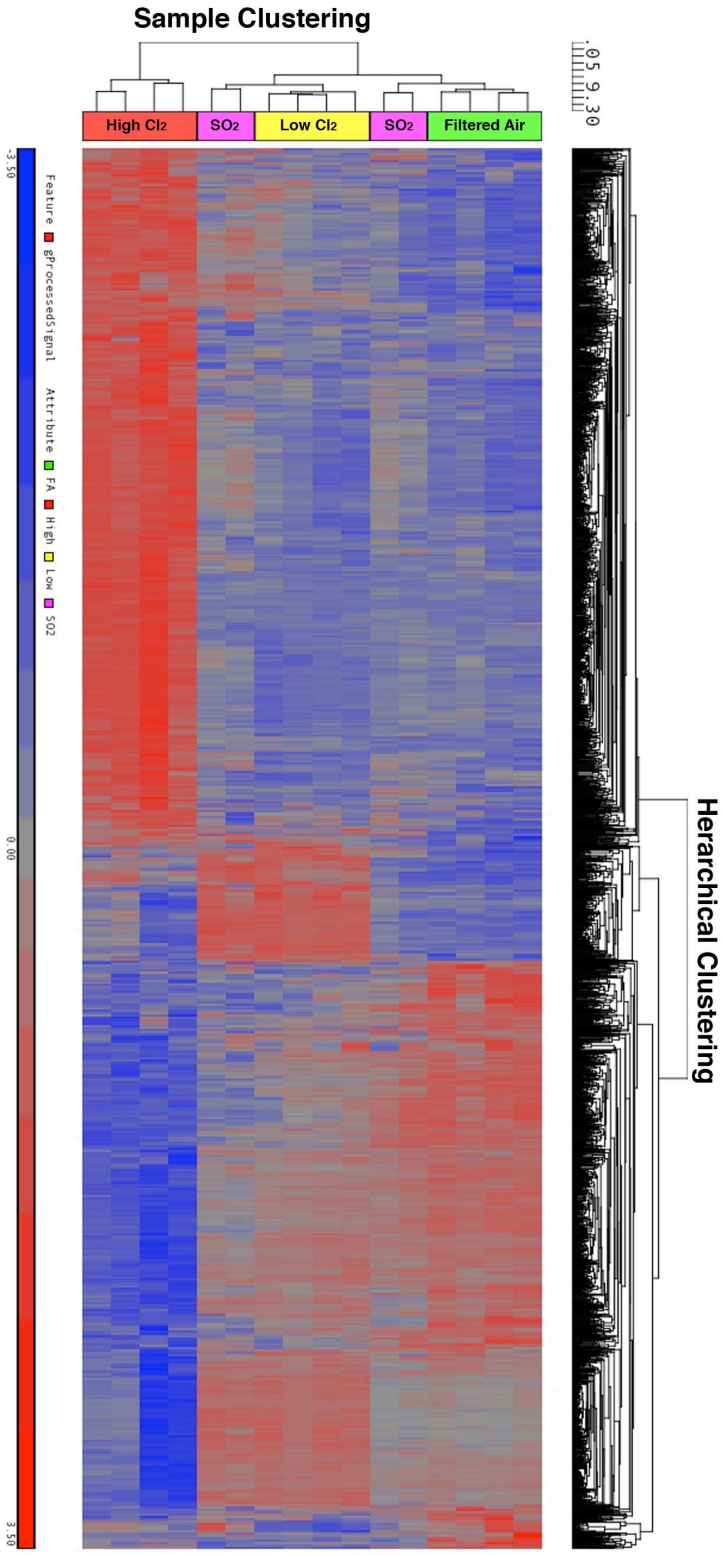

Figure 15: Hierarchical and sample clustering.

Above is a heatmap of all genes with >3 or <-3 fold expression and p>0.05, generated by individual ANOVA comparisons of low Cl_2, high Cl_2, and SO_2 exposure groups to filtered air. The samples were also clustered based on the similarity of their expression profiles.

5.3.2 Identification of enriched biological functions and canonical pathways in exposure-specific gene profiles

Using Ingenuity Pathway Analysis (IPA), we evaluated the functional categories enriched within the transcription profiles induced by low and high Cl_2. Table 2 lists significantly enriched functional annotations as compared to FA controls. Exposure to low Cl_2 is primarily associated with cell cycle/proliferation functions (e.g. "refolding of protein", "differentiation of cells", "response of cyclic AMP"). The functions predicted by IPA were compatible with histologic features of the airway 5 days after low dose Cl_2 exposure. Specifically, the airway showed few inflammatory infiltrates and was covered with differentiating epithelium. Conversely, the analysis of high Cl_2 revealed functions related to "inflammatory responses", "activation of leukocytes", and "cell movement". These findings strongly corresponded to our histologic observations; 5 days after high dose Cl_2 exposure, large areas of the trachea were denuded, and $CD11b^+$ myeloid and collagen-producing cells were infiltrating the intraluminal compartment. The statistical significance of functions associated with high Cl_2 are orders of magnitudes greater than low Cl_2, and all high Cl_2 annotations were strongly predicted to be activated (as indicated by the z-score).

Next we used IPA to identify canonical pathways that were represented in our high vs. low Cl_2 dataset. IPA compares the input gene list to libraries of canonical pathway gene lists and then determines a p value that represents the probability that the overlap between the two lists was generated by chance. Table 3 summarizes the top ten canonical pathways that are enriched after high Cl_2 compared to low Cl_2 exposure. In agreement with the functional analysis, pathways reflecting immune cell migration and activation are upregulated. These include granulocyte and agranulocyte adhesion and

diapedesis, LPS/IL-1 mediated inhibition of RXR function, communication between innate and adaptive immune cells, and TREM-1 signaling. Interestingly, two anti-inflammatory pathways are predicted to be activated, inhibition of matrix metalloproteases and IL-10 signaling. This suggests that there may exist a natural process for dampening the inflammatory response.

Table 2: IPA generated function annotations.

	Low Cl_2 vs Filtered Air	p-value	predicted activation	z-score
1	refolding of protein	5.67E-08		
2	senescence of cervical cancer cell lines	6.34E-05		
3	trophoblastic tumor	6.85E-05		
4	systemic inflammation	7.84E-05		
5	differentiation of cells	2.96E-04	Increased	2.747
6	aggregation of pigment granules	3.76E-04		
7	response of cyclic AMP	3.76E-04		
8	upper aerodigestive tract carcinoma	5.91E-04		
9	secretion of glycosphingolipid	6.24E-04		
10	adenocarcinoma	7.68E-04		
11	gestational trophoblastic disease	7.85E-04		
12	bladder carcinoma	8.92E-04		
13	keratinization of epidermis	9.31E-04		
14	meiosis of germ cells	1.13E-03		
15	germ cell tumor	1.34E-03		
16	epithelial neoplasia	1.37E-03		
17	meiosis of male germ cells	1.61E-03		
18	endoplasmic reticulum stress response	1.96E-03		
19	tumorigenesis of cells	2.04E-03		
20	survival of organism	2.05E-03		

	High Cl_2 vs Filtered Air	p-value	predicted activation	z-score
1	inflammatory response	2.86E-30	Increased	6.358
2	activation of leukocytes	2.75E-28	Increased	4.892
3	cell movement of granulocytes	2.98E-27	Increased	6.001
4	activation of blood cells	2.63E-26	Increased	4.924
5	activation of phagocytes	3.77E-26	Increased	4.889
6	activation of cells	2.02E-25	Increased	4.960
7	cell movement of myeloid cells	8.81E-25	Increased	6.354
8	activation of myeloid cells	2.40E-24	Increased	5.228
9	leukocyte migration	4.03E-24	Increased	5.882
10	cell movement of neutrophils	5.88E-24	Increased	5.436
11	infection of mammalia	7.23E-24	Decreased	-2.246
12	cell movement of leukocytes	2.88E-22	Increased	6.451
13	cell movement of phagocytes	4.47E-22	Increased	6.311
14	chemotaxis of phagocytes	6.60E-21	Increased	5.809
15	chemotaxis of myeloid cells	8.53E-21	Increased	5.856
16	activation of granulocytes	1.44E-20	Increased	4.211
17	accumulation of cells	1.62E-20	Increased	3.011
18	adhesion of blood cells	5.33E-20	Increased	6.218
19	recruitment of cells	7.78E-20	Increased	4.439
20	chemotaxis of leukocytes	9.92E-20	Increased	6.105

Table 3: IPA generated canonical pathways.

Top 10 Canonical Pathways

	High vs Low Chlorine	p-value	# array genes/ total pathway genes
1	Granulocyte Adhesion and Diapedesis	9.19E-25	58/178
2	Agranulocyte Adhesion and Diapedesis	8.16E-20	54/189
3	LPS/IL-1 Mediated Inhibition of RXR Function	8.01E-12	48/241
4	Communication between Innate and Adaptive Immune Cells	1.60E-10	24/109
5	TREM1 Signaling	2.54E-09	20/71
6	LXR/RXR Activation	3.79E-08	28/136
7	Atherosclerosis Signaling	3.79E-08	28/137
8	Altered T Cell and B Cell Signaling in Rheumatoid Arthritis	8.19E-08	15/40
9	Inhibition of Matrix Metalloproteases	1.36E-07	20/78
10	IL-10 Signaling	1.42E-07	22/92

5.3.3 Predicted activation of signaling molecules

Pathway identification can be difficult because not all molecules in a biological pathway need be upregulated at the transcriptional level in order for the pathway to be biological significant. To overcome this challenge, we used IPA's upstream regulator tool to predict transcriptional regulators that most likely account for our observed gene expression profiles (Table 4). IPA generated these predictions using extensive knowledge databases complied from publications on protein interactions, transcriptional factors and signaling networks. The algorithm assigns each factor a z-score that is indicative of the factor's activity. A z-score > 2 or <-2 is considered to be significantly active or inactive, respectively. The most strongly predicted transcriptional regulators are *NFκB*, *TBX2*, *SPI1*, *E2F1* and *RELA*. Transcripts for *SPI1* and *E2F1* are elevated in our array dataset and regulate myeloid cell differentiation and cell cycle, respectively [106, 107]. RELA is one component of the NFκB complex, a major regulator of inflammatory genes [108]. TBX2 is a master regulator of organogenesis and has been implicated as an inducer of epithelial-mesenchymal transition [109].

To broaden our list of potential therapeutic candidates we used IPA to explore predicted upstream signaling molecules other than transcription factors. Table 5 lists all predicted signaling kinases, growth factors, and transmembrane receptors with a z-score > 3. The fold increase of the molecule is indicated when applicable, but the majority of molecules were not elevated > 3 fold in our dataset (based on our ANOVA criteria). We will focus on some of these molecules in the discussion section.

Table 4: IPA predicted upstream transcription regulators.

IPA analysis was based on the dataset generated by ANOVA comparison of high vs. low Cl_2 exposure; the dataset was restricted to genes with >3 or <-3 fold expression changes and a $p<0.01$.

	Transcription Regulators	z-score
1	NFkB (complex)	6.823
2	TBX2	4.869
3	SPI1*	4.566
4	E2F1*	4.345
5	RELA	4.32
6	STAT3	4.309
7	ETS1	4.249
8	EGR1	4.087
9	Ap1	4.023
10	FOXO1	3.847
11	FOXM1*	3.662
12	NFKBIA	3.451
13	STAT1	3.44
14	STAT4*	3.44
15	HMGB1	3.439
16	NfkB1-RelA	3.388
17	JUN	3.377
18	GLI1	3.223
19	NfkB-RelA	3.153
20	HIF1A	3.087

Table 5: IPA predicted upstream regulators.

IPA analysis was based on the dataset generated by ANOVA comparison of high vs. low Cl_2 exposure; the dataset was restricted to genes with >3 or <-3 fold expression changes and a $p<0.01$.

	Top Kinaes	actual fold change		z-score	p-value
1	IKBKB	n/a	kinase	6.026	3.22E-15
2	CHUK	n/a	kinase	5.569	5.45E-13
3	ERK1/2	n/a	group	5.388	7.45E-12
4	ERK	n/a	group	5.200	1.13E-07
5	Jnk	n/a	group	4.987	1.30E-07
6	P38 MAPK	n/a	group	4.880	3.61E-07
7	PI3K (complex)	n/a	complex	4.551	4.90E-06
8	IKBKG	n/a	kinase	3.997	8.60E-08
9	MAP3K1	n/a	kinase	3.799	4.16E-05
10	MAPK14	n/a	kinase	3.728	1.46E-06
11	PRKCE	n/a	kinase	3.663	3.15E-04
12	MET	n/a	kinase	3.639	6.82E-05
13	RAF1	n/a	kinase	3.521	1.92E-05
14	MAP3K8	n/a	kinase	3.311	2.03E-09
15	PRKCA	n/a	kinase	3.309	2.63E-05
16	Akt	n/a	group	3.284	7.89E-07
17	RET	n/a	kinase	3.214	1.50E-07
18	MAP2K1	n/a	kinase	3.156	5.20E-08
19	Mapk	n/a	group	3.098	5.48E-05
20	JAK2	n/a	kinase	3.081	2.48E-03
21	MAPKAPK2	n/a	kinase	3.079	8.15E-07
22	MAPK8	n/a	kinase	3.062	2.25E-06
23	AKT1	n/a	kinase	3.054	7.56E-05

	Top Growth Factors	actual fold change	z-score	p-value
1	EGF	n/a	6.368	2.49E-06
2	HGF	10.990	5.590	1.52E-12
3	AGT	n/a	4.719	1.54E-04
4	TGFB1	n/a	4.488	3.83E-10
5	KITLG	n/a	4.244	1.93E-04
6	VEGFA	n/a	3.482	2.16E-05
7	FGF2	n/a	3.298	7.51E-02
8	IGF1	n/a	3.172	9.15E-05
9	PDGFB	n/a	3.087	3.27E-03
	Top Transmembrane Receptor			
1	TLR3	n/a	5.896	1.72E-13
2	TLR9	n/a	5.408	3.22E-14
3	TLR4	n/a	5.096	3.46E-12
4	TLR2	3.713	3.863	3.77E-08
5	IL17RA	n/a	3.837	4.31E-11
6	TNFRSF1A	n/a	3.711	1.26E-09
7	OLR1	56.374	3.691	1.08E-09
8	TLR7	3.394	3.545	6.28E-06
9	TLR5	n/a	3.238	1.96E-06
10	CD14	n/a	3.147	1.22E-09
11	TYROBP	8.010	3.132	4.46E-06

5.3.4 Increased transcripts of soluble receptor-binding ligands

We also evaluated our original dataset without the assistance of IPA. In table 7 we simply listed all soluble proteins from our original dataset generated from the ANOVA comparison of high vs. low Cl_2. Dynamic changes in ligand transcription could implicate ligand-associated signaling pathways as biologically significant in our injury model. We specifically identified guanosine nucleotide-binding protein (G-protein) ligands, because G-protein receptors make efficient therapeutic targets due to their signal amplification ability. Additionally, we identified ligands capable of inducing growth factor activity. Some of these molecules have already been implicated in fibrotic processes but not necessarily in BO development.

Table 6: Upregulated soluble receptor-binding ligands.

Using the Database for Annotation, Visualization and Integrated Discovery (DAVID), we identified receptor-binding ligands and divided them by their growth factor or G-protein coupled receptor binding associations. Our input dataset was generated by ANOVA comparison of high vs. low Cl_2 exposure; the dataset was restricted to genes with > 5 fold expression changes and a $p<0.01$.

Receptor Binding				Growth Factor Activity	G-protein Coupled Receptor Binding	
1 SFRP1	16 CXCL1	31 TNFSF14	46 CCL4	1 EREG	1 SFRP1	16 WNT7A
2 TNFSF18	17 GDF15	32 GDF3	47 IL1F9	2 TFF1	2 CCL22	17 CCL7
3 CCL22	18 TIGIT	33 FGR	48 CXCL2	3 CXCL1	3 CCL24	18 CXCL5
4 CCL24	19 ITGB2	34 CCL6	49 F7	4 GDF15	4 PROK2	19 CCL4
5 ULBP1	20 CSF3	35 CCL2	50 CCL3	5 CSF3	5 PF4	20 CXCL2
6 PROK2	21 EPGN	36 WNT7A	51 IL6	6 EPGN	6 CCL12	21 CCL3
7 EREG	22 CCL9	37 CCL7	52 IL1B	7 OSM	7 CCL17	22 CXCL3
8 HILPDA	23 CTHRC1	38 IL1A	53 CXCL3	8 HGF	8 CXCL10	
9 PF4	24 CCL8	39 IL1RN		9 GDF3	9 CXCL1	
10 ITGA2	25 TNC	40 SPP1		10 CSF2	10 CCL9	
11 CCL12	26 OSM	41 CXCL5		11 IL6	11 CTHRC1	
12 CCL17	27 TNFSF11	42 GPNMB		12 IL1B	12 CCL8	
13 CCNB1	28 HGF	43 FGG			13 NPY	
14 TFF1	29 TNFSF8	44 PRL2C5			14 CCL6	
15 CXCL10	30 NPY	45 CSF2			15 CCL2	

5.3.5 Transcripts related to the angiogenic CXCR2 pathway are increased

In chapter 2, we presented data suggesting that neovascualrization was VEGF-independent in our BO model. In recent years, an alternative angiogenic pathway has emerged; several publications demonstrated CXCR2 mediates angiogenisis in multiple disease models, including a hetertrophic transplant BO model and tumor models [73, 88]. To determine if our microarray data implicates either angiogenic pathway, we searched our dataset for upregulated surface receptors and ligands associated with VEGFR and CXCR2 pathways; we used the dataset generated from our ANOVA comparison of high vs. low Cl_2. Table 8 lists our findings. For the CXCR2 pathway, the receptor itself was highly upregulated at the transcript level (77.7 fold change). Transcripts of the following CXCR2 ligands were upregulated; Cxcl7, 3, 2, 5, and 1 (listed in order of decreasing fold expression). In stark contrast, our search for VEGF receptors and ligands generated no results. This strongly suggests that the CXCR2 pathway is more active than the VEGFR pathway in our model.

Table 7: Upregulated transcripts associated with the CXCR2 or VEGFR pathways.

Our input dataset was generated by ANOVA comparison of high vs. low Cl_2 exposure; the dataset was restricted to genes with > 3 fold expression changes and a $p<0.01$.

CXCR2 Pathway

	fold change
Cxcr2	77.6879
Ligands	
Cxcl7 (Ppbp)	684.441
Cxcl3	466.162
Cxcl2	42.8214
Cxcl5	19.9393
Cxcl1	7.90773

VEGFR Pathway

no upregulated
receptors or ligands

5.4 Discussion

The signaling pathways contributing to the pathogenesis of BO are unclear. To our knowledge, we are the first to use microarray technology to obtain a transcription profile of chemically induced BO. By comparing BO-inducing to non-BO-inducing injuries we reasoned that our datasets would reflect biological processes of BO exceeding normal airway repair. Our findings add support to suspected pathways in BO development and more importantly, suggest potential new pathways as mediators of BO. Future exploration of these pathways will require extensive validation and therapeutic evaluation *in vivo*. For now, we will discuss the merits of our findings in the context of histopathologic evidence and current literature on BO and other fibrotic diseases. We will divide our discussion into several parts, focusing on canonical pathways, upstream regulators and soluble ligands, CXCR2 angiogenesis, and final remarks.

5.4.1 Canonical Pathways

The top 5 canonical pathways enriched in our analysis included three overt pathways and two less common pathways that have not yet been associated with BO development. The three overt pathways include 1) granulocyte and 2) agranulocyte adhesion and diapedesis, and 3) communication between innate and adaptive immune cells. By histological observation, it is obvious that tracheas of high Cl_2-exposed mice have robust airway infiltration of granulocytes (neutrophils) and agranulocytes (monocytes, macrophages) into the airspace at day 5. This robust infiltration is not observed after low dose Cl_2 exposure. Therefore, upregulation of migration and adhesion molecules is requisite for these cells to enter and remain in the airway. The canonical pathway "communication between innate and adaptive immune cells" is not

as overt because, as of yet, we have not extensively quantified immune cells traditionally associated with adaptive immunity (e.g. lymphocytes). However, the canonical pathways are chosen based on the number of overlapping molecules in the canonical pathway and the dataset of interest. The majority of overlapping molecules represented more strongly innate cells and/or immature myeloid cells than adaptive cell types. In the next two sections we will discuss the less obvious canonical pathways and how they might contribute to BO pathology.

5.4.1.1 IL-1β/LPS inhibition of retinoid x receptors

IL-1β/LPS inhibition of retinoid x receptors (RXR) is the third canonical pathway predicted to be activated. RXRs are nuclear hormone receptors that function as ligand-dependent transcription factors. The ligands for RXRs are retinoids, more commonly known as vitamin A and its derivates. RXRs are capable of forming homodimers and are common dimerization partners for other nuclear hormone receptors (e.g. retinoic acid receptors (RAR), peroxisome proliferator-assoicated receptor, liver X receptor) [110]. The distinct roles of RXR homo- and heterodimerization are not fully understood, but it is clear that responses are influenced by the nuclear receptor combination[110].

The IL-1β/LPS inhibition of RXR pathway was initially described in the liver upon observation that LPS stimulation resulted in a rapid repression of hepatic genes; this response is known as the negative hepatic acute phase response [111]. Later, it was demonstrated in the liver that LPS or IL-1β caused rapid reductions in nuclear levels of RXR, the major regulator of the hepatic genes involved in the acute phase response [112, 113]. It is unclear if a similar mechanism of RXR inhibition occurs in other tissues during infection or inflammation.

To our knowledge the IL-1β/LPS inhibition of RXR pathway has not been identified in the development of BO. Out of the 241 genes that comprise this canonical

pathway, 48 genes overlap with our high vs. low Cl_2 dataset. Transcripts of major upstream regulators of this pathway are increased, including IL-1β, TNFs, and TLRs (i.e. TLR1, 2, 6, 7, 8, and 13). Many transcripts of genes regulated by RXR are downregulated (data not shown). But without additional interrogation of the pathway in our model there is no implicit data to support this finding. However, there are several lines of evidence demonstrating that therapeutic agonism of RXR or RXR/PPAR elicits anti-inflammatory and anti-fibrotic responses; therefore such a therapy may be beneficial in our model. For example, *in vitro* retinoid treatment of activated macrophages resulted in decreased production of TNF-α, IL-12, and nitric oxide and increased production of the anti-inflammatory cytokine, IL-10 [114-116]. As shown in chapter 2, our BO model includes early invasion and accumulation of activated myeloid cells in the tracheal airspace. As a mechanism of action, we would predict that RXR angonism might suppress myeloid cell production of pro-inflammatory cytokines. Additionally, treatment of mice with RXR or RXR/RAR agonists resulted in the attenuation of liver fibrosis, kidney fibrosis, and radiation- and bleomycin-induced pulmonary fibrosis [117-119]. Our array data has predicted that the RXR pathway is turned "off" during the progression of BO. Turning "on" the pathway merits therapeutic consideration based on its anti-inflammatory and anti-fibrotic effects.

5.4.1.2 TREM-1 signaling

Triggering receptor expressed on myeloid cells 1 (TREM-1) is a 30kDa glycoprotein receptor and a member of the Ig superfamily. Myeloid cells constitutively express TREM-1 and upregulate it further when activated. This receptor was initially thought to be myeloid cell specific but increasing reports of TREM-1 expression on human airway epithelium suggest a broader distribution [120]. Activation of TREM-1 leads to the production of pro-inflammatory cytokines such as, TNFα, IL-1β, and IL-6.

Recently, platelets were confirmed as a ligand for TREM-1, but most likely there exist other unknown self and non-self ligands [121]. A soluble form of TREM-1 is generated by matrix metalloproteinase-mediated catalytic shedding; soluble TREM-1 is thought to compete for ligand as an inhibitory mechanism [122].

TREM-1 functions as an initiator and amplifier of inflammation in both infectious and non-infectious scenarios. For example, in a murine sepsis model, inhibition of TREM-1 signaling using either the soluble form of TREM-1, a small peptide TREM-1 antagonist, or siRNA techniques decreased inflammatory cytokines and improved survival [123-125]. The bulk of TREM-1 research has been investigated in the context of infections, but recently TREM-1 has gained recognition for its emerging role in the pathogenesis of non-infections diseases. Therapeutic targeting of TREM-1 has resulted in attenuation of collagen-induced arthritis, and mice deficient for *Trem1* demonstrated attenuated hepatocellular carcinogenesis [126, 127]. TREM-1's contribution to sterile inflammation requires further investigation.

Due to its shot intracellular domain, TREM-1 must associate with DAP12, a transmembrane adaptor protein, for signal transmission. Upstream signaling molecules include, Src, Syk, and Btk [128, 129]. Engagement of TREM-1 with DAP12 results in Src-mediated phosphorylation of DAP12, followed by phosphorylation of Syk and then Btk. Subsequent signaling molecules include, but are not restricted to, PI3K, PLCy, ERK 1/2 and NTAL. Increasing evidence shows that TREM-1 is capable of synergistic crosstalk with pattern recognition receptors, namely TLRs and NLRs [128].

TREM-1 signaling is the fifth canonical pathway predicted by IPA to be activated after exposure to high Cl_2. Out of the 71 genes that comprise TREM-1 signaling, 20 genes overlap with our high vs. low Cl_2 dataset. As of yet, TREM-1 signaling is not implicated in the pathogenesis of BO. However it is reasonable to predict activation of

TREM-1 in our BO model for the following reasons. 1) TREM-1 is primarily expressed on myeloid cells, and we histologically confirmed that activated myeloid cells infiltrate the airspace. 2) Transcripts of vital TREM-1 signaling components, DAP12, Syk and Btk are elevated in our dataset. 3) Transcripts of TREM-1 target genes are elevated (Il-1β, Il-6, TNFα, CCL2, CD86). 4) The TREM-1 pathway can be activated by and synergize with TLR pathways. Our data indicated increases in several TLR transcripts.

A proposed mechanism of action for TREM-1 in BO pathology is as follows: TREM-1 may initiate inflammation or enhance TLR-activated inflammatory processes of the myeloid cells infiltrating the airway. A persistent pro-inflammatory environment may sustain immune-mediated airway damage, resulting in delayed repair or, alternatively, it could perpetuate a program of inappropriate mesenchymal activation and chemoattraction into the airway. Due to the predicted activation of TREM-1 in our BO model and a successful history of TREM-1 therapeutic inhibition in other disease models, it will be interesting to evaluate the effects of TREM-1 inhibition in reducing inflammation and progression of BO in our model.

5.4.2 Predicted upstream regulators and enriched soluble mediators.

Kinases are attractive therapeutic targets; in the last decade small molecule inhibitors were developed that prevent kinase-specific signal transduction. For this reason we used IPA to query predicted upstream kinases. The top two candidates are a part of the inflammatory NFκB signaling pathway. This predicted activation is reasonable given the severe injury observed post Cl_2 exposure. The ERK 1/2 pathway was also identified. Previous literature suggests a role for this pathway in BO pathogenesis. In a heterophic transplant model of BO, CCR1 and CCR5 antagonism resulted in an approximately 60% reduction of tracheal occlusion. The authors correlated this to reduced ERK inhibition[130]. In humans, prophylactic treatment of BO with

macrolides such as azithromycin reduced the incidence of BO two years post transplant [131]. The drug was reported to inhibit ERK 1/2 as well as NFκB signaling[132]. However, it remains to be shown whether the drug's mechanism of action is via the prevention of inflammation-induced epithelial damage or suppression of fibrotic processes or both. Our model would be ideal to test the role of ERK 1/2 in the fibrotic processes leading to BO.

The top IPA predicted growth factors include epidermal growth factor (EGF) and hepatic growth factor (HGF). Dysregulation of EGF is associated with cancer and to a lesser extent with fibrosis. It has been reported to enhance mesenchymal survival and proliferation [133]. However, it is also important for epithelial cell survival and wound healing[133, 134]. The pleiotropic nature of the EGF pathway may preclude its use as a therapeutic. To our knowledge, EGF has not been associated with BO, and EGF was not identified as an upregulated transcript in our ANOVA analysis. In contrast, the other predicted growth factor, HGF, was upregulated 11-fold. Therapeutic administration of this ligand was demonstrated to reverse fibrosis in a bleomycin-induced murine model of pulmonary fibrosis. Evidence suggested that HGF induced myofibroblast apoptosis and extracellular matrix degradation [135, 136]. The role of HGF in BO is not known. We can speculate that our detected HGF upregulation indicates a natural anti-fibrotic response in the injured trachea. However, if there is a natural anti-fibrotic response, it is not strong enough to prevent fibrosis in our model. It would be interesting to test if augmenting natural HGF with recombinant HGF could attenuate fibrosis.

Our query of upregulated soluble ligands resulted in the identification of pro-inflammatory molecules including IL-6, IL-1β, IL-1α and TNFs. In particular, TNFs were enriched in our dataset suggesting that the TNF pathway is an important mediator of BO. Several lines of evidence in the literature support this idea. One particularly

informative study used a herterotopic transplant BO model to demonstrate that neutralization of TNF prevented transplant obstruction[137]. Neutralization of IL-1β was partially protective while neutralization of INF-γ or IL-6 was ineffective. In humans, elevated levels of TNF, IL-1β, TGFβ, and IL-8 have been reported in BALF from BO positive transplant patients[138-140]. However, these human clinical findings are highly variable. As mentioned above, azithromycin is a promising therapy for preventing BO; it is proposed to work via inhibition of the ERK and NFκB signaling pathways[141, 142]. Inhibition of these pathways it is thought to reduce pro-inflammatory cytokines, TNFα in particular. Whether the benefits in the above studies are a result of reduced tissue damage or suppression of fibrotic processes or both is unclear. Our data suggests that the TNF pathway may be an important regulator or initiator of fibrosis since our gene expressions were measured during early fibrotic changes in our model. It will be highly interesting to assess the affect of TNF neutralization or azithromycin on BO development after Cl_2 exposure.

5.4.3 CXCR2

One particularly interesting finding is that CXCR2 and its ligands are enriched in our microarray analysis. In chapter 3, we demonstrated that VEGFR-2 inhibition was insufficient to prevent BO after Cl_2-injury. In the discussion that followed, we proposed that an alternative CXCR2 pathway might mediate angiogenesis in our model. This hypothesis was additionally supported by a previous publication demonstrating that CXCR2 mediates angiogenesis in a heterotrophic transplant model of BO. However we did not have any experimental data to support this claim. Our microarray analysis allowed us to unbiasedly evaluate the enrichment of both VEGFR and CXCR2 pathways via upregulation of their respective receptors and ligands. Strikingly, no upregulated genes were detected in association with VEGFR. In contrast, CXCR2 and five of its

ligands were increased. These findings strongly suggest that the mechanism of neovascularization observed in the transplant model of BO is similarly active in our model. The same transplant publication reported that mRNA expression and protein levels of CXCL2 and 3 increased over the course of BO development, with maximum expression coinciding with fibroproliferation. Similarly, we detected elevated CXCL2 and 3 transcripts.

Our microarray analysis was able to identify an angiogenic pathway already implicated in the pathogenesis of BO. Validation of this pathway in our model could lead to exciting new insights into the pathogenesis of BO. For instance, there are significant differences between a transplant and chemical-induced BO model; including rejection-dependency and airway vs. subcutaneous location of the trachea. Validation of CXCR2-mediated angiogenesis in our model would suggest that it is a universal mechanism of BO shared by all inciting events. However, further experimentation is required before we can make such claims.

5.4.4 Concluding remarks and future directions

To our knowledge, only one study has published microarray-based gene expression analysis for a murine model of BO. Lande et al. conducted microarray anaylsis of isografts and allografts in a murine heterotophic tracheal transplant model of BO [143]. The majority of elevated transcripts were associated with T cell activation and humoral immunity, which limited their ability to identify genes associated with fibrosis and fibroproliferation. Our present analysis offers several advantages over this previous study. 1) Our chemical-induced BO model is not allorejection dependent and 2) avoids possible off-target findings that could arise from surgical tissue damage or 3) arise from exposure to extrapulmonary environments (subcutaneous relocation). 4) The BO developmental timeline is more synchronized in our model since mature epithelial

damage is immediate upon chemical inhalation and occlusive fibrosis occurs approximately 9 days post injury. Conversely, transplant BO models have longer timelines since immune-mediated epithelial damage occurs approximately 7 days post transplant, followed by fibrosis approximately 20 days post transplant. A more synchronized pathogenesis may lead to less variation in gene expression among individuals. Taken together, we argue that our gene expression increases are less likely to be dominated by alloimmune responses, allowing for greater sensitivity in the identification of underlying disease mechanisms. And finally, 5) the previous paper was published in 2005. Over the last eight years, analysis software, like IPA, has greatly improved and provides keen insight into the pathways represented in transcriptional profiles.

Studies in humans have attempted to link genetic polymorphisms to the occurrence of BO after lung transplantation. The most prominent findings are *IFNG*, *TGFB1*, and *IL6* functional polymorphisms that generally exacerbate inflammation and fibrosis[144]. However the sample sizes for many of these studies are small and findings between studies have been inconsistent. It is unclear which pathogenic events these genetic variations most greatly influence or if they are applicable to non-transplant BO. In our analysis, only IL-6 is upregulated. But as mentioned previously neutralization of INF-γ or IL-6 was ineffective at preventing airway obliteration in a herterotopic transplant BO model[137]. In sum, we do not consider INF-γ, TGF- β or IL-6 primary candidates for mediators of BO in our model.

We must concede that microarray analysis and subsequent pathway analysis is not without its limitations. It is important to note that a normal trachea is very different after injury, in terms of activation and cellular content. Due to such dramatic changes in cellular composition, it can be difficult to determine if an enriched pathway is

biologically significant in the pathogenesis of BO or whether the pathway is enriched because it is a bystander pathway in a newly recruited cell type. Additionally, when trying to analyze complex biological processes from a whole genome screen, we assume that some of the analysis will garner false positives or overlook potential pathways entirely. As was the case when we independently queried our dataset and identified CXCR2 as a potential regulator of angiogenesis, a pathway not identified by IPA. However, we were able to confirm the general accuracy of IPA's functional analysis by comparing it with our extensive knowledge of the histopathologic progression of Cl_2-induced BO. But the real power of gene expression analysis is not confirming what is known, but suggesting what is unknown.

Our analysis has narrowed our focus to a few choice pathways for future investigation. To our knowledge, the two canonical pathways, TREM-1 signaling and RXR, have never before been associated with BO. Due to their associations with inflammation and/or fibrosis, both pathways merit future interrogation for their role in BO pathogenesis. These pathways can be targeted using TREM-1 neutralizing antibodies and RXR agonists, respectively. Additionally, we will investigate the role of ERK, NFκB, and TNF signaling pathways. These pathways are already associated with BO although their mechanisms of action are unclear. Using our model, we will be able to assess their pathological contributions to BO, particularly their contributions to fibrotic processes after significant inciting epithelial cell damage. Modulation of these pathways can be achieved using small molecule inhibitors or, in the case of TNF, neutralizing antibodies. We also plan to revisit neovascularization in our model now that our data suggests the process is mediated by CXCR2. CXCR2 has multiple ligands, but by using a CXCR2 antibody antagonist we should be able to prevent CXCR2 signaling and determine its effect on neovascularization of BO lesions post Cl_2 injury. Our findings are only the start

for dissecting apart the complex processes that fuel BO. We will move forward with validating the activation of our chosen targets and evaluating their contribution to BO pathogenesis *in vivo*.

6. Cellular recruitment and accumulation in the lung after exposure to moderate Cl_2 concentrations

6.1 Introduction

Whereas in earlier chapters we focused on fibrotic consequences following high concentrations of Cl_2, in this chapter we will focus on inflammation in the lower airways and lungs following exposure to moderate concentrations of Cl_2. Acute inhalation of toxic chemicals such as Cl_2 causes a spectrum of clinical syndromes in humans. Direct mechanisms of Cl_2 primarily involve oxidative damage to the airway and were discussed in the introduction. Indirect mechanisms are not clearly understood. In chapter 5, we concluded that NOS2 did not contribute to the fibrotic pathology observed in our Cl_2-induced BO model; however, previous studies have highlighted the importance of NOS2 in other Cl_2-induced syndromes by demonstrating that prophylactic pharmacological inhibition of NOS2 mitigated AHR after Cl_2 injury [99]. However, after Cl_2 exposure, the pathology-driving source of NOS2 has not been indentified.

Previously our lab demonstrated that $CCR2^+$ inflammatory monocytes mediated immune pathology in a model of influenza infection and that pharmacologically inhibiting recruitment of these cells to the site of injury mitigated disease severity [92]. Once recruited to the lung, inflammatory monocytes differentiated into inflammatory dendritic cells and exudate macrophages that produced tissue-damaging levels of TNFα and NOS2. Since trafficking of inflammatory monocytes into inflamed tissue is CCR2-dependent, *Ccr2*-deficient mice have impaired recruitment of these cells into the lung after injury [92, 145-147]. We reported that influenza-induced morbidity and mortality were reduced in *Ccr2*-deficient mice and in wild-type mice when treated with a CCR2

antagonist[148]. Correlating with fewer inflammatory monocytes, NOS2 expression was also significantly reduced[92].

Here, we propose that $CCR2^+$ inflammatory monocytes and their derivates, exudate macrophages, are a pathologic source of NOS2 after Cl_2 injury. In this chapter, we evaluated inflammatory monocyte and exudative macrophage accumulation in Cl_2-exposed lungs and determined the effects of CCR2 deficiency and NOS2 deficiency on the accumulation of inflammatory cells in the lungs of Cl_2-exposed mice.

6.2 Materials and methods

Mice. C57BL/6 and *Ccr2*-deficient were purchased from Charles River Laboratories (Wilmington, MA) and *Nos2*-deficient mice (stock # 002596) were purchased from Jackson Laboratory (Bar Harbor, ME). All animal experiments were conducted in accordance with National Institutes of Health guidelines and protocols approved by the Animal Care and Use Committee at Duke University.

Chlorine exposure. Mice were exposed as described in chapter 2 with the exception that all Cl_2 concentrations were 190ppm.

Lung cell isolation and flow-cytometric analysis. Lungs were slowly perfused with 3-5 ml of cold PBS and then maximally inflated with digestion media: 1.5 mg/ml collagenase, 0.4 mg/ml DNase I, 5% FBS and 10mM HEPES in HBSS. The lung lobes were dissected from the rest of the airway and digested in 5 mls of digestion media at 37 degrees C for 30 minutes. Tissues were gently vortexed every 10 minutes during incubation. 25 mls of PBS were added and the tissues were vigorously vortexed for 30 seconds. The disassociated tissue was strained through a 70μm cell strainer. Cells were washed and red blood cells lysed. Cells were resuspended in 5 mls of PBS. $5x10^6$ cells were stained in PBS with Live/Dead Aqua (Molecular Probes, Grand Island, NY). Cells were washed then blocked for 10 minutes at 4 degrees C in a blocking buffer: 10 mM

EDTA, 1% BSA, 5% normal mouse serum, 5% normal rat serum, and 1% Fc block (eBioscience, San Diego, CA) in PBS. Cells were stained with antibodies for 30 min, total volume 100ul, then washed three times and analyzed using a BD LSRII flow cytometer. Antibodies used included: CD49b-PE, CD11c-PerCP-Cy5.5, CD45-Qdot605, IA/IE-Qdot655 from eBioscience and CD11b-PE-Cy7, Gr-1-APC-Cy7, Ly6G-V450 from BD Pharmingen (San Jose, CA).

Statistics. All numerical data are presented as mean ± SD. All data are analyzed by Student's t tests using Prism software (GraphPad, San Diego, CA) as indicated in the figure legends.

6.3 Results

6.3.1 Monocyte-derived macrophages and dendritic cells do not accumulate in the lungs after moderate Cl_2 inhalation

Previous histopathologic and bronchoalveolar lavage data have shown an accumulation of inflammatory cells, such as neutrophils and macrophages, in the airways after Cl_2 exposure [56, 99, 149, 150], but no one has specifically shown inflammatory monocyte and exudate macrophage accumulation in the lung. Monocyte and macrophage subsets have similar morphologies and can only be differentiated using a combination of surface markers that are specific to each subset [151]. Our lab developed a flow cytometry protocol consisting of 10 surface antigens that allowed us to label and quantify the majority of myeloid cell subsets in homogenized lung tissue. Using this protocol we expanded upon previous morphology-based myeloid cell enumerations and quantified phenotypically different myeloid subsets within lung tissue after Cl_2. Our gating strategy for quantifying cell populations is outlined in Figure 16A. We began our investigation by analyzing inflammatory cell recruitment into the lungs 3 and 8 days post exposure to 190ppm of Cl_2. Specifically, we investigated exudate

macrophage accumulation. Lin et al. identified exudate macrophages as $CD11b^{+}$, $CD11c^{+}$, $MHCII^{high}$, and $Gr\text{-}1^{high}$ upon recent recruitment into the lung [92]. In agreement with previous literature, we found that exudate macrophages are not present at baseline (Figure 16B). However, our results also showed that exudate macrophages do not accumulate in the lungs on day 3 (Figure 16B) or day 8 (data not shown) post Cl_2 exposure. Additionally, we did not observe the accumulation of any new populations exceeding baseline populations (data not shown).

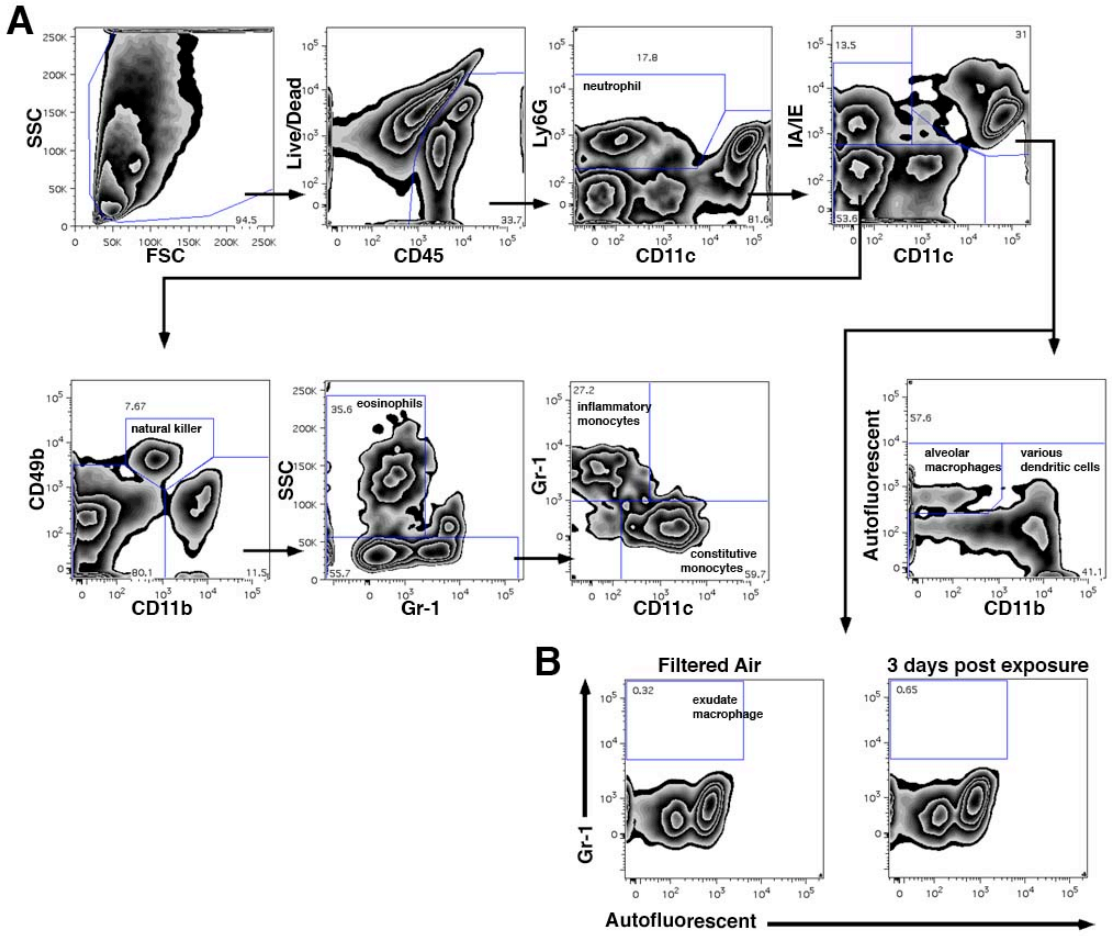

Figure 16: Representative gating strategy for quantification of myeloid subsets.

A) Gating strategy in a FA-exposed mouse. Surface marker expression of myeloid subsets are as follows: neutrophils ($CD45^{+}$, $Ly6G^{high}$); alveolar macrophages ($CD45^{+}$, $CD11c^{high}$, IA/IE^{int}, $Autofluorescent^{+}$, $CD11b^{-}$); dendritic cells ($CD45^{+}$, $CD11c^{int/hi}$, IA/IE^{high}, $Autofluorescent^{-}$, $CD11b^{+/-}$); inflammatory monocytes ($CD45^{+}$, $CD11c^{-}$, IA/IE^{-}, $CD11b^{+}$, $Gr\text{-}1^{+}$); constitutive monocyte ($CD45^{+}$, $CD11c^{int}$, IA/IE^{-}, $CD11b^{+}$, $Gr\text{-}1^{-}$). B) Historically, exudate macrophages are present in the IA/IE^{+}, $CD11c^{+}$ gate and are $Gr\text{-}1^{hi}$. 3 days post Cl_2 exposure, no exudate macrophages are detected.

6.3.2 Effect of CCR2 deficiency on inflammatory cell infiltration and accumulation in the lung

CCR2 and its ligand MCP-1 comprise a major axis of chemoattraction mediating inflammatory monocyte recruitment into inflamed tissue. *Ccr2*-deficient mice have impaired recruitment of these cells into inflamed tissue. We investigated whether CCR2 deficiency affects the accumulation of myeloid cell populations after Cl_2 injury.

In wild-type mice, there was no significant change in myeloid cell populations after Cl_2 inhalation; these include alveolar macrophages, dendritic cells, neutrophils, inflammatory monocytes and constitutive monocytes (Figure 17, white bars). In agreement with previous studies, *Ccr2*-deficient mice have significantly fewer inflammatory monocytes at baseline, approximately 4-fold reduction [92, 152](Figure 17, black lines). This trend was significant and persisted at all timepoints. Additionally, alveolar macrophages and dendritic cell numbers were significantly reduced at baseline compared to wild-type. These reductions have not been previously reported and may be an incidental finding. We found no other differences between wild-type and *Ccr2*-deficient mice that we deemed potentially biologically significant.

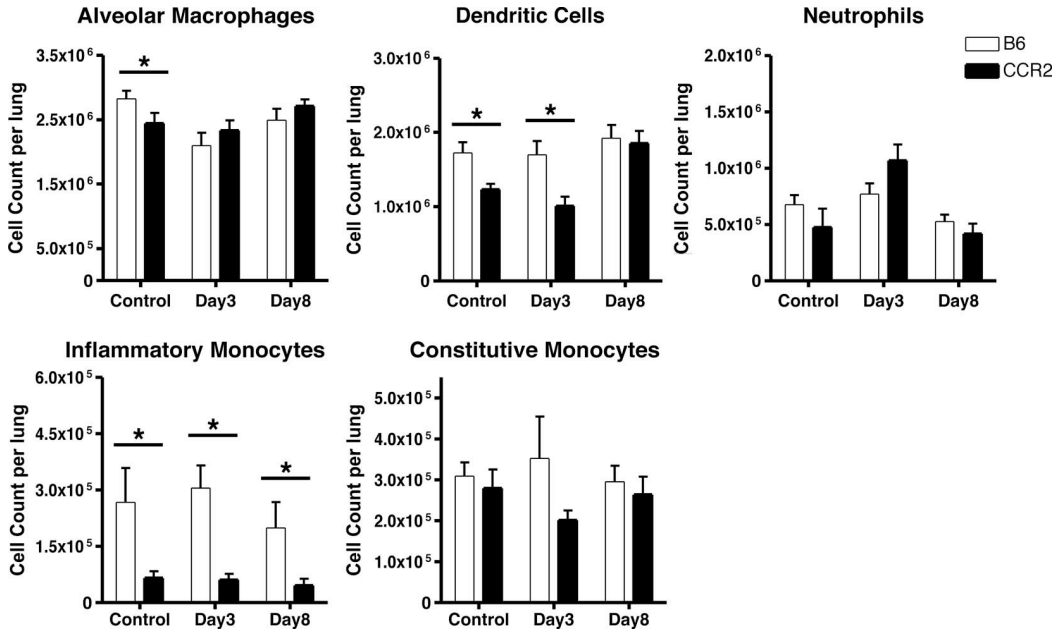

Figure 17: Quantification of lung myeloid cell populations in *Ccr2*-deficient mice.

Mice were exposed to 190 ppm Cl_2. On days 3 and 8 post exposure, lung homogenates were stained for flow cytometric analysis. Using the gating strategy from Figure 16, myeloid cell populations were quantified for wild-type (B6; n=9-10 mice per timepoint) and *Ccr2*-deficient (CCR2; n=8-10 mice per timepoint). *, $p<0.05$ by student's t test, data are presented as mean ± SEM.

6.3.3 Effect of NOS2 deficiency on inflammatory cell infiltration and accumulation in the lung.

Since a previous paper demonstrated that elevated AHR after Cl_2 inhalation was NOS2-dependent, we investigated whether *Nos2*-deficient mice had different inflammatory cell accumulation after injury. Our results showed baseline differences between wild-type and *Nos2*-deficient mice, specifically, a 3-fold increase in inflammatory monocytes and a 2-fold decrease in dendritic cells (Figure 18). There was a trend toward fewer constitutive monocytes; this trend persists across all timepoints. To our knowledge these differences have not been previously reported and may be an incidental finding. Another possible explanation is that the *Nos2*-deficient mice are on a 129 genetic background and the control is a wild-type C57Bl/6. It is known that tissue resident cell numbers can differ according to genetic background. After Cl_2 injury, cell populations in *Nos2*-deficient mice did not significantly change from baseline measurements. We found no accumulation of exudate macrophages in *Nos2*-deficient mice (data not shown) and no other cellular differences that we deemed potentially biologically significant.

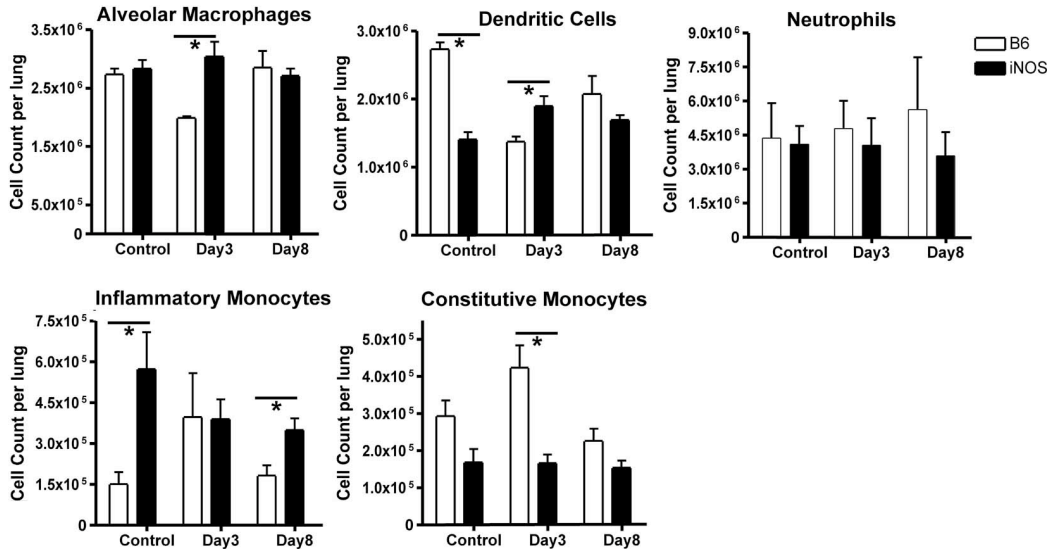

Figure 18: Quantification of lung myeloid cell populations in *Nos*2-deficient mice.

Mice were exposed to 190 ppm Cl_2. On days 3 and 8 post exposure, lung homogenates were stained for flow cytometric analysis. Using the gating strategy from Figure 16, myeloid cell populations were quantified for wild-type (B6; n=4-5 mice per timepoint) and *Nos*2-deficient (iNOS; n=4 mice per timepoint). *, $p<0.05$ by student's t test, data are presented as mean ± SEM.

6.4 Discussion

Cl_2 inhalation results in airway abnormalities that are in part mediated by inflammation[99]. In this chapter, we demonstrated that $CCR2^+$ monocyte-derived cells are not major contributors to inflammation after Cl_2 injury. We based this conclusion on our findings that $CCR2^+$ inflammatory monocytes did not significantly accumulate in the lung and, accordingly, $CCR2^+$ monocyte-derived cells were not detected after injury. Multiple factors could contribute to our observed lack of recruitment into lung tissue. Firstly, moderate Cl_2 exposure primarily damages the airway [149, 153, 154]. We take into consideration that our whole lung analysis may not be sensitive enough to reflect leukocyte infiltration and accumulation specific to the airway. Previous reports in Cl_2-injury models quantified cells from BALF[99, 149, 153]. This technique results in direct leukocyte sampling along the route of injury and not in the lung parenchyma. In addition, Cl_2 injury is a sterile form of inflammation with no foreign immunogen to activate time-honed pathogen-associated molecular patterns (PAMPs). Significant recruitment and accumulation of myeloid cells in the lung is observed during PAMP-activating viral [92, 97] or bacterial lung infection [155] suggesting that different inflammatory stimuli are more effective at recruiting inflammatory monocytes than others.

We also observed that inflammatory cell populations in *Nos2*-deficient mice did not fluctuate from the *Nos2*-deficient baseline. Our findings share the limitations mentioned above. Additionally, *Nos2*-deficiency most likely affects immune cell activation and effector functions instead of directly affecting immune cell trafficking.

However, it is impossible to make conclusions about the effects of cellular accumulation or activation on the pathogenesis of Cl_2-induced acute lung injury or

RADS without data linking observed changes to physiologic outcomes. The above studies were preliminary experiments to confirm the presence of exudate macrophages, a potential cellular source of NOS2. In this goal, we successfully confirmed that there was no accumulation of exudate macrophages in the lungs of Cl_2 exposed mice. Therefore, exudate macrophages are not a pathogenic source of NOS2 in our model. Due to the meager recruitment of inflammatory cells into the lung, we suggest that future research should focus on resident immune cells, including alveolar macrophages, and non-immune cells, including the epithelial cells, as pathogenic sources of NOS2 in Cl_2 injury.

7. Final remarks

This dissertation advances the field of BO research in several ways. First, we characterized a novel murine model of Cl_2-induced BO. It is our hope that this model becomes a staple in BO research as it offers several distinct advantages over traditional transplant BO models, including allorejection independence and greater feasibility in terms of technique and throughput. Additionally, the well-demarcated series of pathological changes in our model will allow a more detailed analysis of the individual cellular and molecular events that lead from basal cell loss to airway occlusion. Secondly, by using this model we demonstrated that in the absence of basal cells, epithelial regeneration does not occur and regions of epithelial denudation persist from which an aberrant repair process is initiated, leading to obliterative airway lesions. Our findings suggest that, irrespective of the cause, loss of epithelial progenitor cells may be a critical factor leading to the development of BO. We encourage further analysis of epithelial progenitor populations in other models of BO to fully ascertain the commonality of this inciting event. Epithelial progenitor cells may become a novel therapeutic target for which therapies protect and sustain critical progenitor cells in the face of injury. And finally, to our knowledge, we are the first to use microarray technology to analyze gene expression profiles in a chemical-induced BO model. Our data identified molecular mediators already associated with BO pathogenesis, including CXCR2, TNFs, ERK, and NFkB. But more importantly, it identified novel molecular mediators, including TREM-1, RXRs and HGF. However, these therapeutic targets require further validation. Our findings are only the start for dissecting the complex processes that drive BO pathogenesis. We fully expect that our Cl_2-induced BO model will be an invaluable resource to systematically test our therapeutic targets for the prevention of BO.

References

1. **Rock, J.R. and B.L. Hogan,** ***Epithelial progenitor cells in lung development, maintenance, repair, and disease.*** **Annu Rev Cell Dev Biol, 2011. 27: p. 493-512.**

2. **Rackley, C.R. and B.R. Stripp,** ***Building and maintaining the epithelium of the lung.*** **J Clin Invest, 2012. 122(8): p. 2724-30.**

3. **Vareille, M., et al.,** ***The airway epithelium: soldier in the fight against respiratory viruses.*** **Clin Microbiol Rev, 2011. 24(1): p. 210-29.**

4. **Rock, J.R., et al.,** ***Basal cells as stem cells of the mouse trachea and human airway epithelium.*** **Proc Natl Acad Sci U S A, 2009. 106(31): p. 12771-5.**

5. **Rock, J.R., S.H. Randell, and B.L. Hogan,** ***Airway basal stem cells: a perspective on their roles in epithelial homeostasis and remodeling.*** **Dis Model Mech, 2010. 3(9-10): p. 545-56.**

6. **Hong, K.U., et al.,** ***In vivo differentiation potential of tracheal basal cells: evidence for multipotent and unipotent subpopulations.*** **Am J Physiol Lung Cell Mol Physiol, 2004. 286(4): p. L643-9.**

7. **Demoly, P., et al.,** ***Cell proliferation in the bronchial mucosa of asthmatics and chronic bronchitics.*** **Am J Respir Crit Care Med, 1994. 150(1): p. 214-7.**

8. **Yahaya, B.,** ***Understanding cellular mechanisms underlying airway epithelial repair: selecting the most appropriate animal models.*** **ScientificWorldJournal, 2012. 2012: p. 961684.**

9. **Borthwick, D.W., et al.,** ***Evidence for stem-cell niches in the tracheal epithelium.*** **Am J Respir Cell Mol Biol, 2001. 24(6): p. 662-70.**

10. **O'Koren, E.G., B.L. Hogan, and M.D. Gunn,** ***Loss of Basal Cells Precedes Bronchiolitis Obliterans-Like Pathological Changes in a Murine Model of Chlorine Gas Inhalation.*** **Am J Respir Cell Mol Biol, 2013. 49(5): p. 788-97. Reprinted with permission of the American Thoracic Society. Copyright © 2012 American Thoracic Society.**

11. **Erjefalt, J.S., et al.,** ***In vivo restitution of airway epithelium.*** **Cell Tissue Res, 1995. 281(2): p. 305-16.**

12. **Puchelle, E., et al.,** ***Airway epithelial repair, regeneration, and remodeling after injury in chronic obstructive pulmonary disease.*** **Proc Am Thorac Soc, 2006. 3(8): p. 726-33.**

13. **Hajj, R., et al.,** ***Basal cells of the human adult airway surface epithelium retain transit-amplifying cell properties.*** **Stem Cells, 2007. 25(1): p. 139-48.**

14. **Weiss, D.J., et al.,** ***Stem cells and cell therapies in lung biology and lung diseases.*** **Proc Am Thorac Soc, 2011. 8(3): p. 223-72.**

15. **Coraux, C., et al.,** ***Epithelial cell-extracellular matrix interactions and stem cells in airway epithelial regeneration.*** **Proc Am Thorac Soc, 2008. 5(6): p. 689-94.**

16. **Epler, G.R.,** ***Constrictive bronchiolitis obliterans: the fibrotic airway disorder.*** **Expert Rev Respir Med, 2007. 1(1): p. 139-47.**

17. **Egan, J.J.,** ***Obliterative bronchiolitis after lung transplantation - A repetitive multiple injury airway disease.*** **American Journal of Respiratory and Critical Care Medicine, 2004. 170(9): p. 931-932.**

18. **Scott, A.I., L.D. Sharples, and S. Stewart,** ***Bronchiolitis obliterans syndrome: risk factors and therapeutic strategies.*** **Drugs, 2005. 65(6): p. 761-71.**

19. **Kuo, E., et al.,** ***Animal models for bronchiolitis obliterans syndrome following human lung transplantation.*** **Immunol Res, 2005. 33(1): p. 69-81.**

20. **Hayes, D., Jr.,** ***A review of bronchiolitis obliterans syndrome and therapeutic strategies.*** **J Cardiothorac Surg, 2011. 6: p. 92.**

21. **Boswell, R.T. and R.J. McCunney,** ***Bronchiolitis obliterans from exposure to incinerator fly ash.*** **J Occup Environ Med, 1995. 37(7): p. 850-5.**

22. **Palmer, S.M., et al.,** ***Severe airway epithelial injury, aberrant repair and bronchiolitis obliterans develops after diacetyl instillation in rats.*** **PLoS One, 2011. 6(3): p. e17644.**

23. **King, M.S., et al.,** ***Constrictive bronchiolitis in soldiers returning from Iraq and Afghanistan.*** **N Engl J Med, 2011. 365(3): p. 222-30.**

24. **Epler, G.R.,** ***Bronchiolitis obliterans organizing pneumonia, 25 years: a variety of causes, but what are the treatment options?*** **Expert Rev Respir Med, 2011. 5(3): p. 353-61.**

25. **King, T.E., Jr.,** ***Overview of bronchiolitis.*** **Clin Chest Med, 1993. 14(4): p. 607-10.**

26. **Gottlieb, J., et al.,** ***Long-term azithromycin for bronchiolitis obliterans syndrome after lung transplantation.*** **Transplantation, 2008. 85(1): p. 36-41.**

27. **Johnson, B.A., et al.,** ***Statin use is associated with improved function and survival of lung allografts.*** **Am J Respir Crit Care Med, 2003. 167(9): p. 1271-8.**

28. **Pettersson, G.B., et al.,** ***Comparative study of bronchial artery revascularization in lung transplantation.*** **J Thorac Cardiovasc Surg, 2013. 146(4): p. 894-900 e3.**

29. **Norgaard, M.A., C.B. Andersen, and G. Pettersson,** ***Does bronchial artery revascularization influence results concerning bronchiolitis obliterans syndrome and/or obliterative bronchiolitis after lung transplantation?*** **Eur J Cardiothorac Surg, 1998. 14(3): p. 311-8.**

30. **Zinkernagel, A.S., R.S. Johnson, and V. Nizet,** ***Hypoxia inducible factor (HIF) function in innate immunity and infection.*** **J Mol Med (Berl), 2007. 85(12): p. 1339-46.**

31. **Hachem, R.R., et al.,** ***The significance of a single episode of minimal acute rejection after lung transplantation.*** **Transplantation, 2005. 80(10): p. 1406-13.**

32. **Wilkes, D.S.,** ***Airway hypoxia, bronchiolar artery revascularization, and obliterative bronchiolitis/bronchiolitis obliterans syndrome: are we there yet?*** **Am J Respir Crit Care Med, 2010. 182(2): p. 136-7.**

33. **Magro, C.M., et al.,** ***Association of humoral immunity and bronchiolitis obliterans syndrome.*** **Am J Transplant, 2003. 3(9): p. 1155-66.**

34. **Nicod, L.P.,** ***Mechanisms of airway obliteration after lung transplantation.*** **Proc Am Thorac Soc, 2006. 3(5): p. 444-9.**

35. **Chong, A.S. and M.L. Alegre,** ***The impact of infection and tissue damage in solid-organ transplantation.*** **Nat Rev Immunol, 2012. 12(6): p. 459-71.**

36. **Okazaki, M., et al.,** ***Maintenance of airway epithelium in acutely rejected orthotopic vascularized mouse lung transplants.*** **Am J Respir Cell Mol Biol, 2007. 37(6): p. 625-30.**

37. **Fernandez, F.G., et al.,** ***Airway epithelium is the primary target of allograft rejection in murine obliterative airway disease.*** **Am J Transplant, 2004. 4(3): p. 319-25.**

38. **Perl, A.K., D. Riethmacher, and J.A. Whitsett,** ***Conditional depletion of airway progenitor cells induces peribronchiolar fibrosis.*** **Am J Respir Crit Care Med, 2011. 183(4): p. 511-21.**

39. **Sisson, T.H., et al.,** ***Targeted injury of type II alveolar epithelial cells induces pulmonary fibrosis.*** **Am J Respir Crit Care Med, 2010. 181(3): p. 254-63.**

40. **Sato, M., S. Keshavjee, and M. Liu,** ***Translational research: animal models of obliterative bronchiolitis after lung transplantation.*** **Am J Transplant, 2009. 9(9): p. 1981-7.**

41. **Jungraithmayr, W., et al.,** ***Small animal models of experimental obliterative bronchiolitis.*** **Am J Respir Cell Mol Biol, 2013. 48(6): p. 675-84.**

42. **Lai, R.S., et al.,** ***Outbreak of bronchiolitis obliterans associated with consumption of Sauropus androgynus in Taiwan.*** **Lancet, 1996. 348(9020): p. 83-5.**

43. **Svetlecic, J., A. Molteni, and B. Herndon,** ***Bronchiolitis obliterans induced by intratracheal papaverine: a novel animal model.*** **Lung, 2004. 182(2): p. 119-34.**

44. **Li, B., et al.,** ***Chronic aspiration of gastric fluid induces the development of obliterative bronchiolitis in rat lung transplants.*** **Am J Transplant, 2008. 8(8): p. 1614-21.**

45. **Li, X., et al.,** ***Oleic acid-associated bronchiolitis obliterans-organizing pneumonia in beagle dogs.*** **Vet Pathol, 2006. 43(2): p. 183-5.**

46. **Parrish, J.S. and D.A. Bradshaw,** ***Toxic inhalational injury: gas, vapor and vesicant exposure.*** **Respir Care Clin N Am, 2004. 10(1): p. 43-58.**

47. **Evans, R.B.,** ***Chlorine: state of the art.*** **Lung, 2005. 183(3): p. 151-67.**

48. **Van Sickle, D., et al.,** ***Acute health effects after exposure to chlorine gas released after a train derailment.*** **The American journal of emergency medicine, 2009. 27(1): p. 1-7.**

49. **Leroyer, C., et al.,** ***Changes in airway function and bronchial responsiveness after acute occupational exposure to chlorine leading to treatment in a first aid unit.*** **Occup Environ Med, 1998. 55(5): p. 356-9.**

50. **Mrvos, R., B.S. Dean, and E.P. Krenzelok,** ***Home exposures to chlorine/chloramine gas: review of 216 cases.*** **South Med J, 1993. 86(6): p. 654-7.**

51. **Jones, R., B. Wills, and C. Kang,** ***Chlorine gas: an evolving hazardous material threat and unconventional weapon.*** **West J Emerg Med, 2010. 11(2): p. 151-6.**

52. **Courteau, J.P., et al.,** *Survey of construction workers repeatedly exposed to chlorine over a three to six month period in a pulpmill: I. Exposure and symptomatology.* **Occup Environ Med, 1994. 51(4): p. 219-24.**

53. **Yadav, A.K., et al.,** *Mechanisms and modification of chlorine-induced lung injury in animals.* **Proc Am Thorac Soc, 2010. 7(4): p. 278-83.**

54. **Song, W., et al.,** *Inhibition of lung fluid clearance and epithelial Na+ channels by chlorine, hypochlorous acid, and chloramines.* **J Biol Chem, 2010. 285(13): p. 9716-28.**

55. **Leustik, M., et al.,** *Mitigation of chlorine-induced lung injury by low-molecular-weight antioxidants.* **Am J Physiol Lung Cell Mol Physiol, 2008. 295(5): p. L733-43.**

56. **Winder, C.,** *The toxicology of chlorine.* **Environ Res, 2001. 85(2): p. 105-14.**

57. **Schwartz, D.A., D.D. Smith, and S. Lakshminarayan,** *The pulmonary sequelae associated with accidental inhalation of chlorine gas.* **Chest, 1990. 97(4): p. 820-5.**

58. **Bherer, L., et al.,** *Survey of construction workers repeatedly exposed to chlorine over a three to six month period in a pulpmill: II. Follow up of affected workers by questionnaire, spirometry, and assessment of bronchial responsiveness 18 to 24 months after exposure ended.* **Occup Environ Med, 1994. 51(4): p. 225-8.**

59. **Babu, A.N., et al.,** *Microvascular destruction identifies murine allografts that cannot be rescued from airway fibrosis.* **J Clin Invest, 2007. 117(12): p. 3774-85.**

60. **Snell, G.I. and G.P. Westall,** *The contribution of airway ischemia and vascular remodelling to the pathophysiology of bronchiolitis obliterans syndrome and chronic lung allograft dysfunction.* **Curr Opin Organ Transplant, 2010. 15(5): p. 558-62.**

61. **Ropponen, J.O., et al.,** *Innate and adaptive immune responses in obliterative airway disease in rat tracheal allografts.* **J Heart Lung Transplant, 2011. 30(6): p. 707-16.**

62. **Bitron, M.D. and E.F. Aharonson,** *Delayed mortality of mice following inhalation of acute doses of CH2O, SO2Cl2, and Br2.* **Am Ind Hyg Assoc J, 1978. 39(2): p. 129-38.**

63. **Basset, F., et al.,** *Intraluminal fibrosis in interstitial lung disorders.* **Am J Pathol, 1986. 122(3): p. 443-61.**

64. **Musah, S., J. Chen, and G.W. Hoyle,** *Repair of tracheal epithelium by basal cells after chlorine-induced injury.* **Respir Res, 2012. 13: p. 107.**

65. **Rock, J.R., et al.,** *Notch-dependent differentiation of adult airway basal stem cells.* **Cell Stem Cell, 2011. 8(6): p. 639-48.**

66. **Daniels, G.M. and S.G. Amara,** *Selective labeling of neurotransmitter transporters at the cell surface.* **Methods Enzymol, 1998. 296: p. 307-18.**

67. **Liu, X., R.R. Driskell, and J.F. Engelhardt,** *Stem cells in the lung.* **Methods Enzymol, 2006. 419: p. 285-321.**

68. **Hubbs, A.F., et al.,** *Respiratory toxicologic pathology of inhaled diacetyl in sprague-dawley rats.* **Toxicol Pathol, 2008. 36(2): p. 330-44.**

69. **Ghanei, M., et al.,** *Use of immunohistochemistry techniques in patients exposed to sulphur mustard gas.* **Patholog Res Int, 2011. 2011: p. 659603.**

70. **Mo, Y., et al.,** *Differential susceptibility of inbred mouse strains to chlorine-induced airway fibrosis.* **Am J Physiol Lung Cell Mol Physiol, 2013. 304(2): p. L92-102.**

71. **Costa, C.L., et al.,** *Nitric acid-induced bronchiolitis in rats mimics childhood Bronchiolitis obliterans.* **Respiration, 2005. 72(6): p. 642-9.**

72. **Teisanu, R.M., et al.,** *Functional analysis of two distinct bronchiolar progenitors during lung injury and repair.* **Am J Respir Cell Mol Biol, 2011. 44(6): p. 794-803.**

73. **Belperio, J.A., et al.,** *Role of CXCR2/CXCR2 ligands in vascular remodeling during bronchiolitis obliterans syndrome.* **J Clin Invest, 2005. 115(5): p. 1150-62.**

74. **Simons, M.,** *An inside view: VEGF receptor trafficking and signaling.* **Physiology (Bethesda), 2012. 27(4): p. 213-22.**

75. **Hoeben, A., et al.,** *Vascular endothelial growth factor and angiogenesis.* **Pharmacol Rev, 2004. 56(4): p. 549-80.**

76. **Vieira, J.M., et al.,** *Expression of vascular endothelial growth factor (VEGF) and its receptors in thyroid carcinomas of follicular origin: a potential autocrine loop.* **Eur J Endocrinol, 2005. 153(5): p. 701-9.**

77. **Sawano, A., et al.,** *Flt-1, vascular endothelial growth factor receptor 1, is a novel cell surface marker for the lineage of monocyte-macrophages in humans.* **Blood, 2001. 97(3): p. 785-91.**

78. **Selheim, F., H. Holmsen, and F.S. Vassbotn,** *Identification of functional VEGF receptors on human platelets.* **FEBS Lett, 2002. 512(1-3): p. 107-10.**

79. **Tabernero, J.,** *The role of VEGF and EGFR inhibition: implications for combining anti-VEGF and anti-EGFR agents.* **Mol Cancer Res, 2007. 5(3): p. 203-20.**

80. **Kuo, C.J., et al.,** *Comparative evaluation of the antitumor activity of antiangiogenic proteins delivered by gene transfer.* **Proc Natl Acad Sci U S A, 2001. 98(8): p. 4605-10.**

81. **Bruns, C.J., et al.,** *Effect of the vascular endothelial growth factor receptor-2 antibody DC101 plus gemcitabine on growth, metastasis and angiogenesis of human pancreatic cancer growing orthotopically in nude mice.* **Int J Cancer, 2002. 102(2): p. 101-8.**

82. **Facemire, C.S., et al.,** *Vascular endothelial growth factor receptor 2 controls blood pressure by regulating nitric oxide synthase expression.* **Hypertension, 2009. 54(3): p. 652-8.**

83. **Maynard, S.E., et al.,** *Excess placental soluble fms-like tyrosine kinase 1 (sFlt1) may contribute to endothelial dysfunction, hypertension, and proteinuria in preeclampsia.* **J Clin Invest, 2003. 111(5): p. 649-58.**

84. **Meyer, K.C., et al.,** *Vascular endothelial growth factor in human lung transplantation.* **Chest, 2001. 119(1): p. 137-43.**

85. **Keane, M.P., et al.,** *Neutralization of the CXC chemokine, macrophage inflammatory protein-2, attenuates bleomycin-induced pulmonary fibrosis.* **J Immunol, 1999. 162(9): p. 5511-8.**

86. **Garkavtsev, I., et al.,** *The candidate tumour suppressor protein ING4 regulates brain tumour growth and angiogenesis.* **Nature, 2004. 428(6980): p. 328-32.**

87. **Keane, M.P., et al.,** *Imbalance in the expression of CXC chemokines correlates with bronchoalveolar lavage fluid angiogenic activity and procollagen levels in acute respiratory distress syndrome.* **J Immunol, 2002. 169(11): p. 6515-21.**

88. **Keane, M.P., et al.,** *Depletion of CXCR2 inhibits tumor growth and angiogenesis in a murine model of lung cancer.* **J Immunol, 2004. 172(5): p. 2853-60.**

89. **Matsuo, Y., et al.,** *CXC-chemokine/CXCR2 biological axis promotes angiogenesis in vitro and in vivo in pancreatic cancer.* **Int J Cancer, 2009. 125(5): p. 1027-37.**

90. **Alderton, W.K., C.E. Cooper, and R.G. Knowles,** *Nitric oxide synthases: structure, function and inhibition.* **Biochem J, 2001. 357(Pt 3): p. 593-615.**

91. **Farley, K.S., et al.,** *Effects of macrophage inducible nitric oxide synthase in murine septic lung injury.* **Am J Physiol Lung Cell Mol Physiol, 2006. 290(6): p. L1164-72.**

92. **Lin, K.L., et al.,** *CCR2+ monocyte-derived dendritic cells and exudate macrophages produce influenza-induced pulmonary immune pathology and mortality.* **J Immunol, 2008. 180(4): p. 2562-72.**

93. **Hughes, M.N.,** *Relationships between nitric oxide, nitroxyl ion, nitrosonium cation and peroxynitrite.* **Biochimica Et Biophysica Acta-Bioenergetics, 1999. 1411(2-3): p. 263-272.**

94. **Pacher, P. and C. Szabo,** *Role of the peroxynitrite-poly(ADP-ribose) polymerase pathway in human disease.* **Am J Pathol, 2008. 173(1): p. 2-13.**

95. **Eguchi, Y., S. Shimizu, and Y. Tsujimoto,** *Intracellular ATP levels determine cell death fate by apoptosis or necrosis.* **Cancer Res, 1997. 57(10): p. 1835-40.**

96. **Zhang, J., et al.,** *Nitric oxide activation of poly(ADP-ribose) synthetase in neurotoxicity.* **Science, 1994. 263(5147): p. 687-9.**

97. **Virag, L., et al.,** *Peroxynitrite-induced cytotoxicity: mechanism and opportunities for intervention.* **Toxicol Lett, 2003. 140-141: p. 113-24.**

98. **Fischer, S.R., et al.,** *Nitric oxide synthase inhibition restores hypoxic pulmonary vasoconstriction in sepsis.* **Am J Respir Crit Care Med, 1997. 156(3 Pt 1): p. 833-9.**

99. **Martin, J.G., et al.,** *Chlorine-induced injury to the airways in mice.* **Am J Respir Crit Care Med, 2003. 168(5): p. 568-74.**

100. **Jang, A.S., et al.,** *Expression of nitric oxide synthase, aquaporin 1 and aquaporin 5 in rat after bleomycin inhalation.* **Intensive Care Med, 2004. 30(3): p. 489-95.**

101. **Genovese, T., et al.,** *Inhibition or knock out of inducible nitric oxide synthase result in resistance to bleomycin-induced lung injury.* **Respir Res, 2005. 6: p. 58.**

102. **Enkhbaatar, P., et al.,** *The inducible nitric oxide synthase inhibitor BBS-2 prevents acute lung injury in sheep after burn and smoke inhalation injury.* **Am J Respir Crit Care Med, 2003. 167(7): p. 1021-6.**

103. **Han, X., et al.,** *Increased iNOS activity is essential for intestinal epithelial tight junction dysfunction in endotoxemic mice.* **Shock, 2004. 21(3): p. 261-70.**

104. **Hill, B.G., et al.,** *What part of NO don't you understand? Some answers to the cardinal questions in nitric oxide biology.* **J Biol Chem, 2010. 285(26): p. 19699-704.**

105. **Rawlins, E.L. and B.L. Hogan,** *Ciliated epithelial cell lifespan in the mouse trachea and lung.* **Am J Physiol Lung Cell Mol Physiol, 2008. 295(1): p. L231-4.**

106. **Zakrzewska, A., et al.,** *Macrophage-specific gene functions in Spi1-directed innate immunity.* **Blood, 2010. 116(3): p. e1-11.**

107. **Biswas, A.K. and D.G. Johnson,** *Transcriptional and nontranscriptional functions of E2F1 in response to DNA damage.* **Cancer Res, 2012. 72(1): p. 13-7.**

108. **Lawrence, T.,** *The nuclear factor NF-kappaB pathway in inflammation.* **Cold Spring Harb Perspect Biol, 2009. 1(6): p. a001651.**

109. **Wang, B., et al.,** *The T box transcription factor TBX2 promotes epithelial-mesenchymal transition and invasion of normal and malignant breast epithelial cells.* **PLoS One, 2012. 7(7): p. e41355.**

110. **Lefebvre, P., Y. Benomar, and B. Staels,** *Retinoid X receptors: common heterodimerization partners with distinct functions.* **Trends Endocrinol Metab, 2010. 21(11): p. 676-83.**

111. **Baumann, H. and J. Gauldie,** *The acute phase response.* **Immunol Today, 1994. 15(2): p. 74-80.**

112. **Zimmerman, T.L., et al.,** *Nuclear export of retinoid X receptor alpha in response to interleukin-1beta-mediated cell signaling: roles for JNK and SER260.* **J Biol Chem, 2006. 281(22): p. 15434-40.**

113. **Beigneux, A.P., et al.,** *The acute phase response is associated with retinoid X receptor repression in rodent liver.* **J Biol Chem, 2000. 275(21): p. 16390-9.**

114. **Mehta, K., et al.,** *Inhibition by all-trans-retinoic acid of tumor necrosis factor and nitric oxide production by peritoneal macrophages.* **J Leukoc Biol, 1994. 55(3): p. 336-42.**

115. **Wang, X., C. Allen, and M. Ballow,** *Retinoic acid enhances the production of IL-10 while reducing the synthesis of IL-12 and TNF-alpha from LPS-stimulated monocytes/macrophages.* **J Clin Immunol, 2007. 27(2): p. 193-200.**

116. **Na, S.Y., et al.,** *Retinoids inhibit interleukin-12 production in macrophages through physical associations of retinoid X receptor and NFkappaB.* **J Biol Chem, 1999. 274(12): p. 7674-80.**

117. **Hisamori, S., et al.,** *All-trans-retinoic acid ameliorates carbon tetrachloride-induced liver fibrosis in mice through modulating cytokine production.* **Liver Int, 2008. 28(9): p. 1217-25.**

118. **Zhong, Y., et al.,** *Novel retinoic acid receptor alpha agonists for treatment of kidney disease.* **PLoS One, 2011. 6(11): p. e27945.**

119. **Tabata, C., et al.,** *All-trans-retinoic acid prevents radiation- or bleomycin-induced pulmonary fibrosis.* **Am J Respir Crit Care Med, 2006. 174(12): p. 1352-60.**

120. **Rigo, I., et al.,** *Induction of triggering receptor expressed on myeloid cells (TREM-1) in airway epithelial cells by 1,25(OH)(2) vitamin D(3).* **Innate Immun, 2012. 18(2): p. 250-7.**

121. **Haselmayer, P., et al.,** *TREM-1 ligand expression on platelets enhances neutrophil activation.* **Blood, 2007. 110(3): p. 1029-35.**

122. **Gomez-Pina, V., et al.,** *Metalloproteinases shed TREM-1 ectodomain from lipopolysaccharide-stimulated human monocytes.* **J Immunol, 2007. 179(6): p. 4065-73.**

123. **Bouchon, A., et al.,** *TREM-1 amplifies inflammation and is a crucial mediator of septic shock.* **Nature, 2001. 410(6832): p. 1103-7.**

124. **Gibot, S., et al.,** *A soluble form of the triggering receptor expressed on myeloid cells-1 modulates the inflammatory response in murine sepsis.* **J Exp Med, 2004. 200(11): p. 1419-26.**

125. **Gibot, S., et al.,** *TREM-1 promotes survival during septic shock in mice.* **Eur J Immunol, 2007. 37(2): p. 456-66.**

126. **Murakami, Y., et al.,** *Intervention of an inflammation amplifier, triggering receptor expressed on myeloid cells 1, for treatment of autoimmune arthritis.* **Arthritis Rheum, 2009. 60(6): p. 1615-23.**

127. **Wu, J., et al.,** *The proinflammatory myeloid cell receptor TREM-1 controls Kupffer cell activation and development of hepatocellular carcinoma.* **Cancer Res, 2012. 72(16): p. 3977-86.**

128. **Arts, R.J., et al.,** *TREM-1: intracellular signaling pathways and interaction with pattern recognition receptors.* **J Leukoc Biol, 2013. 93(2): p. 209-15.**

129. **Ormsby, T., et al.,** *Btk is a positive regulator in the TREM-1/DAP12 signaling pathway.* **Blood, 2011. 118(4): p. 936-45.**

130. **Uchida, O., et al.,** *Met-RANTES ameliorates fibrous airway obliteration and decreases ERK expression in a murine model of bronchiolitis obliterans.* **Ann Thorac Cardiovasc Surg, 2007. 13(2): p. 82-6.**

131. **Vos, R., et al.,** *A randomised controlled trial of azithromycin to prevent chronic rejection after lung transplantation.* **Eur Respir J, 2011. 37(1): p. 164-72.**

132. **Culic, O., V. Erakovic, and M.J. Parnham,** *Anti-inflammatory effects of macrolide antibiotics.* **Eur J Pharmacol, 2001. 429(1-3): p. 209-29.**

133. **Bonner, J.C.,** *Mesenchymal cell survival in airway and interstitial pulmonary fibrosis.* **Fibrogenesis Tissue Repair, 2010. 3: p. 15.**

134. **Repertinger, S.K., et al.,** *EGFR enhances early healing after cutaneous incisional wounding.* **J Invest Dermatol, 2004. 123(5): p. 982-9.**

135. **Lee, Y.H., et al.,** *Hepatocyte growth factor inhibits apoptosis by the profibrotic factor angiotensin II via extracellular signal-regulated kinase 1/2 in endothelial cells and tissue explants.* **Mol Biol Cell, 2010. 21(23): p. 4240-50.**

136. **Mizuno, S., et al.,** *HGF reduces advancing lung fibrosis in mice: a potential role for MMP-dependent myofibroblast apoptosis.* **FASEB J, 2005. 19(6): p. 580-2.**

137. **Smith, C., et al.,** *Neutralization of tumor necrosis factor-alpha or interleukin-1 prevents obliterative airway disease in HLA-A2 transgenic murine tracheal allografts.* **J Heart Lung Transplant, 2001. 20(2): p. 166-167.**

138. **Borthwick, L.A., et al.,** *TNFalpha from classically activated macrophages accentuates epithelial to mesenchymal transition in obliterative bronchiolitis.* **Am J Transplant, 2013. 13(3): p. 621-33.**

139. **Elssner, A., et al.,** *Elevated levels of interleukin-8 and transforming growth factor-beta in bronchoalveolar lavage fluid from patients with bronchiolitis obliterans syndrome: proinflammatory role of bronchial epithelial cells. Munich Lung Transplant Group.* **Transplantation, 2000. 70(2): p. 362-7.**

140. **DiGiovine, B., et al.,** *Bronchoalveolar lavage neutrophilia is associated with obliterative bronchiolitis after lung transplantation: role of IL-8.* **J Immunol, 1996. 157(9): p. 4194-202.**

141. **Cheung, P.S., E.C. Si, and K. Hosseini,** *Anti-inflammatory activity of azithromycin as measured by its NF-kappaB, inhibitory activity.* **Ocul Immunol Inflamm, 2010. 18(1): p. 32-7.**

142. **Tsai, W.C., et al.,** *Azithromycin blocks neutrophil recruitment in Pseudomonas endobronchial infection.* **Am J Respir Crit Care Med, 2004. 170(12): p. 1331-9.**

143. **Lande, J.D., et al.,** *Gene expression profiling in murine obliterative airway disease.* **Am J Transplant, 2005. 5(9): p. 2170-84.**

144. **Kastelijn, E.A., et al.,** *Genetic polymorphisms and bronchiolitis obliterans syndrome after lung transplantation: promising results and recommendations for the future.* **Transplantation, 2012. 93(2): p. 127-35.**

145. **Peters, W., et al.,** *CCR2-dependent trafficking of F4/80dim macrophages and CD11cdim/intermediate dendritic cells is crucial for T cell recruitment to lungs infected with Mycobacterium tuberculosis.* **J Immunol, 2004. 172(12): p. 7647-53.**

146. **Belperio, J.A., et al.,** *Critical role for the chemokine MCP-1/CCR2 in the pathogenesis of bronchiolitis obliterans syndrome.* **J Clin Invest, 2001. 108(4): p. 547-56.**

147. **Moore, B.B., et al.,** *Protection from pulmonary fibrosis in the absence of CCR2 signaling.* **J Immunol, 2001. 167(8): p. 4368-77.**

148. **Lin, K.L., et al.,** *CCR2-antagonist prophylaxis reduces pulmonary immune pathology and markedly improves survival during influenza infection.* **J Immunol, 2011. 186(1): p. 508-15.**

149. **Demnati, R., et al.,** *Histopathological effects of acute exposure to chlorine gas on Sprague-Dawley rat lungs.* **J Environ Pathol Toxicol Oncol, 1995. 14(1): p. 15-9.**

150. **Gunnarsson, M., et al.,** ***Exposure to chlorine gas: effects on pulmonary function and morphology in anaesthetised and mechanically ventilated pigs.*** **J Appl Toxicol, 1998. 18(4): p. 249-55.**

151. **Gordon, S. and P.R. Taylor,** ***Monocyte and macrophage heterogeneity.*** **Nat Rev Immunol, 2005. 5(12): p. 953-64.**

152. **Yu, Y.R., et al.,** ***CCR2 deficiency, dysregulation of Notch signaling, and spontaneous pulmonary arterial hypertension.*** **Am J Respir Cell Mol Biol, 2013. 48(5): p. 647-54.**

153. **Koohsari, H., et al.,** ***The role of gamma delta T cells in airway epithelial injury and bronchial responsiveness after chlorine gas exposure in mice.*** **Respir Res, 2007. 8: p. 21.**

154. **White, C.W. and J.G. Martin,** ***Chlorine gas inhalation: human clinical evidence of toxicity and experience in animal models.*** **Proc Am Thorac Soc, 2010. 7(4): p. 257-63.**

155. **Jin, C., et al.,** ***Particulate allergens potentiate allergic asthma in mice through sustained IgE-mediated mast cell activation.*** **J Clin Invest, 2011. 121(3): p. 941-55.**

Biography

Emily Grace O'Koren was born on February 28, 1986 in Enid, Oklahoma. She is the daughter of Anthony and Mari O'Koren and has one older brother, Anthony O'Koren. During her early years, science and vocal music equally captivated her interest. She pursued both disciplines during her undergraduate studies at Lehigh University in Bethlehem, PA where she obtained dual degrees, a Bachelor of Science in Biology and a Bachelor of Arts in Music, in 2008.

Emily was first introduced to immunology in an undergraduate course. Her interest piqued, she quickly sought to learn more and eventually entered the graduate program of the Department of Immunology at Duke University.

Emily currently lives in Durham, NC where she enjoys the extended gardening season and cheering for Duke University's basketball team, the Blue Devils.

Publications

O'Koren, E. G., B. L. Hogan, et al. "Loss of Basal Cells Precedes Bronchiolitis Obliterans-Like Pathological Changes in a Murine Model of Chlorine Gas Inhalation." *Am J Respir Cell Mol Biol*. 2013. 49(5): p. 788-97.

Cain, D. W., **E. G. O'Koren**, et al. (2013). "Identification of a Tissue-Specific, C/EBPbeta-Dependent Pathway of Differentiation for Murine Peritoneal Macrophages." J Immunol. 2013. 191(9): p. 4665-75.